# Advanced Photon Harvesting Techniques for Organic Solar Cells

Dissertation zur Erlangung des akademischen Grades

## *Doctor Rerum Naturalium*

im Doktoratsstudium der Naturwissenschaften

Angefertigt am Institut für Organische Solarzellen (LIOS)

Eingereicht von:

*Dipl.-Phys. Robert Koeppe*

Betreuung:

*o. Univ. Prof. Mag. Dr. Niyazi Serdar Sariciftci*

Beurteilung:

*o. Univ. Prof. Mag. Dr. Niyazi Serdar Sariciftci*

*Univ. Prof. Dr. Siegfried Bauer*

Linz, Dezember 2007

**Kurzzusammenfassung:**

In der folgenden Arbeit werden verschiedene Ansätze zur Erweiterung des aktiven Spektrums organischer Solarzellen diskutiert und experimentell untersucht. Als Modellsystem einer organischen Solarzelle mit niedriger Energielücke werden hierfür Bauelemente auf Basis der organischen Halbleiter Zink-Phthalocyanin und Fulleren $C_{60}$ (und seiner Derivate) verwendet. Diese Solarzellen weisen eine hohe Quanteneffizienz in der Konversion von Licht zu Strom vor allem im roten und nahen infraroten Spektralbereich auf. Im blauen und grünen Teil des Spektrums ist die Effizienz durch die niedrige Absorption deutlich geringer und führt zu einer kleineren Leistungseffizienz bei der Umwandlung von Sonnenlicht.

Der erste Abschnitt bezieht sich auf Konzepte der Kombination von Solarzellen auf Basis von Zink-Phthalocyanin und Fulleren mit halbleitenden Polymeren, die eine höhere Energielücke aufweisen und somit die Absorptionslücke im blauen und grünen Spektralbereich ausgleichen können.

Diese Kombination kann geschehen durch ein direktes Hineinmischen des Polymers in die Zink-Phthalocyanin-Fulleren-Solarzelle, womit man eine Multikomponentensolarzelle erschafft. Die Effizienz der Ladungstrennung kann hierbei allerdings nur durch ein geschicktes Manipulieren der Übergänge zwischen den verschiedenen Materialien optimiert werden. Dies wird hier durch eine Komplexkoordination zwischen dem Zink-Atom im Zink-Phthalocyanin und einer Pyridyl-Seitengruppe an einem Fullerenderivat erreicht.

Desweiteren können zwei organische Solarzellen mit komplementären Absorptionsspektren über einen Serienkontakt verbunden werden. So kann eine hohe Konversionseffizienz über einen breiten Spektralbereich erlangt werden. Besondere Aufmerksamkeit muss hierbei auf den Rekombinationskontakt zwischen den beiden Bauelementen gelegt werden, damit eine vollständige Serienverschaltung realisiert werden kann. Im vorliegenden Falle wurde dieser Kontakt über eine dünne, nichtkontinuierliche Lage aus Gold zwischen einer Fulleren- und einer Zink-Phthalocyanin-Schicht zwischen einer Polymer-Fullerensolarzelle mit hoher Energielücke und einer Zink-Phthalocyanin-Fullerensolarzelle mit niedriger Energielücke realisiert. Die resultierende organische Tandemsolarzelle zeigt eine hohe Konversionseffizienz über einen sehr breiten Spektralbereich.

Im zweiten Abschnitt wird die Möglichkeit untersucht, externe Absorber an eine organische Solarzelle zu koppeln. Zwei grundsätzliche Mechanismen stehen hierbei für den Transport der Energie zwischen dem externen Absorber, welcher selbst nicht photovoltaisch aktiv ist, und der Solarzelle zur Verfügung.

Als erstes wird der Mechanismus der Photolumineszenz untersucht. Hierbei absorbiert ein Farbstoff mit hoher Lumineszenzquantenausbeute das einfallende Licht im Spektralbereich geringer Absorption der Solarzelle und reemittiert das Licht in einer passenderen Farbe. Die Lumineszenz geschieht isotrop, deswegen muss eine Wellenleiterkonstruktion eingesetzt werden, um das emittierte Licht zur Solarzelle zu führen. Eine solche Anordnung, auch bekannt als Lumineszenzkonzentrator, wurde im Zusammenspiel mit organischen Solarzellen untersucht und es wurde eine deutliche Steigerung der Konversionseffizienz im blauen und grünen Spektralbereich durch den Konzentrator erreicht.

Als weitere Möglichkeit, externe Absorber an eine Solarzelle zu koppeln, steht der resonante Energietransfer zur Verfügung. Dieser Prozess geschieht gerichtet und in geeigneten Systemen mit sehr hoher Effizienz. Allerdings bedingt die geringe Reichweite eine Nanostrukturierung des Absorbers, um einen guten Kontakt zu den Solarzellenmaterialien zu gewährleisten. Es werden Systeme auf der Basis von Halbleiter-Nanokristallen und farbstoffbeladener Zeolit L Mikrokristalle untersucht. Der Energietransfer zu Zink-Phthalocyanin als organischem Solarzellenmaterial wurde in beiden Fällen nachgewiesen und detailliert untersucht.

1

**Abstract:**

In the following thesis, different approaches towards the extension of the spectral bandwidth of organic solar cells are dicussed and explored experimentally. As a model system for an organic solar cell with low energy gap, devices based on the organic semiconductors zinc-phthalocyanine and fullerene $C_{60}$ (and derivatives thereof) are used. These solar cells show a high quantum efficiency in the conversion of light to electrical current especially in the red and near infrared part of the spectrum. In the blue and green spectral range, the efficiency is severely limited by the low absorption cross section of the active materials. This leads in total to a reduced solar power conversion.

The first part describes concepts of combining the solar cells based on zinc-phthalocyanine and fullerenes with semiconducting polymers with a higher energy gap which therefore can offset the low absorption in the blue and the green.

This can be done by mixing the polymer directly into the zinc phthalocyanine-fullerene solar cell and thus creating a multicomponent solar cell. The efficency of the charge transfer can only be optimized by a direct manipulation of the interfaces between the materials. In this case, this is achieved by employing a complex coordination between the Zinc atom in zinc phthalocyanine and a pyridyl sidegroup attached to a fullerene derivative.

Furthermore, two organic solar cells with complementary absorption spectra can be connected by a series contact. This can yield a high conversion efficiency over a broad spectral range. Special emphasis lies here on the recombination contact between the two cells to establish a full series contact. In this thesis, a thin, noncontinouos gold layer was used to provide a contact between a high energy gap polymer-fullerene and a low energy gap zinc phthalocyanine-fullerene solar cell. The resulting organic tandem solar cell shows a high conversion efficiency over a very large spectral range.

In the second part the possibility of coupling external absorbers to an organic solar cell is studied. Two general mechanisms are useful to transport the energy from an absorber that is itself not photovoltaically active to the solar cell active materials.

In the first case, photoluminescence is used to that effect. Here, a dye with very high luminescence quantum yield absorbs the light in the spectral region of low absorbance of the solar cell active materials. The energy is then re-emitted as light of a better suitable colour. Luminescence is an isotropic process, making a waveguide construction necessary to guide the light to the solar cell. Such a contraption, known as a luminescent concentrator, is studied in conjunction with a low energy gap organic solar cell. A significant increase of the conversion efficiency in the blue and green spectral region is achieved.

A further possibility for coupling external absorbers to an organic solar cell is resonant energy transfer. This process is directional and can reach very high efficiencies in well tuned systems. The limited range of only a few nanometers makes a precise control of the nanostructure of such a setup necessary. Systems based on semiconductor nanocrystals and dye-loaded zeolite L microcrystals are studied. An efficient energy transfer to zinc phthalocyanine as organic solar cell material was studied in detail for both systems.

## I. Introduction

Over the last twenty years, the development of organic or "plastic" solar cells made significant progress from the first working devices [1, 2, 3] to more and more refined concepts [4, 5, 6, 7] that are slowly able to enter the competition with the mature technology of silicon solar cells. Major advantages of organic active materials are the ease of fabrication with low processing temperatures and the possible use of high-throughput production techniques such as printing or low temperature physical vapour deposition on endless flexible substrates.

The flexibility of organic synthesis makes a huge range of possible molecular structures for organic semiconducting materials available, with an unlimited number of possibilities yet untried. Two main classes of these materials can be identified by the process in which the semiconducting thin film phase is formed.

First, small molecules with high thermal stability can be evaporated in vacuum usually forming a neat film upon condensing on the relatively cold surface of the substrate. Secondly, many organic molecules, most noteably polymers can be dissolved in various solvents and deposited from solution. After evaporation of the solvent, a solid layer of the semiconducting material is formed. Often, the requirements in the molecular structure are contradictory and many molecules show either high enough thermal stability for evaporation or good enough solubility required for an acceptable film formation after solution processing, but not both.

The basic working principle of efficient organic solar cells is the dissociation of photogenerated excitations at the interface between electron donor and acceptor phases by a photoinduced charge transfer process [8]. Subsequently, the charge carriers have to be transported in the respective phase to the electrodes [4, 5, 6]. Critical parameters for the photocurrent generation are therefore the light absorption in the active layer, the efficiency of the charge transfer and the charge carrier transport properties of the materials involved.

As the excitations in materials consisting of organic molecules are usually not very mobile with diffusion lengths in the range of 10nm, only a small volume around the interface between donor and acceptor material is active in the photocurrent generation. A very good method to extend the charge carrier generation volume is the distribution of the donor-acceptor interface over the whole bulk of the solar cell active layer. This can be done rather easily with organic materials either by co-evaporation or casting the two materials from a common solution. The resulting solid state blend of a donor and acceptor material is called "bulk-heterojunction".

In these blends, there is always a certain amount of phase separation occuring, the amount of which is determined by many parameters such as solubility in the common solvent, temperature, concentrations, etc. In an optimized blend mixture, almost all excited states generated by absorbed photons will undergo a photoinduced charge transfer and lead to separated charges with the holes in the donor and the electrons in the acceptor phase, respectively [5]. Subsequently, the charges have to travel to their respective electrodes, where they can be extracted as photocurrent.
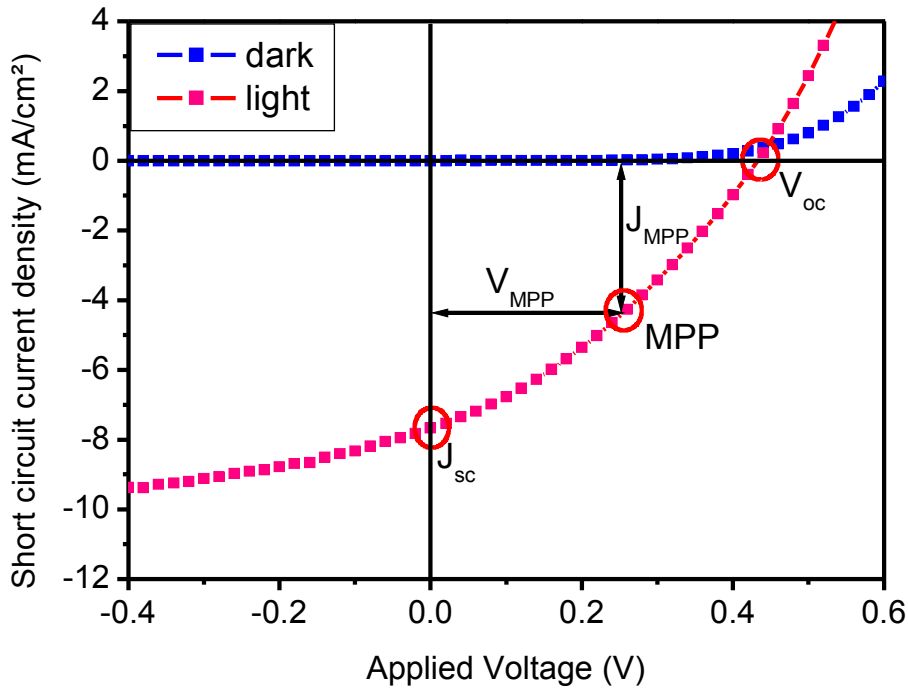


**I.1** Sample J-V curve of a solar cell showing the parameters used to calculate the PCE.

The most basic parameters of solar cells are the power conversion efficiency (PCE) usually measured under simulated AM1.5 solar emission and the spectral dependent external quantum efficiency (EQE), also called incident photon to collected electron efficiency (IPCE).

The PCE can be derived from a J-V-curve under light, where the current density through the device is plotted against a variable applied voltage. Such a J-V-curve is plotted in Fig. I.1. As the solar cell generates power, a certain amount of current density is passing through the device even though no voltage is applied. This is the short circuit current density ($J_{sc}$), corresponding to the short circuit current $I_{sc}$ normalized to the active area. To stop the current flow, a certain voltage has to be applied. This is called the open circuit voltage ($V_{oc}$). As the output power density of the solar cell corresponds to the product of voltage and current

density, the maximal power will be generated somewhere in between at the maximum power point (MPP). The ratio between the power density at the MPP and the product of $V_{oc}$ and $J_{sc}$ is called the fill factor (FF). Taking this into account, the PCE can be calculated as follows:

$$PCE(\%)=\frac{output\ power\ density\ of\ solar\ cell}{intensity\ of\ the\ incoming\ light}*100=\frac{V_{oc}*J_{sc}*FF}{I_{light}}*100 \quad \text{Form I.1}$$

The IPCE is measured by illuminating the solar cell with monochromatic light with the power $P_{ill}$ and recording the short circuit current $I_{sc}$ at different wavelengths $\lambda$. Thus, the IPCE can be calculated as follows:

$$IPCE(\%)=\frac{number\ of\ collected\ electrons}{number\ of\ incident\ photons}*100=\frac{1240\frac{nm}{eV}*J_{sc}}{\lambda(nm)*P_{ill}}*100 \quad \text{Form I.2}$$

In optimized organic solar cells, the IPCE can reach very high values of above 80%, meaning that almost all photons absorbed in the active layer will generate charges that can be collected at the electrodes.
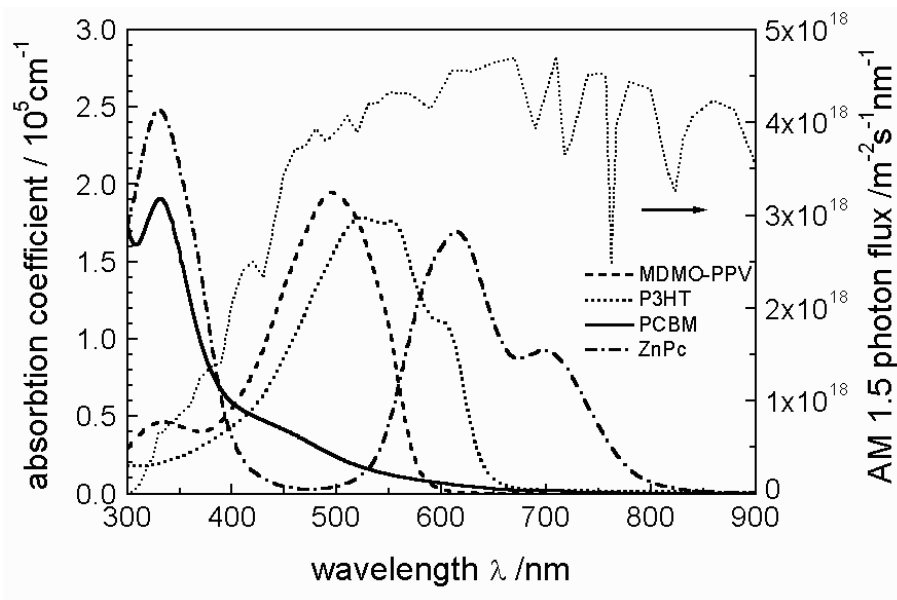


I.2 Absorption spectra of common organic solar cell materials together with the AM1.5 solar photon flux spectrum.

But despite the high quantum efficiencies reachable in organic solar cells, they only show a rather low overall power conversion efficiency of maximally 5% compared with established inorganic solar cell techniques that can reach up to 40%. To a large part, this is due to the fact that the best organic semiconducting materials available have an absorption edge at

comparatively high energy, usually above 2eV [9, 10]. Therefore, a large part of the solar irradiation cannot be converted by organic solar cells, as it is not absorbed in the active layer. This is illustrated in Fig. I.2, where the absorption spectra of several commonly used organic solar cell materials are depicted together with the solar AM1.5 irradiance photon flux. As fullerenes, the most commonly used organic acceptor molecules (represented in Fig. I.2 by the fullerene derivative [6,6]-phenyl-C61 butyric acid methyl ester (PCBM)), show only a weak absorption between 500 and 720nm, most of the solar irradiance will be absorbed in the donor material. In the case of the polymers poly((2-methoxy-5-(3,7-dimethyloctyloxy)-p-phenylene) vinylene (MDMO-PPV) and poly-3-hexyl thiophene (P3HT), the absorption reaches only to 600nm and 650nm, respectively. This means that only less than 25% of the solar photons incident on the surface of the earth are within the absorption range.

An exception in Fig. I.2 is the absorption of the small molecule zinc-phthalocyanine (ZnPc), which is used as a model system for a low bandgap organic material in the studies described in this thesis. The absorption reaches to over 800nm, leading to a much higher potential for photon harvesting, as over 40% of the photons in the AM1.5G solar spectrum have lower wavelengths. So the potential short circuit current density in organic solar cells based on ZnPc is nearly doubled in comparison to MDMO-PPV as absorber material.
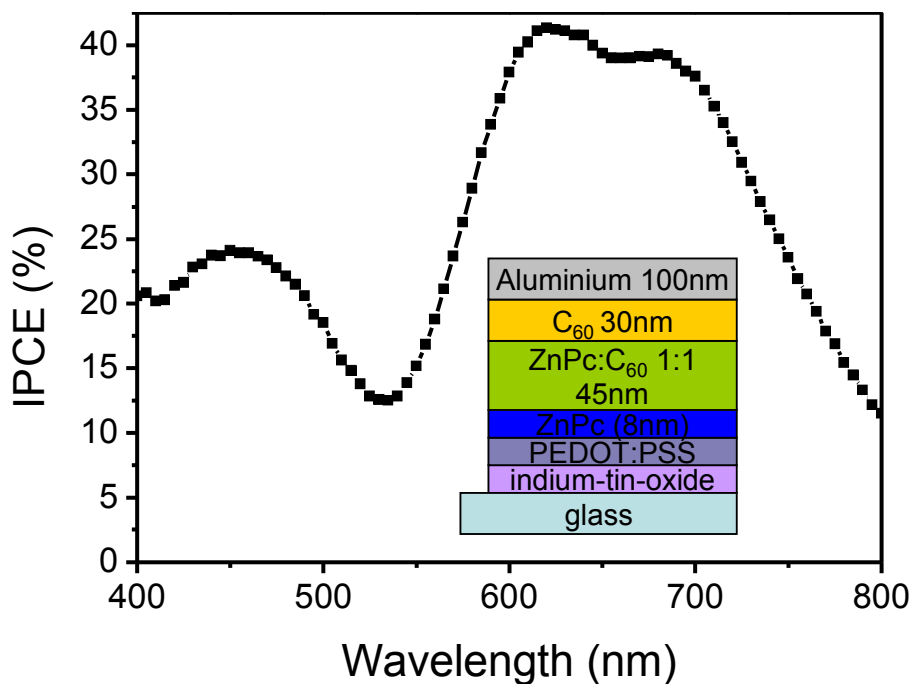


**I.3** Incident photon to converted electron efficiency (IPCE) spectrum of an optimized ZnPc:$C_{60}$ bulk heterojunction solar cell. Conversion efficiencies in the blue and green are lower than in the red due to the low absorption of the active materials in this range. Shown as inset is the structure of the device.
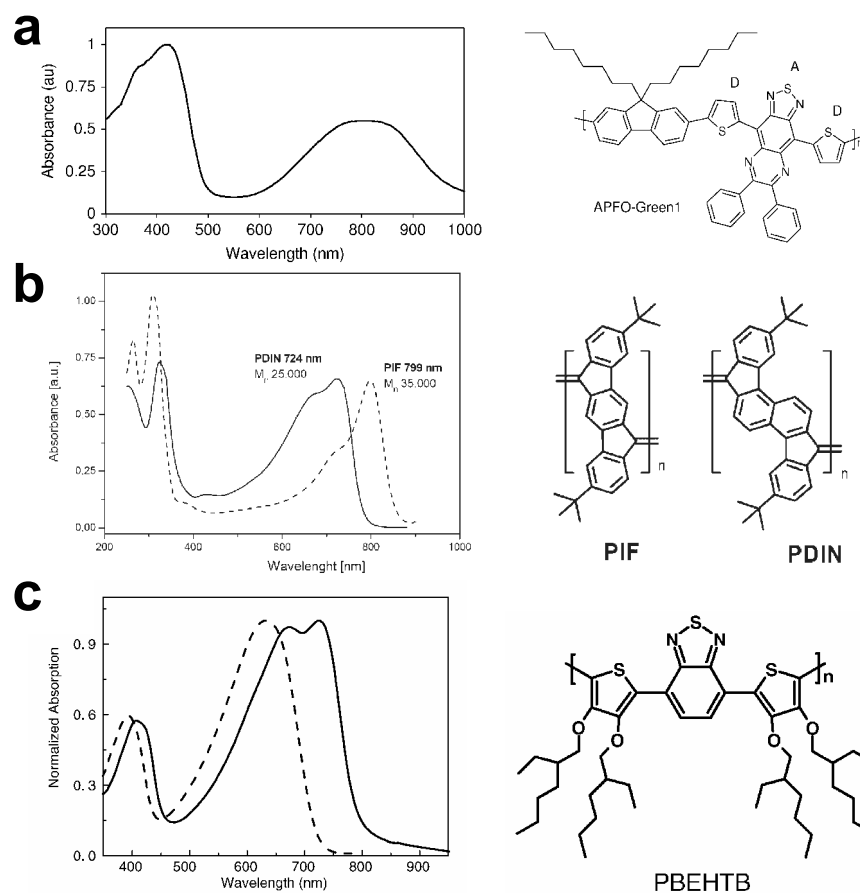
**I.4** Absorption spectra and structure formulae of some low energy gap polymers used in organic solar cells:
**a** APFO-Green 1 from E. Perzon, X.J. Wang, S. Admassie, O. Inganas, M.R. Andersson, Polymer 47(12), (2006) 4261-4268; Copyright 2006 Elsevier
**b** PIF and PDIN from E. Preis and U. Scherf, Macromolecules Rap. Comm. 27(14), (2006) 1105-1109; Copyright 2006 Wiley VCH
**c** PBEHTB from M.M. Wienk, M.P. Struijk and R.A.J. Janssen, Chem. Phys. Lett. 422(4-6), 488-491 (2006); Copyright 2006 Elsevier. The dashed line is the absorption spectrum of a solution in CHCl3, the solid line of a thin film on glass.

But in contrast to inorganic semiconductor materials, the absorption of organic materials usually occurs in spectrally narrow bands with very low absorption in between them. For example, ZnPc shows almost no absorption the region between the Q-band (600-800nm) and the Soret-band (300-400nm). This has severe consequences on the spectrally resolved IPCE of a solar cell fabricated by co-evaporation of ZnPc and $C_{60}$ fullerene as shown in Fig. I.3. The solar cell presented shows high short circuit photocurrent densities of over 11mA/cm² with an open circuit voltage of 0.45 and a fill factor of 0.45 under 100mW/cm² simulated AM1.5

illumination. This leads to a power conversion efficiency of above 2%. Shown as an inset to Fig. I.3 is the structure of the ZnPc:$C_{60}$ solar cell. The solar cell exhibits high quantum efficiencies of over 40% in the deep red, where ZnPc shows the distinct broad absorption, but stays below 15% in the green spectral range.

The gap in the absorption spectrum is a general feature of conjugated organic materials arising from the spacing between the different $\pi$-electron orbital energy levels, e.g. between the transitions $S_0$->$S_1$ and $S_0$->$S_2$. In the literature, there are many reports about low energy gap organic materials, mostly conjugated polymers [11, 12, 13, 14] and Fig. I.4 shows a few examples of such materials and their respective absorption spectra. All of them show a noticeable decrease of absorption in the blue and/or green spectral range. As there are up to now no competitive alternatives to fullerenes as acceptor materials in these solar cells, this feature can lead to a low absorption of green light in thin film organic solar cells built with such materials.

The thickness of organic solar cells is limited to 100-200nm. This is due to the fact that charge carrier mobility in organic semiconductors is rather low (usually below $10^{-3}$ cm$^2$/Vs), leading in thicker devices to large series resistances and to a high possibility that generated charge carriers will recombine before they reach their respective collecting electrodes. Thus, a low absorption cross-section of the materials used will lead directly to a low conversion efficiency in the according spectral region.

One way to adress this is the use of different materials as electron acceptor to extend the absorption range in the blue and green spectral range. This could either be higher fullerenes with a stronger absorption in the visible [15], other acceptors with a stronger absorbance in the blue and green spectral range such as perylene diimides [1, 2] or semiconductor nanocrystals that show a continuous absorption towards the blue [16, 17] (see Fig. I.5). But most of these materials have not yielded higher power efficiencies in organic solar cell devices than those employing $C_{60}$ and its derivatives despite the larger absorption range.

In this thesis, other ways of extending the photon harvesting range of a low energy gap organic solar cell based on ZnPc and derivatives of $C_{60}$ are explored and evaluated. The specific interaction between a novel pyrollidinofullerene compound bearing chelating pyridil groups and ZnPc opens the pathway to specifically engineer the donor-acceptor interfaces in a multicomponent solar cell comprising four materials. These solar cells show an efficient current generation over the full range from 400nm to 800nm. The studies performed on these
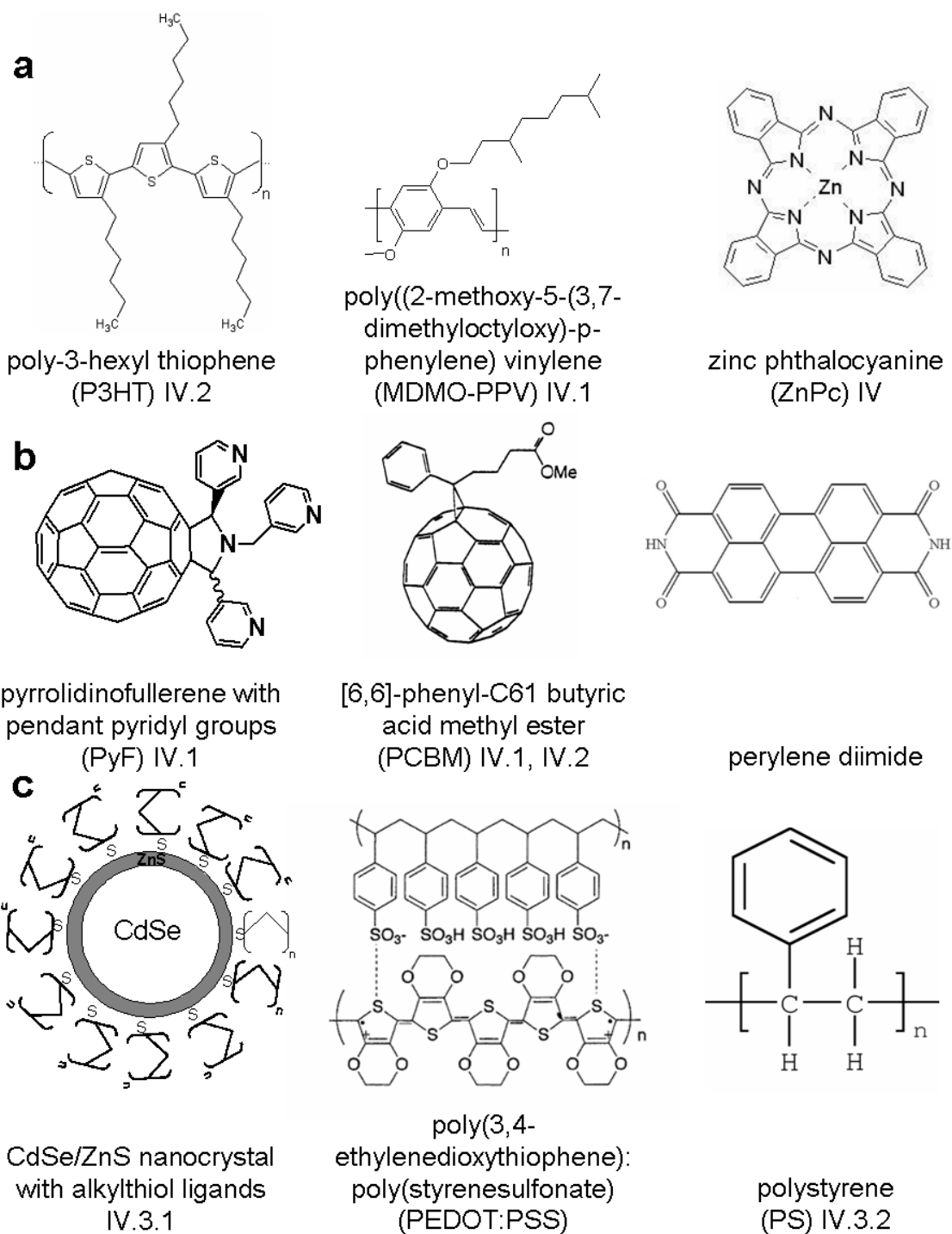
systems are described in chapters II.1 and III.1 of this thesis.

A straight-forward way of combining the spectral response of two organic solar cells with complementary absorption spectra is to stack them on top of each other and connect them in series via a recombination contact, e.g. a very thin, non-continuous gold layer. A device consisting of a $ZnPc:C_{60}$ bulk-heterojunction solar cell stacked on top of a P3HT:PCBM diffuse bilayer device is prepared and characterised as described in III.2. Photocurrent measurements show that these tandem solar cells can efficiently convert photons in a spectral range from 400 to over 800nm.

Extending the absorption range of low energy gap solar cells is also possible by coupling them to external absorbers. One way to achieve the coupling is via photoluminescence. As the emission of light is isotropic, a waveguide structure is needed to channel the emitted light to the solar cell which is best done in an arrangement known as the luminescent concentrator. In this thesis, the application of luminescent concentrators on organic solar cells is studied and discussed in chapter III.3.1.

A very elegant way of concentrating the energy from solar radiation spectrally and spatially is via a cascaded nonradiative resonant energy transfer. This process is directed and can be highly efficient, but the transfer range of less than 10nm requires precise engineering on a nanometer scale to ensure a good coupling of an external absorber to the organic solar cell.

In this thesis, two systems of external absorbers that might be coupled to a solar cell via energy transfer are studied. The first system are semiconductor nanocrystals covered with alkanethiol ligands to prevent direct charge transfer between the nanocrystal and the organic solar cell materials. Studies of the interaction between these nanocrystals and the organic solar cell materials are described in chapter III.3.2.1. The second system are dye-filled zeolite L crystals, in which energy can be funneled efficiently to the interface with the organic solar cell. Studies of the energy transfer processes from a dye filled zeolite L crystal to ZnPc are presented in chapter III.3.2.2.

**a**

poly-3-hexyl thiophene
(P3HT) IV.2

poly((2-methoxy-5-(3,7-dimethyloctyloxy)-p-phenylene) vinylene
(MDMO-PPV) IV.1

zinc phthalocyanine
(ZnPc) IV

**b**

pyrrolidinofullerene with
pendant pyridyl groups
(PyF) IV.1

[6,6]-phenyl-C61 butyric
acid methyl ester
(PCBM) IV.1, IV.2

perylene diimide

**c**

CdSe/ZnS nanocrystal
with alkylthiol ligands
IV.3.1

poly(3,4-ethylenedioxythiophene):
poly(styrenesulfonate)
(PEDOT:PSS)

polystyrene
(PS) IV.3.2

**I.5** Organic solar cell materials of interest **a** donor materials **b** acceptor materials **c** other materials

**II. Transferring Energy - Luminescence and Förster Energy Transfer**

In the following thesis, an important focus lies on the transferring of energy to low energy gap organic solar cell materials such as ZnPc. This can be done by using materials that harvest the light in the region of low absorption of the ZnPc with an subsequent transfer of the excitation energy into the solar cell active layer, where the charge transfer and transport will happen. This transfer of excitation energy can happen either by emission and reabsorption in the active layer (luminescence) or by resonant energy transfer. The photophysics of both phenomena will be described in the next pages.

## II.1 Photoluminescence

Photoluminescence (PL) is very generally a process in which a substance is absorbing light followed by an emission of photons. This requires a transition dipole moment in the substance which will interact with a photon with resonant energy. The interaction leads to an excitation of the substance, which can decay via the same or another transition dipole in the substance, leading to an emission of light. In organic molecules, usually two types of PL occur: fluorescence and phosphorescence. Both processes are sketched in a sample Jablonski diagram in Fig. II.1.
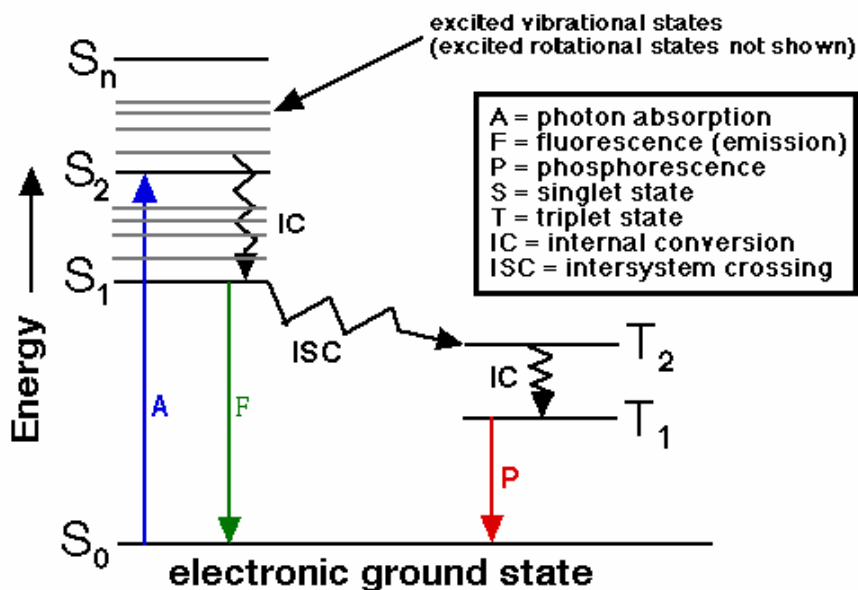


**II.1** Jablonski diagram showing the different pathways for fluorescence (green) and phosphorescence (red)

A state generated by photoexcitation ($S_{exc}$) of a molecule will usually very quickly relax via internal conversion (IC) to the lowest electronic excited state ($S_1$). From there, it can decay radiatively to a vibronic level of the electronic ground state ($S_{0x}$) by emitting a photon. Light emission resulting from this process is called fluorescence. The wavelength of the emitted light will correspond to the energetic difference between the states $S_1$ and $S_{0x}$. As the absorption has happened between the vibronic and electronic ground state ($S_0$) and some vibrational level of the electronically excited state, the fluorescence is always redshifted relative to the absorption spectrum.

An emission is called phosphorescence if the excited state $S_1$ decays via intersystem

crossing (ISC) to a triplet state and the radiative decay occurs between the lowest triplet state and the singlet ground state of the molecule. Due to the spin change necessary in this system, phosphorescence usually happens on a much slower timescale of μs to ms instead of ps to ns for the fluorescence. The redshift of the emission relative to the absorption is more pronounced in the phosphorescence than in the fluorescence as usually additional energy is dissipated in an internal conversion after the ISC.

Photoluminescence quantum yields for isolated organic dye molecules (e.g. in solution or an inert matrix) can reach high values of more than 90%. Competing processes are nonradiative decay channels similar to the internal conversion which dissipate the excitation energy as heat as well as charge or energy transfer processes. Photoluminescence emission is nondirected with only a slight dependency of the emission direction on the orientation of the emission dipole.

## II.2 Förster energy transfer

Theodor Förster's theory [37, 38] describes the coulombic coupling of the transition dipoles of weakly interacting excited donor and ground-state acceptor chromophores. For this, we consider an excited molecule D* and a molecule in the ground state A. Furthermore, the transition dipole for emission in D* (the donor) and the transition dipole for absorption in A (the acceptor) are in resonance. The condition is sketched in Fig. II.2b in the formalism of a Jablonski diagram. This immediately implies a transition of the excited state from the donor to the acceptor.

$$D*+A \rightarrow D+A* \qquad \text{Form II.1}$$
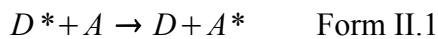
To describe the coupling of the two molecules we have to consider the wavefunctions of the electrons involved, one for each molecule. So to calculate the transition we have to define a wavefunction for the initial and the final state, considering the two electrons (called 1 and 2) involved:

$$\Psi_i = \frac{1}{\sqrt{2}}(\Psi_{D*}(1)\Psi_A(2) - \Psi_{D*}(2)\Psi_A(1))$$
$$\Psi_f = \frac{1}{\sqrt{2}}(\Psi_D(1)\Psi_{A*}(2) - \Psi_D(2)\Psi_{A*}(1)) \qquad \text{Form II.2}$$

Thus, the interaction between initial and final state is calculated as:

$$\beta = \langle \Psi_i | H' | \Psi_f \rangle \qquad \text{Form II.3}$$

H' is the perturbation part in the Hamiltonian of the complete system. Due to the additive nature of the initial and the final wavefunction, the resulting interaction is a sum of two terms:

$$\beta = \beta_C - \beta_{ex} \qquad \text{Form II.4}$$

$\beta_C$ can be called the Coulomb term, as it describes an interaction where the electrons are staying in place on the respective molecules, while only the excitation energy is transferred. $\beta_{ex}$ concerns a process where the energy transfer is mediated by a swapping of the electrons between the molecules. An overlap of the molecular wavefunctions is required for this process, which is therefore only occuring when D* and A are in direct contact. For the further discussion, only the Coulomb interaction will be considered, as it will have a much longer range and can be evaluated without detailed knowledge of the molecular orbital wavefunctions.

The Coulomb term describes a multipole-multipole interaction that can be reliably approximated by a dipole-dipole coupling of the transition dipole moments $\mu_D$ and $\mu_A$ for the

15

transitions D*→D and A→A*, respectively. Thus, by calculating the interaction between two dipoles at a distance $R_{DA}$, $\beta_C$ as Coulombic interaction energy between D and A can be expressed as:

$$\beta_C = \frac{e^2}{4\pi\epsilon_0 n^2} \frac{1}{R_{DA}^3} |\mu_D||\mu_A|\kappa \qquad \text{Form II.5}$$

Here, n is the refractive index of the medium between D and A and $\kappa$ is a factor describing the orientation of the dipoles towards each other.

By using Fermi's golden rule, the rate for resonant energy transfer $k_{RET}$ can be calculated as follows:

$$k_{RET} = \frac{2\pi}{\hbar} \beta_C^2 \rho(D*A; DA*) \qquad \text{Form II.6}$$

$\rho$ is a measure for the density of resonant initial and final states, as shown in Fig. II.2b. It correlates closely with the overlap between the donor emission and acceptor absorption spectrum. Fortunately, the density of states can be directly coupled to the measured absorption and emission spectra of acceptor and donor via the Einstein coefficients for spontaneous emission and induced absorption.

The rate of resonant energy transfer is finally given by the Förster formula:

$$k_{RET} = \frac{9000\ln(10)c^4}{128\pi^5 N_A} \frac{\kappa_{D*A}^2 \Phi_D*}{n^4 R_{DA}^6 \tau_{D*}} * J_{DA}$$

$$\text{Form. II.7}$$

$$J_{DA} = \int_\nu \frac{S_d(\nu)\epsilon_A(\nu)}{\nu^4} d\nu$$

where n is the index of refraction of the medium between the chromophores, c the vacuum speed of light, $N_A$ the Avogadro- or Lohschmidt-number, $\kappa_{D*A}$ is an orientation factor ranging between -2 and 2, $\Phi_{D*}$ is the luminescence quantum efficiency of the donor, $\tau_{D*}$ the donor luminescence lifetime, $S_D(\nu)$ the normalized donor emission spectrum, $\epsilon_A(\nu)$ the acceptor extinction coefficient, $\nu$ the frequency and $R_{DA}$ the distance between donor and acceptor.

Prerequisite for energy transfer is an overlap between the donor emission and the acceptor absorption correlating to a resonance between the transition dipoles of the involved chromophores. If this is the case, then the leading dependency is in the distance between donor and acceptor. In a system with matching donor emission and acceptor absorption, the

characteristic radius $R_0$, where the transfer probability is 50%, can reach values up to 10nm. As the probability for energy transfer is 50% if the rates for luminescence and energy transfer are equal, $R_0$ is calculated as follows:

$$R_0 = \sqrt[6]{J_{DA}\frac{9\ln(10)\Phi_D\kappa_{DA}^2}{128\pi^5 n^4 N_A}} \qquad \text{Form II.8}$$

With this, the probability for energy transfer can be expressed using the ratio between the distance of D and A and the Förster radius:

$$P_{RET} = \frac{1}{1+(\dfrac{R}{R_0})^6} \qquad \text{Form II.9}$$

The dependence of the transfer probability on the distance between donor and acceptor chromophore for certain values of $R_0$ is sketched in Fig. II.2a, while Fig. II.2b illustrates the resonance condition.
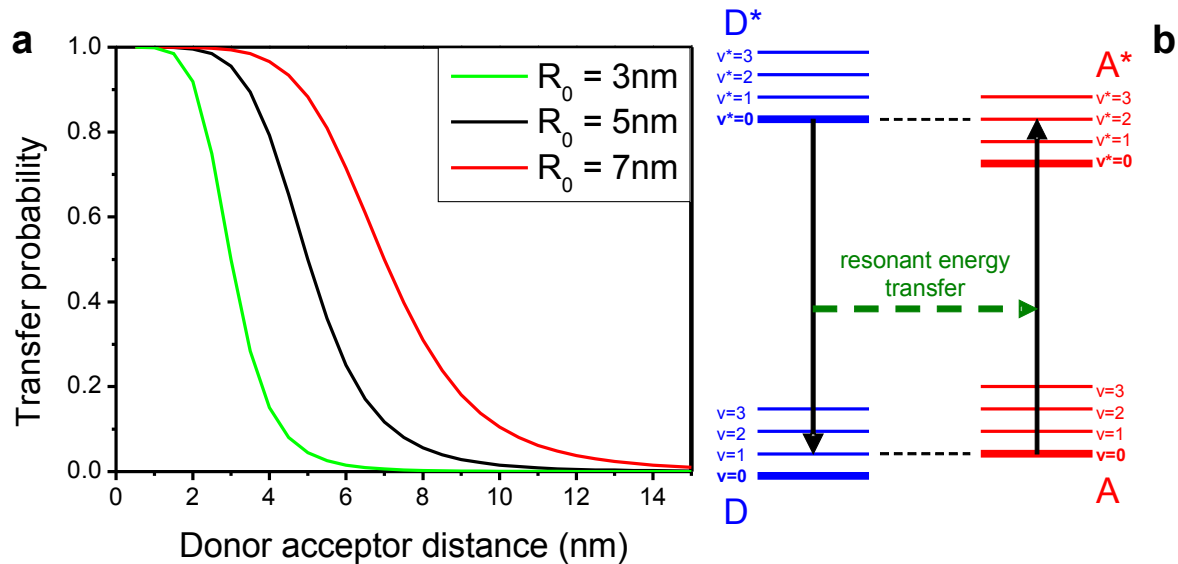


**II.2 a** distance dependence of the energy transfer probability according to Förster's theory. **b** energy level diagram illustrating the resonance condition for energy transfer

**III. Experimental**

**III.1 Fabrication of solar cells based on zinc-phthalocyanine and fullerenes**

The semiconducting properties of tightly packed conjugated molecule crystals and thin films have been studied since a long time [18]. In the early 1980s, the first efficient solar cells could be fabricated as a heterojunction between copper-phthalocyanine and a perylene-diimide [1]. Metalized phthalocyanines still are interesting compounds due to their strong absorption in the red and near infrared spectral region. The best performance is gained in conjunction with fullerenes which provide a very efficient charge separation and transport [6, 7]. In the following chapter, a brief overview over recent developments in the field of phthalocyanine:fullerene heterojunction solar cells is given.

## III.1.1 Zinc-phthalocyanine and pyrollidinofullerene diffuse bilayer solar cells

In the following, a study on the complexation between a pyrrolidinofullerene compound bearing three chelating pyridyl groups (PyF) and ZnPc is presented. A route to combine these materials in a bilayer thin-film organic solar cell is described and the performance of these cells is studied in comparison with reference cells fabricated using PCBM as electron acceptor, which shows no specific interaction with ZnPc. The results show a strong enhancement of the photovoltaic activity due to the complexation of the donor and acceptor molecules as compared to non-complexed structures.
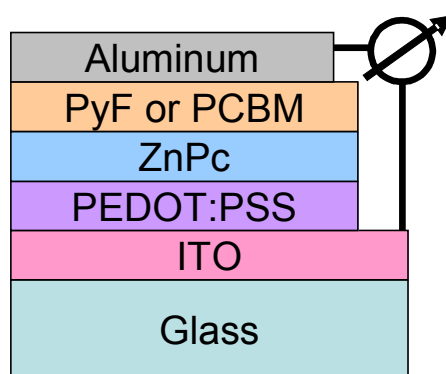
**III.1** structure of the diffuse bilayer solar

The materials used are shown in Fig. I.5, the solar cell structure in Fig. III.1. Absorbance spectra of the fullerene solutions (0.5mg fullerene per 1ml dichloromethane (DCM)) are measured before and after adding 2mg ZnPc in 3ml solution followed by gentle stirring and filtering through a 0.45μm membrane filter. As reference, 2mg ZnPc is added to 3ml pyridine, stirred and filtered through a 0.45μm membrane filter.

The solar cells are prepared on glass covered by a ITO layer of ~200nm thickness showing a sheet resistance of below 20Ω/ . On this, a layer of PEDOT:PSS with a thickness of about 70nm is spincoated from aqueous solution. About 40nm of ZnPc is deposited by thermal evaporation in high vacuum (approximately $10^{-6}$ mbar), followed by placing a single drop of the fullerene solution in DCM on the substrate at high spinning speeds (6000 to 8000 rpm). The samples are transferred to a glovebox filled with inert gas, where 100nm of aluminum is evaporated as a back electrode. The active area is approximately 4x2 mm². The PyF solution is prepared and stored in ambient atmosphere while the PCBM solution is kept protected against oxygen and water except for the time of spincoating.

I-V-characteristics are recorded on a solar simulator (AM1.5, 100mW/cm²). The incident photon to collected electron efficiency is measured using chopped monochromatized light from a Xe lamp and a lock-in amplifier. All solar cell measurents are performed in inert atmosphere.

ZnPc shows very poor or no solubility in most organic solvents, with the exception of pyridine, where a complex with a coordination bond between the zinc and the nitrogen of the pyridine ring is formed. Between ZnPc and DCM there is no complexation and ZnPc is completely insoluble in DCM.
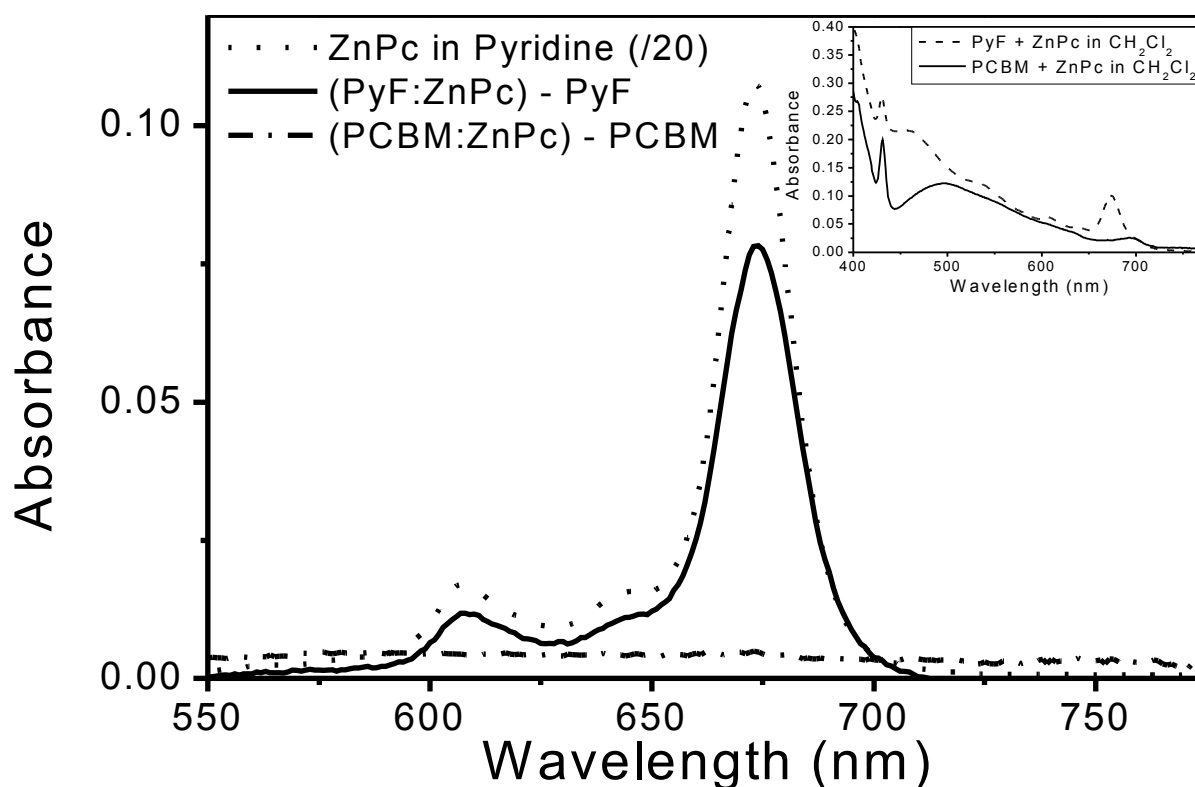
**III.2** Difference between the spectra of a fullerene (solid line PyF; dash-dotted line PCBM) solution in CH₂Cl₂ with and without addition of ZnPc. The dotted line is the absorption spectrum of ZnPc dissolved in pyridine. Inset: absorbance spectra of the fullerene solutions with added ZnPc

As shown in Fig. III.2, this changes significantly upon adding PyF to the solution. The absorption spectrum of a solution of 0.5mg PyF per 1 ml DCM (solid line in Fig. III.2) shows a clear contribution of the ZnPc Q-band absorption. The difference between the spectra shows a high similarity with the absorption spectrum of ZnPc in pyridine (dotted line in Fig. III.2). This indicates the formation of a complex between the pyridyl groups in PyF and the zinc atom in ZnPc leading to an increased solubility of ZnPc in DCM. A concentration of about 15 µg ZnPc per 1 ml solution can be deduced, using a literature value for the molar extinction coefficient ($\varepsilon_{674nm}$=2.8 $10^5$cm$^{-1}$/M) of ZnPc in pyridine[19]. This corresponds to a ratio of one ZnPc per ~19 PyF molecules.

The difference spectrum of PCBM in DCM before and after addition of ZnPc (dash-dotted line in Fig. III.2) shows no changes. This means no increase in ZnPc solubility, an indication that there is no coordinative interaction between PCBM and ZnPc.

Fig. III.3 shows the I-V-characteristics of the solar cell structures. The amount of PCBM

and PyF in the solar cells in both cases corresponds roughly to 50nm thick films, nearly independent on the concentration (10mg/ml to 25mg/ml) of the fullerene solution and the spincoating speed (6000rpm to 8000rpm) used, what is probably due to the special spincoating technique as described above and the high volatility of DCM (boiling point $T_b = 40°C$). Exchanging DCM with chlorobenzene results in a large amount of ZnPc washed away during the spincoating, leading to significantly reduced solar cell output parameters and lower reproducibility.
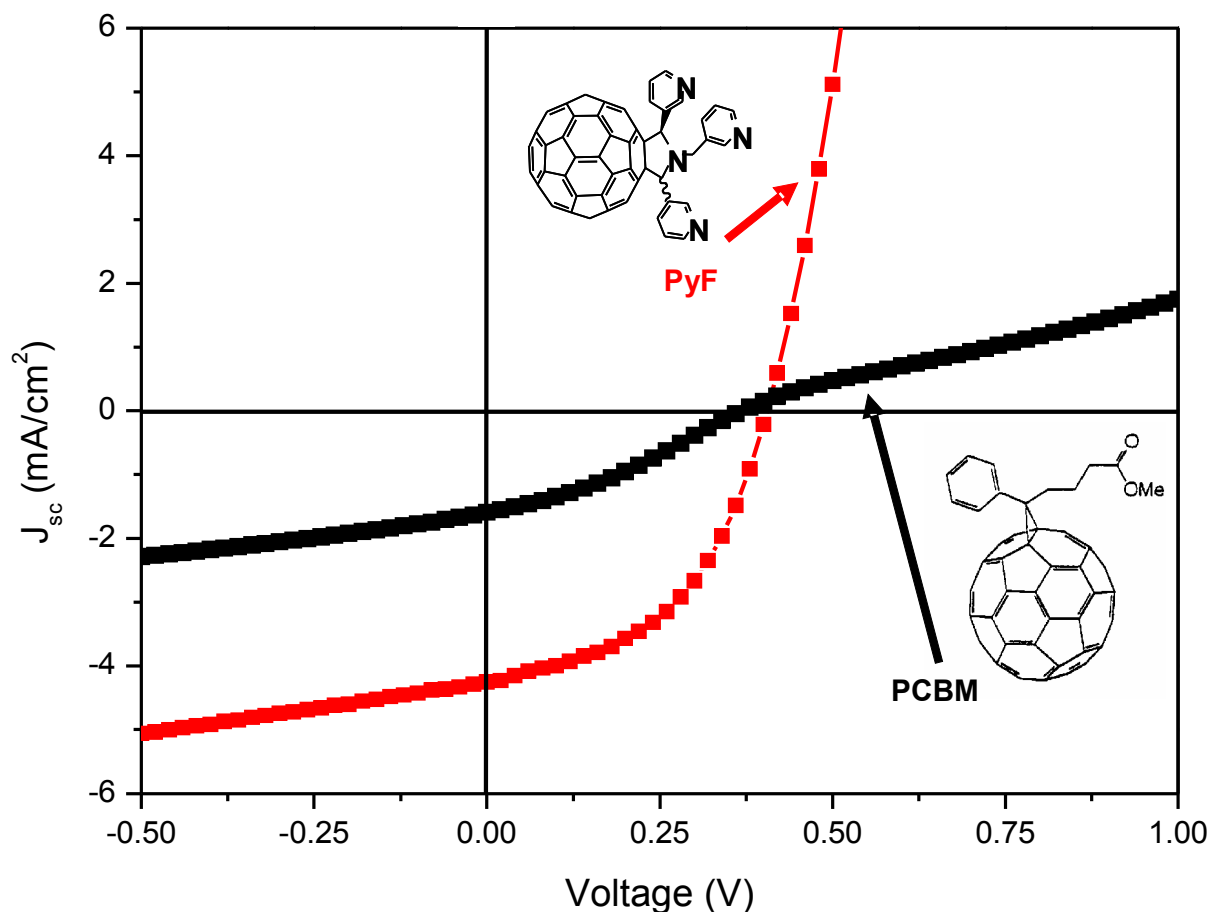


**III.3** I-V characteristics of diffuse bilayer solar cells fabricated with either PyF or PCBM.

In an optimized configuration, solar cells fabricated from ZnPc and PyF show short circuit current densities of around 4.2 mA/cm², open circuit voltages of around 400mV and fill factors of around 0.45. This corresponds to a power conversion efficiency of approximately 0.75% under 100mW/cm² simulated AM1.5 illumination.

Solar cells fabricated from ZnPc and PCBM show short circuit current densities of around 1.3 mA/cm², open circuit voltages of around 380mV and fill factors of around 0.3. The I-V-

22

curve shows a distinct negative curvature at positive voltages, a so-called counterdiode. This behaviour of the I-V-curve can be modelled by assuming two unequal diodes connected in series, but with opposite directions. Usually, it is associated with an interfacial barrier inside the device leading to a build-up of charges.

To explain the superior photocurrent generation in the PyF solar cells, we propose that a higher interfacial interaction between the donor and the acceptor is happening due to the specific organometallic coordination interaction between the PyF and the ZnPc. The ordering between ZnPc and PyF[20] may result in a higher overlap of the π-electron wavefunctions of the donor and acceptor moieties. Additionally, the solubility of the PyF-ZnPc-complex may lead to a more diffuse interface, which can increase the charge transfer probability[21].
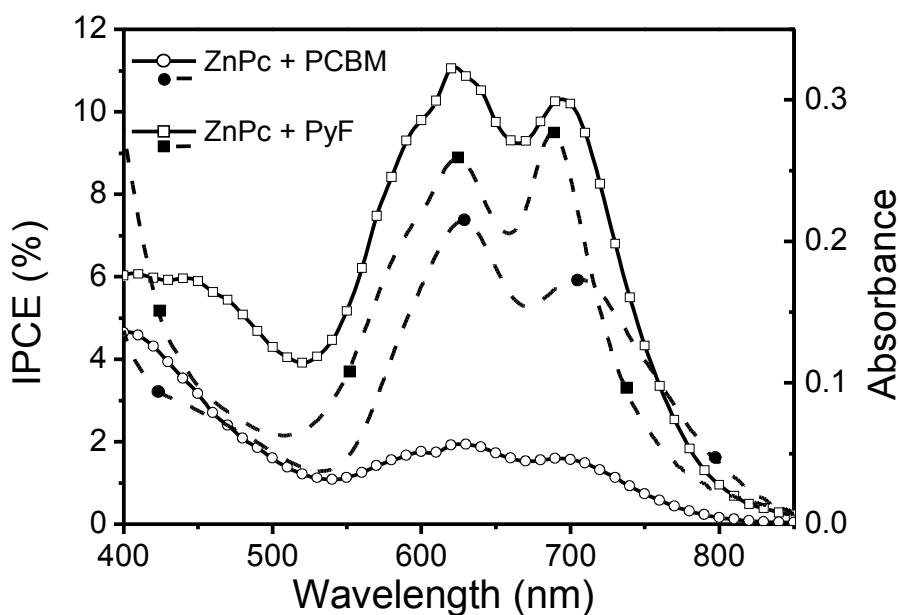


**III.4** Incident Photon to Converted Electron efficiency (IPCE) (solid) and active layer absorbance (dashed) spectra of diffuse bilayer solar cells fabricated with PyF (square symbols) and PCBM (round symbols).

Fig. III.4 shows the incident photon to collected electron efficiency (IPCE) spectra of the solar cells (solid) and the absorption spectra of the active layers (dashed). Especially dominant in both spectra is the broad Q-band of the solid state ZnPc between 600 and 800nm. Below 550nm, the fullerenes give the stronger contribution to the photocurrent. The lower values for the IPCE in the PCBM cell correspond to the lower short circuit current densities in the I-V measurements on the solar simulator.

Noteworthy is a change in shape of the ZnPc Q-band in the cells fabricated with PyF visible both in the absorption and IPCE spectra. The ZnPc Q-band double peak spectrum

shifts and narrows reproducibly under the influence of PyF. This is probably due to the interaction of ZnPc and PyF, leading to a weakened π-stacking of the ZnPc molecules at the interface and hence a stronger contribution of the ZnPc single molecule absorption with the pronounced peak at 675nm (see Fig. III.2) in the spectra.

In conclusion, solar cells are prepared by combining an evaporated layer of ZnPc and a novel highly soluble pyridyl-substituted fullerene derivative and the intermolecular interactions are investigated. Relatively high short-circuit current densities of over 4 mA/cm² were achieved with diffuse bilayer solar cells of ZnPc and PyF using a special spincoating technique to deposit the fullerene layer.

It is proposed that the complex formation of the pyridyl-substituted fullerenes with ZnPc increases the photovoltaic performance in this kind of diffuse bilayer organic solar cells. This specific interaction might also help in increasing the performance in other kinds of solar cells. Most noteworthy is the application in a multicomponent organic solar cell comprising 4 different compounds in the active layer, where the specific interaction can help to induce and maintain a favourable nanomorphology with the appropriate donor/acceptor interfaces (see chapter IV.1). Although, the performance is increased relative to ZnPc/PCBM and ZnPc/$C_{60}$ (not shown) bilayer devices, ZnPc:$C_{60}$ bulk heterojunction as shown in Fig. I.3 and described in III.1.2 can give much higher quantum as well as power conversion efficiencies.

### III.1.2. Zinc-phthalocyanine:$C_{60}$ bulk heterojunction solar cells

In the following, studies on films of a blend of ZnPc and $C_{60}$ between electrodes of the conducting polymer PEDOT:PSS and Aluminum are presented. I-V characteristics of these solar cells in light and dark are measured together with the spectral photoresponse. Additionally, the influence of 'buffer' layers of pure ZnPc and $C_{60}$ between the mixed layer and the electrodes is studied. An optimized device with layers of the pure materials is presented that reaches over 2.5% power conversion efficiency under 100mW/cm² simulated AM1.5 illumination.

To prepare the substrates, an aqueous solution of PEDOT:PSS (Baytron P) is spincoated onto a 1.5x1.5mm² glass slide covered by a transparent electrode of ITO. The active layer is deposited in high vacuum (<$10^{-5}$ mbar) by coevaporation of ZnPc and $C_{60}$ (both materials purified by vacuum sublimation) onto substrates kept at room temperature. Both materials are deposited at approx. 0.1nm/s to yield a 1:1 by volume blend. The buffer layers of the pure materials are deposited under the same conditions also with a deposition rate of approx. 0.1nm/s. Afterwards the samples are transferred to a glovebox filled with inert gas, where 100nm of Al is deposited by evaporation in a high vacuum chamber. In both evaporation chambers, the thickness of the deposited films is monitored by a quartz crystal microbalance.
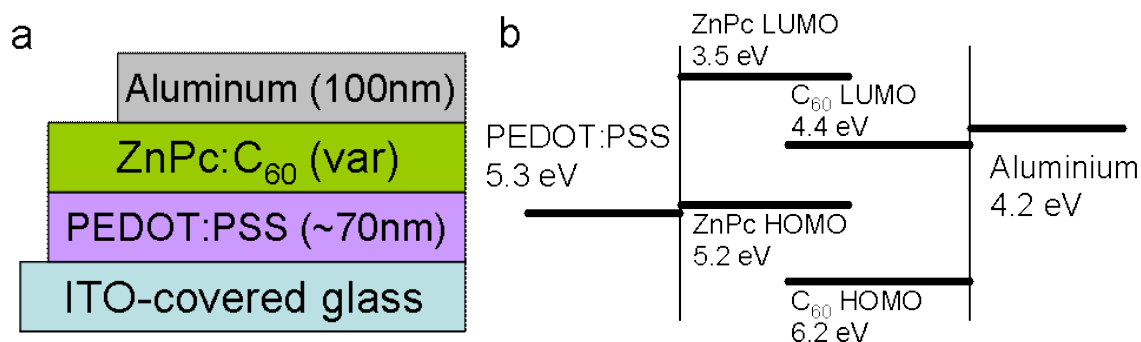
**III.5 a** structure of the ZnPc:$C_{60}$ solar cells. **b** the corresponding energy level diagram

The measurements of the solar cell characteristics are performed in the inert atmosphere of a nitrogen glovebox. I-V characteristics are recorded with a Keithley 236 sourcemeter, illumination is provided by a KHS Steuernagel solar simulator adjusted by a calibrated silicon solar cell to 100mW/cm². Incident Photon to Converted Electron (IPCE) spectra are recorded with a EG&G lockin amplifier under illumination by chopped light from a Xe lamp transferred into the glovebox by an optical fiber.

The structure of the devices investigated is shown in Fig. III.5a, the corresponding energy levels in Fig. III.5b. Photocurrent generation is taking place in the mixed layer of ZnPc and $C_{60}$ by an efficient photoinduced charge transfer [8]. As the ITO/PEDOT electrode workfunction is well aligned with the HOMO of the ZnPc, the holes generated in the ZnPc phase will be preferentially extracted through the ITO/PEDOT contact. The Al back electrode contacts the $C_{60}$ LUMO and additionally serves as a back reflector to increase the optical path of the incident light.

26

At first, the influence of the thickness of the blend layer is investigated. For this purpose, nine substrates of PEDOT covered ITO glass are coated with a coevaporated blend layer. A moving shutter ends the evaporation for three devices at 35nm thickness, for another three at 85nm and for the last three at 135nm. Thus, equal deposition conditions for all devices are ensured.
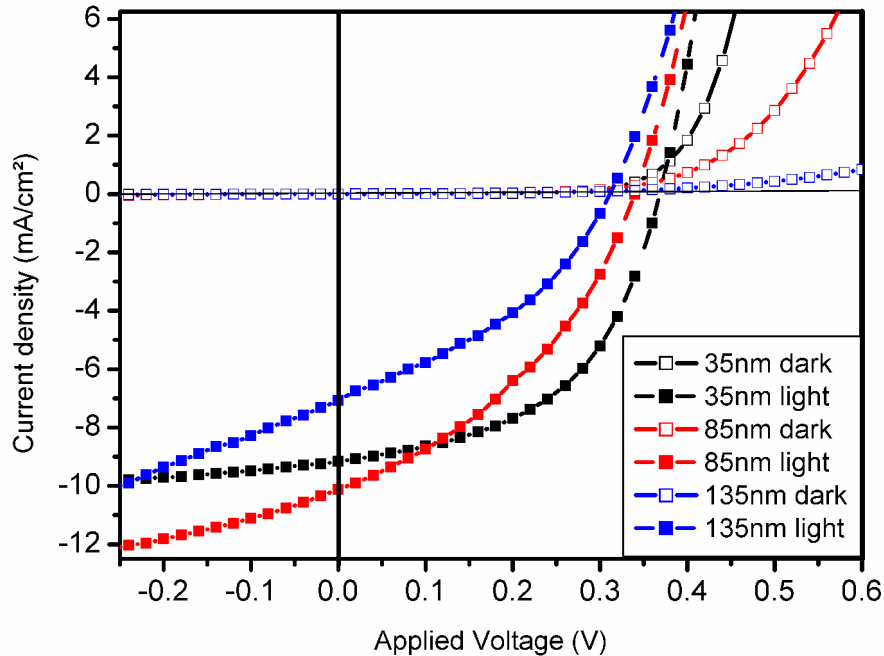


**III.6** Dark and light I-V-characteristics of ZnPc:$C_{60}$ solar cells with different active layer thicknesses

Fig. III.6 shows the I-V characteristics of the devices. As expected of this material combination, a rather low open circuit voltage ($V_{oc}$) is accompanied by very high short circuit current densities ($J_{sc}$) and a moderate fill factor. The devices typically yield the following characteristics under 100mW of simulated AM1.5 illumination:

| thickness: | $V_{oc}$: | $J_{sc}$: | fill factor: |
|---|---|---|---|
| 35nm | 0.36V | 9.5mA/cm² | 0.52 |
| 85nm | 0.34V | 10.8mA/cm² | 0.38 |
| 135nm | 0.32V | 7.2mA/cm² | 0.36 |

The first clear tendency is the decrease of the fill factor with increasing thickness which is due to the bad charge carrier transport requiring high fields for charge extraction. Thus,

charge carriers cannot exit the device under load and the current breaks down early.

A second feature is in the behaviour of the $J_{sc}$. Even in the very thin device, the Isc reaches nearly 10mA/cm², increases slightly in the 85nm layer and drops significantly in the very thick film. This is probably due to the bad charge carrier transport in the materials, so that at least one type of charge carriers is not able to leave the device before recombining if it is generated too far away from the electrode. As $C_{60}$ is known as one of the best organic electron transporting materials [22], the most likely explanation is that the generated holes can only be collected in a certain range lose to the ZnPc-PEDOT interface.
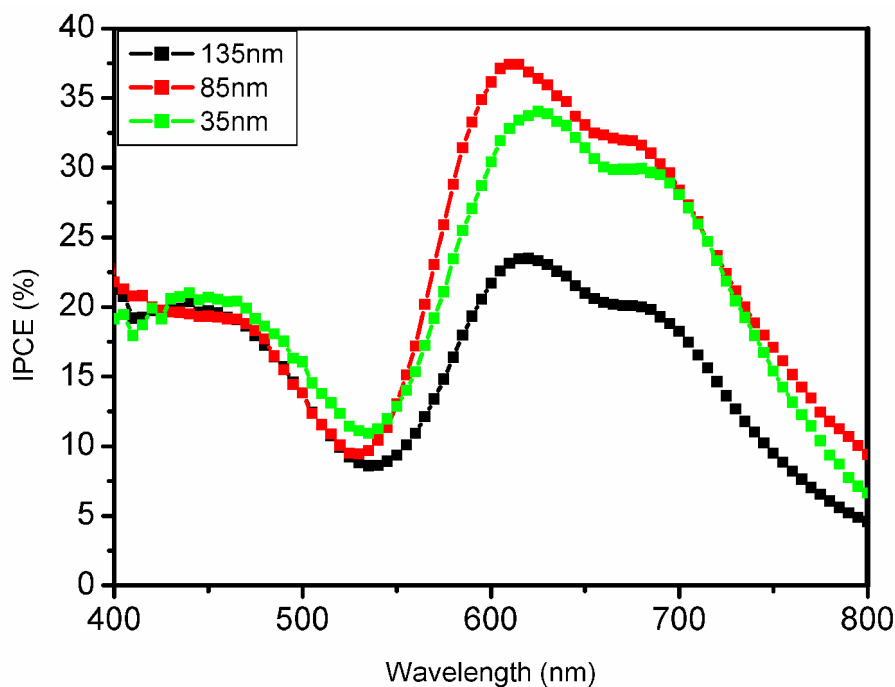


**III.7** Incident Photon to Converted Electron efficiency spectra of ZnPc:$C_{60}$ solar cells with different active layer thicknesses

To further clarify the picture, the spectrally resolved incident photon to collected electron ratio (IPCE) or external quantum efficiency of the devices depicted in Fig. III.7 is considered. The main features in the red between 600 and 800nm as well as below 450nm correlate with the absorption of the materials. In the gap around 520nm, both materials show very low absorption coefficients. Although the absolute values of the quantum efficiency vary according to the change in short circuit current of the different devices, the shape of the curves is not changing very much.

This supports the explanation that only a certain volume near the transparent electrode

contributes to the photocurrent. Another explanation such as the high absorption limiting the penetration depth of the incoming light would result in a much larger distortion of the spectrum of the thick device.

To study the influence of "buffer" layers around the blend of ZnPc and $C_{60}$, a shutter is applied during the deposition process to yield three samples of just the blend layer between the electrodes, three samples with 30nm of $C_{60}$ between the blend layer and the Al electrode and three samples with 20nm of ZnPc between the PEDOT electrode and the blend layer. The blend layer is deposited under the same conditions for all cells compared and has a thickness of 50nm.

The I-V characteristics of these devices are shown in Fig. III.8. Under 100mW/cm² simulated AM1.5 illumination, they show the following characteristics:

| layer structure: | $V_{oc}$: | $J_{sc}$: | fill factor: |
|---|---|---|---|
| blend | 0.34V | 9.2mA/cm² | 0.51 |
| blend/$C_{60}$ | 0.36V | 12.0mA/cm² | 0.38 |
| ZnPc/blend | 0.46V | 7.9mA/cm² | 0.23 |
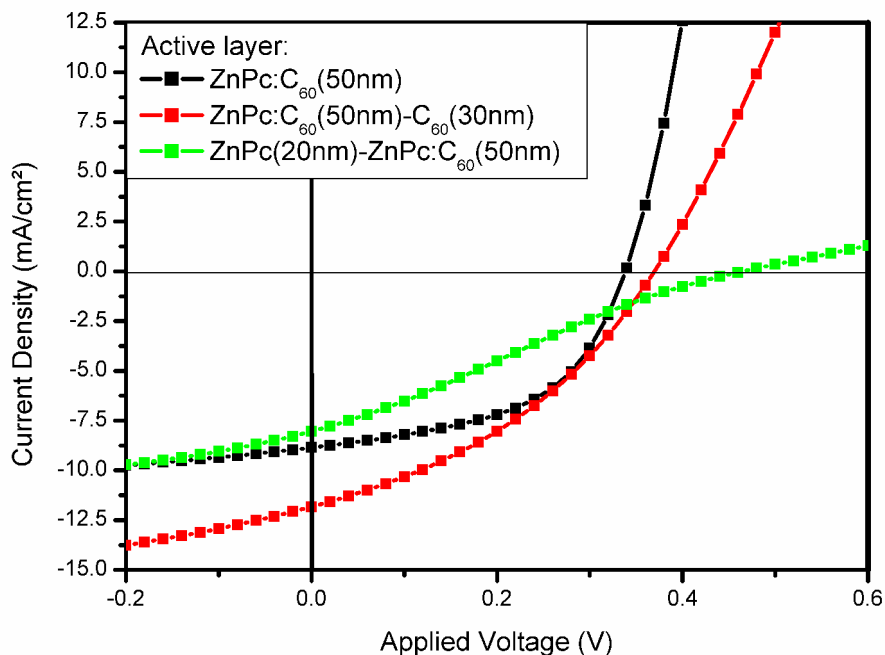


**III.8** I-V characteristics of ZnPc:$C_{60}$ solar cells with buffer layers of pure materials around the blend layer

29

As expected, the pure blend devices show a similar performance to the thin devices from Fig. III.6. Adding 30nm of $C_{60}$ between the blend and the aluminium electrode increases the $J_{sc}$ significantly while retaining the $V_{oc}$ on a similar level as the blend. The increase in photocurrent is probably due to an enhancement of the absorption inside the active layer of the device. As shown previously, the thin layer structure gives rise to interference effects that vary very much with the thickness of the layers used. A thicker layer can move the interference induced maximum of the electric field intensity to a more favourable location inside the device [23]. This is, however, accompanied by a lower fill factor.

The most evident change occurs when inserting a pure ZnPc layer between the PEDOT electrode and the blend layer. On one hand, the $V_{oc}$ increases noticeably, while the current and especially the fill factor drop very strongly. The latter effect is induced by a pronounced distortion of the I-V curve. This so called "counterdiode" behaviour is probably due to a build-up of charges at an interface leading to a breakdown of the current under load.

This effect depends critically on the thickness of the inserted layer of ZnPc. If the thickness is kept below 5nm, no significant effect either on $V_{oc}$ or on the I-V curve shape is observed. If the thickness is above 10nm, both an increase in $V_{oc}$ and the counterdiode behaviour are reproducibly appearing. In the thickness range between 5nm and 10nm, usually an increase in $V_{oc}$ is observed without counterdiode behaviour. In Fig. III.9 the I-V characteristics of a device where such a case is realized are shown. The following layer structure is used: PEDOT-ZnPc (10nm) - ZnPc:$C_{60}$ (45nm) - $C_{60}$ (15nm). The simulated AM1.5 power conversion efficiency of close to 3% is a very respectable value for organic solar cells. The IPCE spectrum of this device is plotted in Fig. I.3.

The solar cells presented here are a very promising step towards the realisation of cheap and flexible organic solar cells and photodetectors. The compatibility with proven and industrially applied high volume production techniques for organic light emitting diodes (OLEDs) might be a major point for introducing devices like these into the market.
Additionally, these solar cells show the highest absorption and quantum yield in the deep red part of the visible spectrum and are severly limited in thickness. This makes them ideal candidates for advanced photon harvesting concepts. Some of these concepts are presented in the chapter IV.
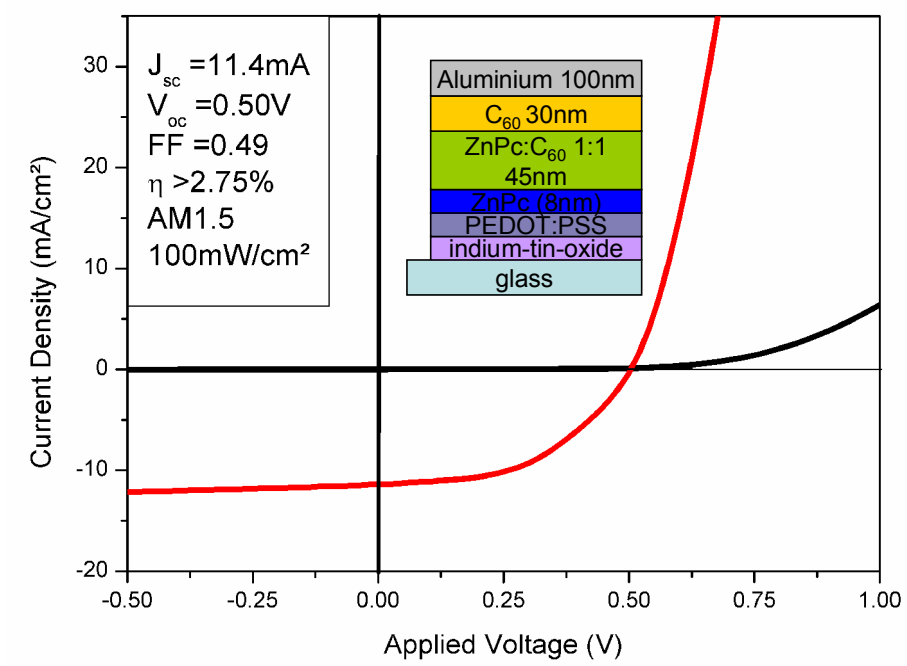
**III.9** Dark and light I-V characteristics of an optimized ZnPc:$C_{60}$ solar cell. The inset shows the solar cell structure

## III.2. Experimental Techniques
## III.2.1. Multicomponent Solar Cells

All organic semiconductor materials (PyF, PCBM, MDMO-PPV and ZnPc) used in this study are shown in Fig. I.5. The fabrication of the solar cells is very similar to that described in III.1.1 for diffuse bilayer ZnPc/PyF solar cells: precleaned substrates of glass covered with ITO are spincoated with an approx. 70nm thick layer of PEDOT:PSS. On this, a film of ZnPc of various thicknesses is deposited by thermal evaporation in high vacuum.

26 mg of PCBM and PyF mixed in different ratios and 6 mg of MDMO-PPV are dissolved per mL of HPLC-grade chlorobenzene and stirred at 50 °C for 36 h to ensure a full solubilization. One drop of the resulting solution is put on the substrate covered with the ZnPc film rotating at 8000 rpm on the spincoater. The device is finished with an electrode deposited by thermal evaporation of 0.6nm of LiF followed by approx. 100nm of Al.
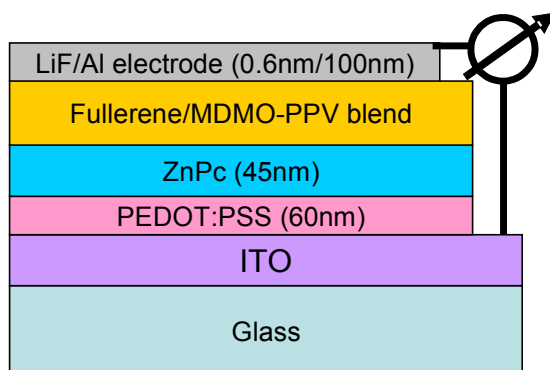


**III.10** Schematic layout of the multicomponent solar cells.

The schematic layout of the resulting multicomponent solar cell is shown in Fig. III.10. Devices are kept and measured under inert atmosphere in a nitrogen glovebox.

To estimate the active layer absorption, devices are prepared without deposition of the back electrodes and the transmission T is measured in a Cary 3G spectrophotometer. By measuring the transmission $T_0$ of a substrate without active layer, the absorbance can be calculated according to the following equation:

$$\text{abs} = \log\left(-\frac{T}{T_0}\right) \qquad \text{Form III.1}$$

I-V measurements are carried out with a Keithley 236 source measure unit. The solar cell parameters as described in I are determined by measuring the I-V-curves on a solar simulator

calibrated to 100mW/cm² of AM1.5 illumination. IPCE spectra are taken by recording the short circuit current from the solar cell under chopped illumination from a monochromated 75W Xe lamp transferred into the glovebox via an optical fiber using a EG&G lockin amplifier. By comparing the signal with the signal from a calibrated silicon solar cell, the IPCE can be determined as described in I.

## III.2.2. Organic Tandem Solar Cells
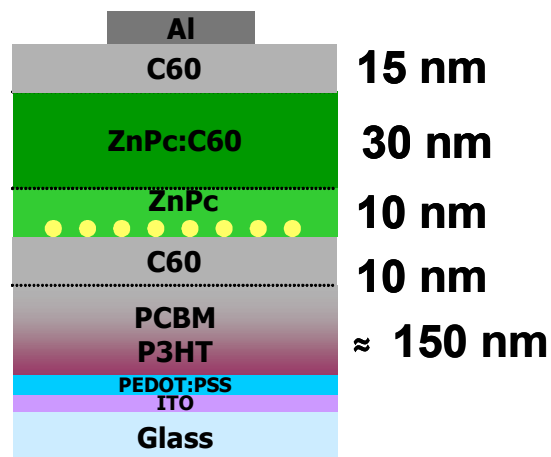


**III.11** Device structure of the organic tandem solar cells

The structure of the tandem cells studied is depicted in Fig. III.11. Indium tin oxide (ITO) coated glass having a sheet resistance of about $15\Omega/\square$ and covered by an about 70nm thick layer of PEDOT:PSS (Baytron P®, HC Starck) is used as substrate. Then, poly-3-hexyl-thiophene (P3HT) (1 %wt in chlorobenzene) is spin-cast, followed by [6,6]-phenyl $C_{61}$-butyric acid methyl ester (PCBM) (1 %wt in dichloromethane) at high rotation speeds of about 7000rpm.

Photoluminescence (PL) investigations performed on this structure reveal a strong PL signal from PCBM, suggesting that some PCBM rich (potentially continuous) environment is present on the top of the layer, indicative of a diffuse bilayer structure as in the case of the ZnPc:PyF solar cells presented in III.1.1. The rest of the tandem cell is realized by thermal evaporation under high vacuum. First of all, a 10nm layer of $C_{60}$ is evaporated at a rate of 0.03nm/sec, followed by the evaporation of the recombination layer (1 nm of Au) at a higher rate (0.5nm/sec) in order to hamper its diffusion in the sub-layer. Finally, the second cell, consisting of 10nm of ZnPc (0.03nm/sec), 40 nm of a mixture of co-evaporated ZnPc and $C_{60}$ (1:1, 40nm, 0.03nm/sec), and 15nm of $C_{60}$ (0.03nm/sec) is realized. The whole structure is closed by an electrode comprising 5nm of Cr and 95nm of Al (0.1nm/sec). The solar cells are characterized under 100 mW/cm² simulated AM 1.5 white light illumination. The current-voltage (I-V) measurements have been carried out under argon atmosphere in a glove box

with a Keithley 236 source-measure unit.

For the wavelength dependent photocurrent measurement, a 900W Xenon lamp combined with a monochromator (dλ<2nm resolution) is used as the light source. The light is focused on the active area of the solar cells and an I-V-curve is measured for each wavelength.

In a second experiment, the wavelength dependent photocurrent is measured using two light sources. The first light source, a halogen lamp with attached monochromator, is scanned through the entire visible spectrum, the second one, the Xe-lamp used before, stays fixed to a certain wavelength in order to selectively activate the desired sub-cell. Only the light from the halogen lamp is modulated by a mechanical chopper and by using a lock-in technique, the photocurrent generated by this illumination is recorded selectively. Fig. III.12 shows a schematic of the setup.
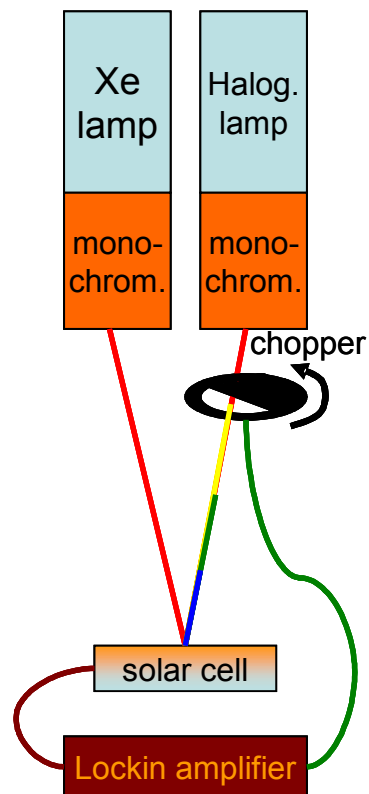


**III.12** Schematic of the photocurrent response setup with background illumination.

### III.2.3. Coupling external absorbers by luminescence

The organic solar cells used in the luminescent concentrator setup are based on a blend of ZnPc and fullerene $C_{60}$ [6, 7] as described in III.1.2. An approx. 70nm thick film of PEDOT:PSS (Baytron P) is spincoated on a 0.75mm thick glass substrate covered with a 200nm thick transparent electrode of Indium-Tin-Oxide (ITO). After thorough drying, a 60nm thick film of a blend of ZnPc:$C_{60}$ (1:1 by volume) followed by a 30nm thick film of $C_{60}$ is thermally evaporated in high vacuum ($<10^{-5}$ mbar). This active layer is covered by a 100nm thick evaporated aluminium electrode.

The luminescent concentrator is a 3x15x15mm³ polymethylmetacrylate (PMMA) plate fabricated by thermal polymerisation of a methylmetacrylate monomer solution (Plexit) doped with 0.007%wt of the dye Makrolex Fluorescence Red G from Bayer with a luminescence quantum yield of 89%. It is fabricated by the Fraunhofer IAP and has been used already in conjunction with a Silicon solar cell [36]. The absorbance spectrum of the concentrator plate is shown in Fig III.13b together with the luminescence spectrum of the used dye.
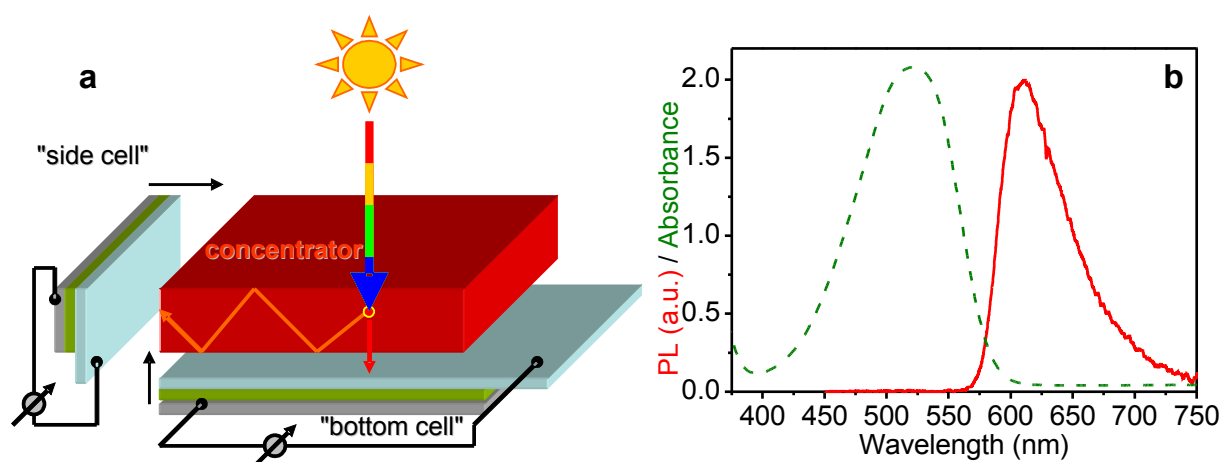


**III.13 a** the setup of the luminescent concentrator solar cell. The concentrator plate (red) absorbs the green and blue spectral parts of the incoming light and re-emits it as red light which is mainly guided to an organic solar cell attached to the side of the plate ("side cell"). Air gap mirrors on the other small sides (not shown) divert the light emitted away from the side cell back towards it. The red spectral part of the incoming light is transmitted to the bottom cell. **b** absorbance and emission spectrum of the concentrator plate

Two solar cells are used on different sides of the concentrator plate; the "bottom cell" has an active area of 15x15mm², the "side cell" of 3x15mm². Both are fixed onto the respective sides of the concentrator plate as shown in Fig. III.13a. The glass substrate of the side cell is

bonded to the Plexit plate by a highly transparent two-component epoxy glue. As the waveguiding properties of the plastic plate have to be conserved, the bottom cell is just loosely placed onto the concentrator, leaving an air gap. Aluminum mirrors are applied to the other small faces of the concentrator plate with an air gap to increase the waveguiding towards the side cell.

I-V-characteristics and incident photon to collected electron efficiency (IPCE) spectra of both solar cells are measured before and after application to the concentrator plate. The light source for the I-V-characteristics is a Steuernagel KHS solar simulator adjusted by a calibrated silicon diode to give 100mW/cm² AM1.5 illumination. IPCE spectra are recorded by monitoring the short circuit current of the solar cells with a SRS830 lockin amplifier using the chopped, monochromated (dλ<2nm) light from a Hg lamp as illumination. The incident light is focused in a 3x2mm² spot which can be moved across the surface of the concentrator. Thus, the quality of the waveguiding structure can be probed. If the quantum efficiency is not decreasing with the distance of the incident light spot from the side cell, the waveguiding works efficiently.

**III.2.4. Energy transfer between semiconductor nanocrystals and zinc-phthalocyanine**

The CdSe/ZnS nanocrystals were purchased as solution in toluene from NN-labs Inc. (www.nn-labs.com). Nominal diameter of the particles is 3.0nm and the emission maximum in solution is at 605nm. The CdSe core is epitaxially coated with an effectively 0.3nm thick ZnS layer to passify surface states. The PL quantum yield in solution is approximately 40%. The original octadecylamine (ODA) ligands providing solubility and stability were exchanged with a standard ligand exchange procedure [50] to n-alkanethiols of different length: n=18 (T18), 16 (T16), 12 (T12), 9 (T9), 6 (T6). A schematic picture of a nanocrystal is shown in Fig. I.5.

Absorption spectra were taken with a Varian Cary 3G UV-Vis Spectrophotometer. The luminescence of the films was measured with a M.U.T "Tristan light" fiber spectrometer using a Coherent "Innova 400" $Ar^+$-laser as 514 nm excitation source. The nanoparticle PLE was measured with the fibre spectrometer using a monochromated Xe-lamp as light source. The quenching measurements for the Stern-Volmer plot were done in an LP920 flash photolysis setup with a Coherent Nd:YAG ns pulsed laser running at 355nm as pump source.

The energy transfer samples were produced by thermally evaporating 20nm of ZnPc in high vacuum ($p<10^{-5}$mbar) onto a clean glass slide, followed by dropcasting of approximately 30μl solution of T12-coated nanocrystals and subsequent evaporation of another 20nm thick film of ZnPc. A 40nm thick film of ZnPc was evaporated under the same conditions onto a clean glass slide as reference.

The scattered nanoparticle samples were prepared by putting one drop of a solution of 2mg nanoparticles (T18, T16, T12, T9 or T6) in 1ml of toluene onto a clean glass slide (1.5x1.5cm²) rotating at 6000rpm. Subsequently, on one half of the glass slide, a layer of 20nm ZnPc was thermally evaporated in high vacuum. The quenching ratio is determined by averaging the nanoparticle photoluminescence of 5 points each on the parts of the glass slides with and without covering of ZnPc. Similarly strong quenching with less reproducibility was observed when the nanoparticles were deposited onto the ZnPc layer, so we can exclude a loss of luminescence due to damaging of the nanoparticles during the deposition of the ZnPc layer.

The photodiodes were prepared by spincoating a layer of PEDOT:PSS (Baytron PH) onto an ITO-covered glass slide. These substrates were coated with a layer of 40nm ZnPc by thermal evaporation in high vacuum. On some samples, approximately 25μl of T12 coated

nanoparticle solution was dropcast. Then another 20nm of ZnPc and 75nm Al were evaporated to finish the diode structure. Charge separation in these photodiodes is not very efficient, but yields enough photocurrent to record the spectrally resolved photocurrent.

The Incident Photon to Collected Electron conversion efficiency spectra (IPCE) were measured by illuminating the active area of the samples with monochromatised and chopped light from a tungsten halogen lamp. The resulting modulated photocurrent is recorded by a lock-in amplifier. The lamp power is recorded with a silicon diode powermeter (Thorlabs PM100) and is between 3-20 $\mu$W over the measured spectral range.

**IV. Advanced photon harvesting concepts**

In common organic solar cell concepts, two materials are brought in close contact with each other to ensure an efficient photoinduced charge transfer. But often, two materials that give a good miscibility, charge transfer and transport will not give an absorption that matches the solar spectrum for high overall power conversion efficiency. In the following, several strategies to extend the spectral range of efficient photon harvesting are discussed.

## IV.1. Multicomponent solar cells

MDMO-PPV:PCBM bulk heterojunctions are amongst the most efficient and well-studied organic solar cell material combinations, with optimized devices reaching solar power conversion efficiencies of more than 2.5% [5, 24, 25]. They collect the sunlight in a spectral region between 350 and 600 nm, whereas the major fraction of the photocurrent produced by fullerene/ZnPc devices as described in II. arises from the wide Q-band absorption of ZnPc at 580-800 nm. This is illustrated by the IPCE spectra for efficient MDMO-PPV:PCBM and ZnPc/PyF photovoltaic cells (Fig. IV.1).
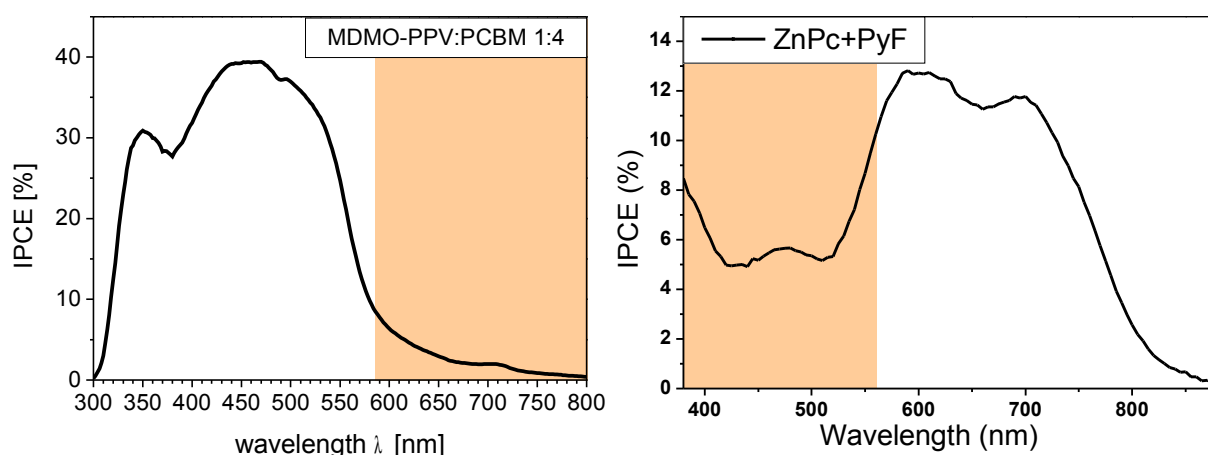


**IV.1** IPCE spectra of organic solar cells based on MDMO-PPV:PCBM (left) and ZnPc/PyF (right) illustrating the limited range of photon harvesting in two-component devices.

Therefore, it looks very promising to combine both types of cells in one device to achieve photocurrent generation over a wide spectral region. One way to do so is to combine both cell concepts via a recombination contact to produce an organic tandem solar cell [26, 27] such as described in IV.2. In the following, a more direct approach utilizing the complex coordination between ZnPc and PyF described in III.1.1 to fabricate a solar cell combining both MDMO-PPV and ZnPc as donor materials is presented.

All pyrrolidinofullerene materials presented in this work were synthesised by Dr. Pavel Troshin in the group of Prof. Rimma Lyubovskaya at the Institute of Problems of Chemical Physics of the Russian Academy of Science in Chernogolovka, Russian Federation. Dr. Troshin was also performing a part of the experimental studies presented here.

Multicomponent solar cells with different ratios of the fullerene compounds, different ZnPc film thicknesses and different solvents used are prepared and I-V-curves measured for at least 8 individual solar cells each. Typical results are shown in Table IV.1. Optimal results were obtained when a mixture of PCBM with a small amount of PyF was used as acceptor material. The first reduction potential of PyF measured by cyclic voltammetry [28] matches perfectly the first reduction potential of PCBM (Table IV.2), indicating that both compounds have very similar electron affinities. Therefore, the addition of small amounts of PyF to PCBM should not affect the electron transport properties of the material significantly.

| composition of acceptor phase | solvent | ZnPc thickness (nm) | $V_{oc}$ (mV) | $J_{sc}$ (mA/cm²) | FF (%) | $\eta$ (%) |
|---|---|---|---|---|---|---|
| 100% PCBM | CB | 45 | 510 | 3.2 | 53 | 0.8 |
| 2% PyF+98% PCBM | CB | 45 | 560 | 5.0 | 52 | 1.5 |
| 4% PyF+96% PCBM | CB | 45 | 570 | 5.8 | 50 | 1.6 |
| 8% PyF+92% PCBM | CB | 45 | 540 | 5.0 | 51 | 1.4 |
| 16% PyF+84% PCBM | CB | 45 | 530 | 3.7 | 43 | 0.8 |
| 33% PyF+67% PCBM | CB | 45 | 490 | 3.8 | 43 | 0.8 |
| 67% PyF+33% PCBM | CB | 45 | 310 | 0.5 | 33 | 0.05 |
| 100% PyF | CB | 45 | 310 | 0.25 | 23 | 0.01 |
| 4% PyF+96% PCBM | CF | 45 | 460 | 0.9 | 27 | 0.11 |
| 4% PyF+96% PCBM | DCM | 45 | 420 | 0.6 | 28 | 0.07 |
| 4% PyF+96% PCBM | CB | 30 | 500 | 4.3 | 44 | 0.9 |
| 4% PyF+96% PCBM | CB | 60 | 470 | 4.7 | 51 | 1.1 |

**Table IV.1** Output parameters of Multicomponent Solar Cells fabricated under different conditions. CB = chlorobenzene, CF = chloroform, DCM = dichloromethane, DCB = 1,2-dichlorobenzene

| $E_{1/2}$, V vs. SCE | | | |
|---|---|---|---|
| compound | $E^1_{1/2}$ | $E^2_{1/2}$ | $E^3_{1/2}$ |
| PyF | -0.8 | -1.2 | -1.75 |
| PCBM | -0.8 | -1.2 | -1.8 |

**Table IV.2** Reduction potentials ($E_{1/2}$) of the fullerene derivatives vs. SCE determined from cyclic voltammetry measurements.
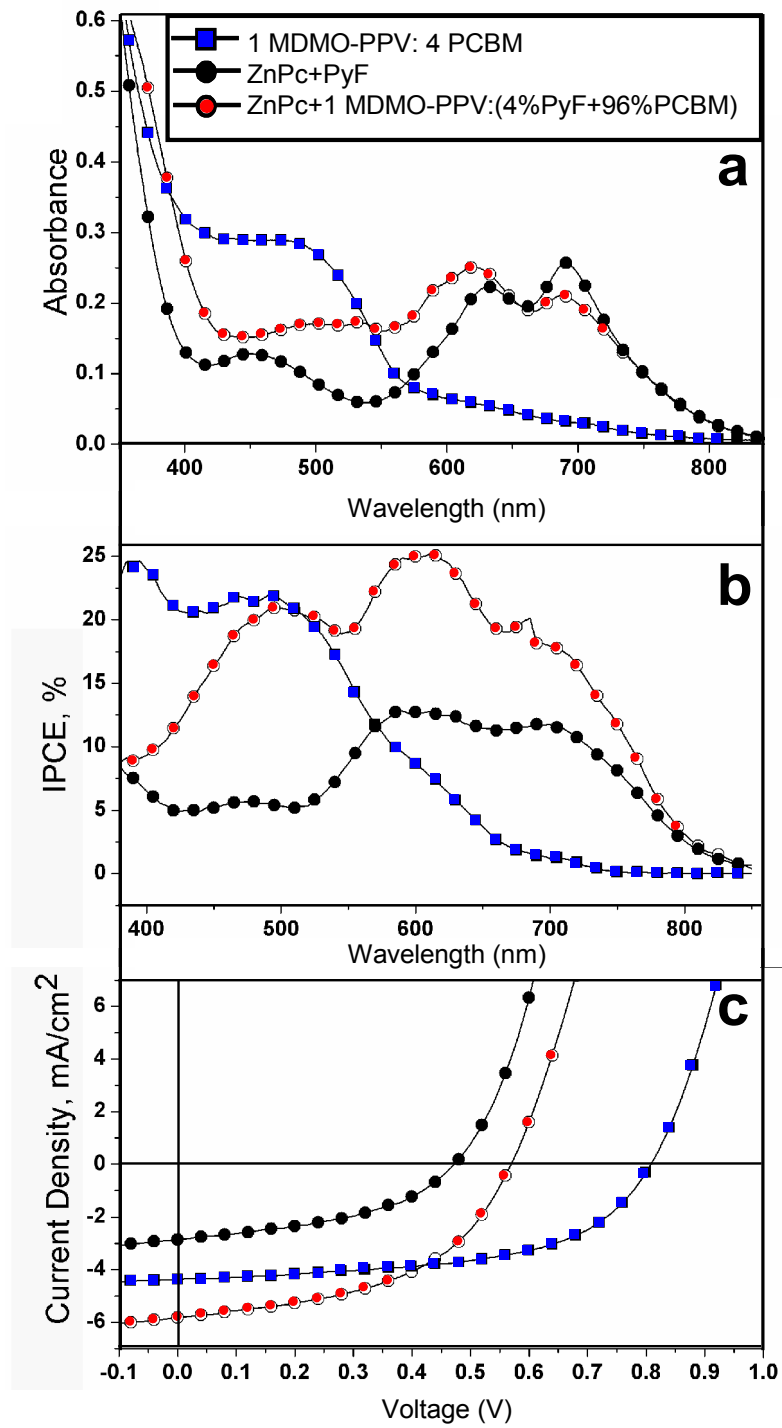
**IV.2** Comparison of Polymer:Fullerene, ZnPc:Fullerene and multicomponent solar cells

**a** absorbance spectra of the active layers

**b** Incident Photon to Collected Electron efficiency (IPCE)

**c** I-V characteristics under 100mW/cm² simulated AM1.5 solar illumination

The proposed working mechanism of the multicomponent cells is absorption of light mainly in the phthalocyanine and polymer phases of the solar cell with subsequent dissociation of the excitation at the nearest interface to a fullerene. The electrons are transported to the aluminum back electrode via the fullerene phase while the holes generated in the polymer can move through the ZnPc layer to the ITO/PEDOT (indium tin oxide/poly(3,4-ethylenedioxy)thiophene) electrode. The rather good fill factor of the best devices (>50%) shows that the transport over the ZnPc layer is not severely limiting the performance of the multicomponent solar cells.

The higher lying hole transport level of the ZnPc results in a significantly lower $V_{oc}$ than in MDMO-PPV:PCBM solar cells [24] which is the biggest drawback of this concept. A better suited material combination with better suited energy levels might reduce this loss. Especially the low ionization potential of the ZnPc limits the achievable $V_{oc}$ considerably.

The active layer absorption covers the whole visible region (350-800 nm) (Fig. IV.2a) and in optimized devices, the full absorption generates photocurrent. This can be concluded from the IPCE spectra of the devices (Fig. IV.2b). The best multicomponent solar cells produce photocurrent densities of up to 6.0 mA/cm²; this is significantly higher than the $I_{sc}$ of either MDMO-PPV:PCBM or ZnPc/PyF solar cells (Fig. IV.2c). Still, the high quantum efficiencies and therefore high photocurrents achieved in the ZnPc:$C_{60}$ evaporated bulk heterojunction solar cells are not yet reached with this concept.

The open circuit voltage and fill factor values are somewhat lower (570 mV and 50%, respectively) than for MDMO-PPV:PCBM bulk heterojunction solar cells; therefore, the best multicomponent cells investigated in this work yield solar power conversion efficiencies of 1.6-1.7%, similar to the performance of solar cells built with low energy gap polymers that collect the sunlight in the same region [17, 29]. Further optimization of the material composition and device fabrication conditions might lead to higher performances.

If fullerene compounds based on $C_{70}$ are used, higher current densities of more than 7mA/cm² and therefore efficiencies of over 2% can be reached. This indicates that the quantum efficiency of the multicomponent devices is limited by the low thickness and therefore also low absorption of the active layer which is increased by the larger absorption coefficient of the higher fullerenes.

The optimal thickness of the ZnPc bottom layer is about 45 nm for solar cells investigated in this work, while devices with 30 and 60 nm films of ZnPc give a worse performance (Table 1). Several different solvents were tested for deposition of the fullerene/polymer blends on the

ZnPc layer; the efficiency of the resulting solar cells decreases in the order chlorobenzene >> chloroform $\cong$ dichloromethane. A similar solvent effect was observed for the conventional bulk heterojunction MDMO-PPV/PCBM solar cells [24]. A number of previous studies showed that the choice of solvent strongly affects the active layer morphology and the use of chlorobenzene as a solvent gives the best results [25]. In the case of the multicomponent cells, the atomic force microscopy (AFM) images show that the nanomorphology of the top fullerene (mix of 4% PyF and 96% PCBM)-polymer blend layer is comparable to the morphology of the PCBM/MDMO-PPV films with good solar cell performances (Fig. IV.3) [30]. Thus, the bottom ZnPc layer seems to have no strong influence on the degree of the phase separation occurring in the fullerene/polymer layer deposited on the top.

An important factor that strongly influences the solar cell performance is the loading of the acceptor phase with PyF; the composition of the acceptor phase is expressed by the weight percent ratios between PCBM and PyF. For instance, the solar cells fabricated on ZnPc using just pure PCBM as acceptor material show relatively low performance (Table IV.1). However, the introduction of even very small amounts of PyF into the PCBM/MDMO-PPV blend (2% of PyF with respect to 98% of PCBM) already significantly improves the power conversion efficiency.
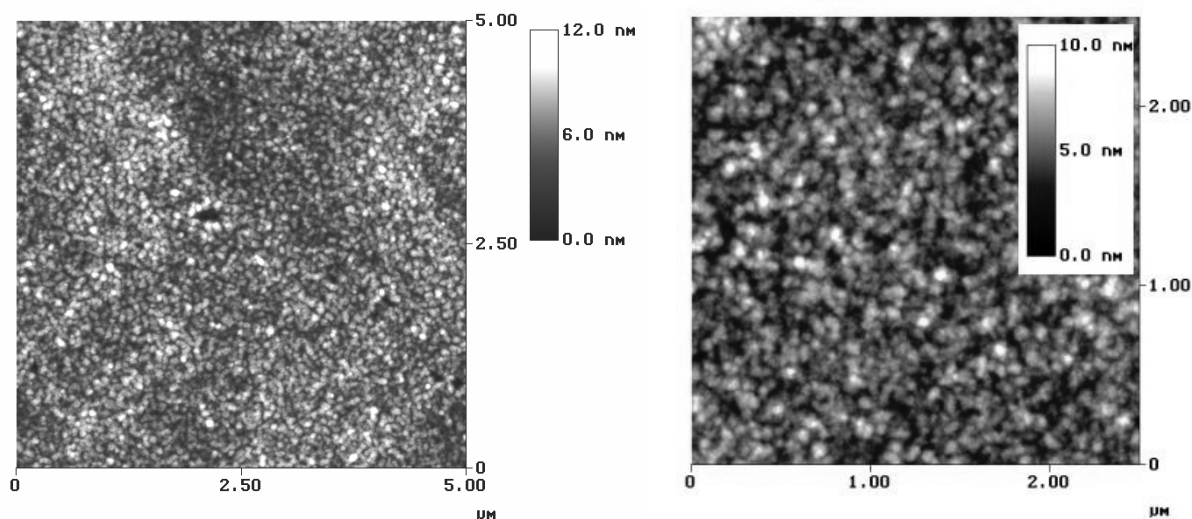


**IV.3** AFM image of the surface of the active layer of a multicomponent solar cell (left) showing a nanoscale morphology comparable to that of a morphology optimized MDMO-PPV:PCBM solar cell (right)
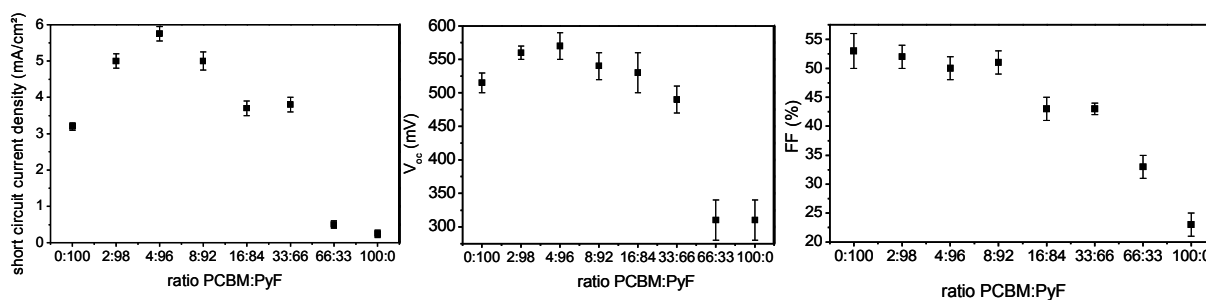
**IV.4 S**olar cell parameters in dependence on the ratio between the fullerenes in the multicomponent solar cell blend

The overall dependence of the solar cell parameters on the PyF-PCBM ratio is illustrated on the diagrams in Fig. IV.4. An acceptor material comprising 4% of PyF with 96% of PCBM gives the best solar cell parameters. Following the increase in the content of PyF and decrease in the content of PCBM in the blend leads again to lower solar cell efficiencies. It is notable that both $V_{oc}$ and $I_{sc}$ are similarly affected by the pyrrolidinofullerene content, while the fill factor is less sensitive but still obeys the same trend.

This drastic change of the solar cell performance upon introduction of a small amount of PyF is most probably connected to the supramolecular interaction between ZnPc and PyF in the multicomponent systems as described in III.1.1. To verify this, the change of the active layer absorption and the IPCE spectra of photovoltaic devices is monitored under different PyF loading.

The active layer absorption spectra (Fig. IV.5a) shows that the addition of PyF leads to a shifting and narrowing of the Q-band double-peak spectrum which intensifies with the amount of PyF added to the solution spin-cast on top of the ZnPc layer. This indicates that the complexation is also occurring in these devices. As described in III.1.1 the complexation separates ZnPc molecules from the π-stacked configuration and therefore, the single sharp Q-band absorption at 675nm starts to appear in the film spectra.

The photocurrent action spectra (IPCE) of the multicomponent solar cells also exhibit a very strong dependence on the ratio between PyF and PCBM used as acceptor materials (Fig. IV.5b). Thus, solar cells made using just PCBM without addition of PyF produce photocurrent mainly in the 350-580 nm spectral region (like conventional PCBM/MDMO-PPV bulk heterojunction devices), whereas the contribution from the ZnPc absorption (580- 800 nm region) is very weak. The addition of small amounts of PyF (2% of PyF with respect to 98% of PCBM) changes the situation remarkably: the intensity of the 580-800 nm features

increases by a factor of 2.5 up to the same intensity as the 350-580 nm part of the IPCE spectrum. At the same time, the addition of 2% of PyF nearly doubles the solar cell power conversion efficiency as seen from the I-V measurements (Table IV.1). The complexation activates the ZnPc contribution to the photocurrent response, as it provides a specific interaction of the ZnPc and the fullerene phase in the blend solution.
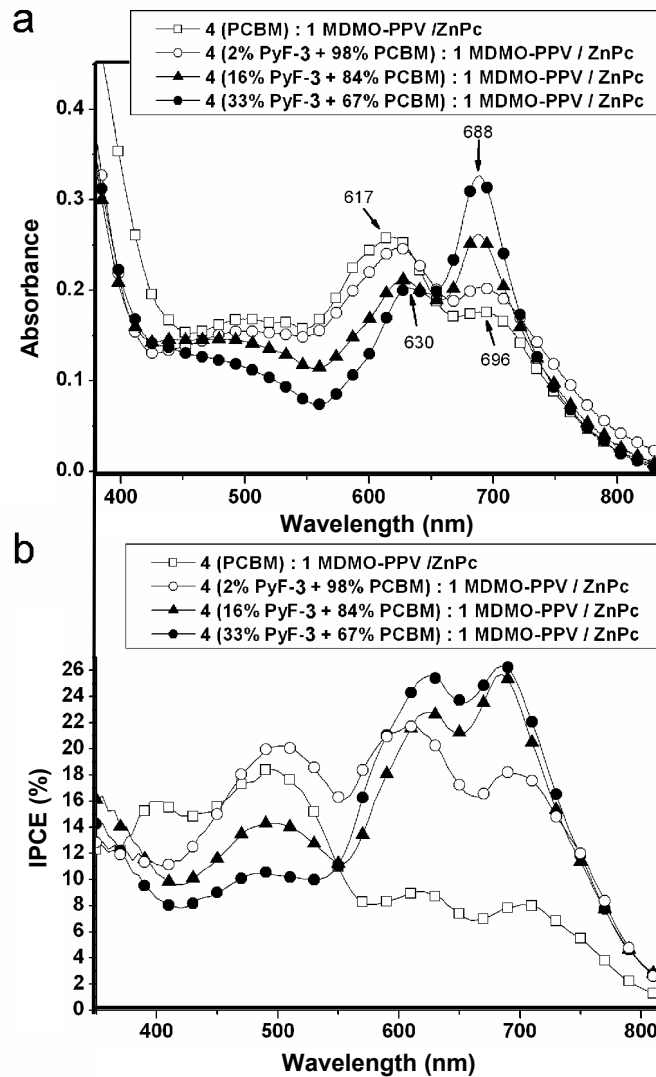


**IV.5** Influence of the PyF:PCBM ratio on **a** the active layer absorbance and **b** the IPCE spectra of multicomponent solar cells

The positive influence of PyF on the efficiency of solar cells stops at the component ratio 8% of PyF to 92% of PCBM; above that the 350-550nm part of IPCE spectrum becomes much weaker, indicating a lower contribution from MDMO-PPV and PCBM to the current generation. This effect becomes even more pronounced when the content of PyF reaches 16%

and 33% (with respect to 84% and 67% of PCBM). The IPCE spectrum of the devices made using a combination of 33% of PyF with 67% of PCBM looks like the typical spectrum of bilayer PyF/ZnPc solar cells (Fig. IV.2b); this means that MDMO-PPV does not contribute significantly to the photocurrent in this case.

Presumably, 33% of PyF is enough to block the ZnPc surface entirely via the complex formation. In this case, the layer of the ZnPc:PyF complexes separates the ZnPc and MDMO-PPV phases blocking the hole transport from the polymer to the ITO electrode. On the other hand, electron transport is not seriously affected: the PyF complexed with ZnPc still communicates with the fullerene-rich phase in the fullerene/polymer blend.

In summary, multicomponent organic solar cells made from MDMO-PPV, ZnPc, PCBM, and PyF exhibit good performance and efficient photocurrent generation in a wide spectral region. The performance of solar cells with pure PCBM as the fullerene phase in the bulk heterojunction is quite low (<1%); however, the addition of small amounts of PyF to the PCBM (ratio 2%/98%, respectively) doubles the power conversion efficiency.

The introduction of PyF into the fullerene phase strongly increases the photocurrent generation in the 600-800 nm spectral region (corresponding to the ZnPc Q-band absorption) due to the complex formation between PyF and ZnPc. The content of PyF in the active layer of the solar cell is a crucial factor that strongly influences the device performance; an optimal PCBM/PyF ratio has to be found to achieve the maximum photocurrent generation from both blue- and red-absorbing materials.

It seems that the combination of bilayer fullerene/ZnPc and bulk heterojunction fullerene/polymer photovoltaic devices can be considered a promising approach to achieve a wide spectral response in organic solar cells while retaining the good charge-transfer and transport properties of established materials. The already achieved PCE are on a similar level as the best low band gap polymer systems reported up to date. Additionally, the rather even photocurrent response of the devices over the whole visible spectrum makes them interesting for photodetector applications.

## VI.2. Organic Tandem Solar Cells

As described in I, organic semiconductors show limited photovoltaic properties because of their spectrally limited optical absorption. Therefore, a further improvement can be envisaged by realizing organic tandem solar cells, based on the superposition of active materials having complementary absorption profiles. The connection between the materials is not done by mixing them in a multicomponent solar cell as described in IV.1, but by connecting separate solar cells in series by a common recombination contact.

This concept is already employed to achieve high efficiency inorganic solar cells by reducing the energetic losses caused by the thermalization of charge carriers [31, 32]. Two or more solar cells with different bandgaps are stacked onto each other with a recombination contact in between. This leads to an adding of the photovoltages. The maximum current that can be extracted from the tandem device equals the lowest current generated in each subcell. This makes the optical engineering of the layer structure extremely important.

In the case of organic materials, the tandem concept can be applied not only to decrease the thermalization losses, but also to increase the photon harvesting by combining semiconductors having complementary absorption spectra. Thus, a low energy gap organic solar cell having a low conversion efficiency in the blue and green can be coupled with an organic solar cell with a high conversion efficiency in this region. Organic tandem solar cells employing this concept to efficiently convert white light in the spectral range from 400 to 800nm will be presented in the following.

A large part of the experiments presented here was performed by DI Hans-Jürgen Prall and Dr. Gilles Dennler. More details on the fabrication of organic tandem solar cells can be found in the Diploma thesis of DI Prall.
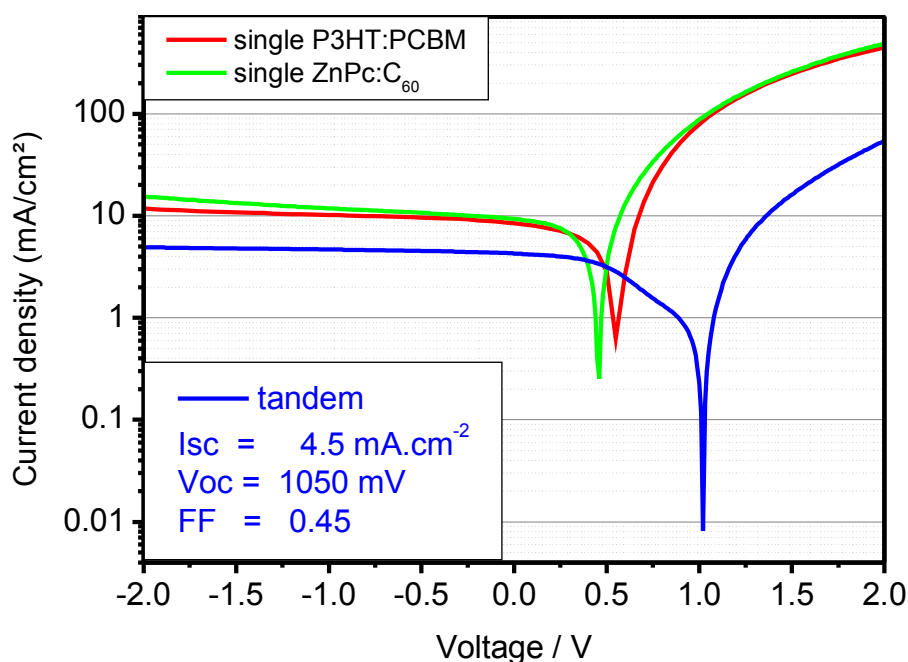
**IV.6** I-V characteristics of solar cells based on a diffuse bilayer of P3HT and PCBM (red), ZnPc and $C_{60}$ (green) as well as a tandem solar cell (blue)

Fig. IV.6 shows the I-V curves of the single P3HT:PCBM cell, the single ZnPc/ZnPc:$C_{60}$/$C_{60}$ cell as well as the tandem cell under 100mW/cm² simulated AM1.5 illumination. It can be observed that the P3HT:PCBM diffuse bilayer approach results in cells exhibiting good performance despite the fact that no post-treatment is used. For this device a $J_{sc}$ of 8.5mA/cm$^2$, a $V_{oc}$ of 550mV and a fill factor (FF) of 0.55 can be measured, yielding a power conversion efficiency of 2.6%. In the case of the single small molecule based cell, a $J_{sc}$ of 9.3mA/cm$^2$, a $V_{oc}$ of 470mV and a fill factor of 0.50 is recorded, leading to an efficiency of about 2.2%. Thus, the fact that the tandem cell shows a $V_{oc}$ of 1050mV, approximately the sum of the individual $V_{oc}$ of the sub-cells suggests that an efficient series connection between the cells is established. Moreover, the FF of the tandem cell is found to be about 0.45, only a bit lower than those of the sub-cells. This observation means that the transport is not strongly limiting the performance of the tandem device. However, the organic tandem solar cell shows a quite reduced $J_{sc}$ equal to 4.8mA/cm$^2$, which corresponds to a solar power conversion efficiency of 2.4%. The limitation of the tandem performance is most likely due to a nonideal balancing of the respective thicknesses of the sub-cells, leading to a bad current matching.
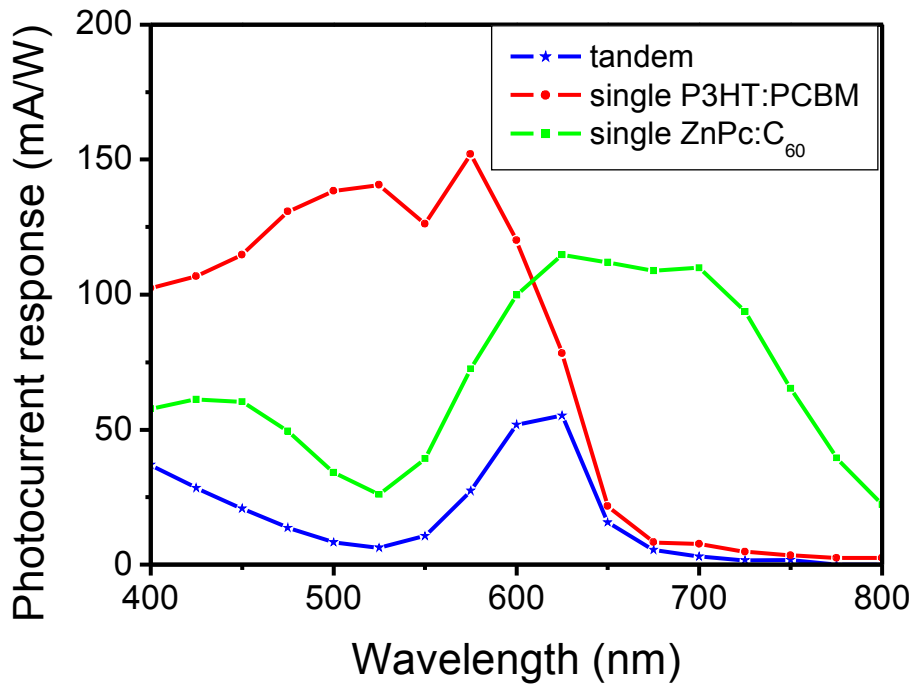
**IV.7** Spectral behaviour of the photocurrent response of solar cells based on a diffuse bilayer of P3HT and PCBM (red), ZnPc and $C_{60}$ (green) as well as a tandem solar cell (blue)

In order to confirm the series connection of the sub-cells and the extension of the photon harvesting in the tandem device, wavelength dependent photocurrent response measurements have been performed. Fig. IV.7 exhibits the results obtained for the single P3HT:PCBM and ZnPc/ZnPc:$C_{60}$/$C_{60}$ sub-cells as well as for the tandem cell. The curve related to the tandem device is always lower than the lowest current given by one of the sub-cells. This perfectly agrees with the expectations arising from the series connection. Moreover, it is visible that the current in the tandem device is equal to the current in the P3HT:PCBM device when this cell is the limiting one. However, in the region 375-630nm where the ZnPc/ZnPc:$C_{60}$/$C_{60}$ cell shows the smaller current, the tandem device shows a current which is consequently smaller.

This observation can be explained by the structure of the tandem device: The incident light crosses first the P3HT:PCBM cell, and then the ZnPc/ZnPc:$C_{60}$/$C_{60}$ one. Therefore, for 375-630nm, a large part of the photons is absorbed in the P3HT:PCBM cell, further reducing the already limiting current delivered by the ZnPc/ZnPc:$C_{60}$/$C_{60}$ cell in this spectral region.

The photon harvesting enhancement being not clearly demonstrated by the direct measurement of the photocurrent response, a further experiment using two illumination

sources has been performed. One source provides a continous illumination at a certain wavelength, while the second is scanned through the entire spectrum. Only the photocurrent generated by the light from the second source is recorded. The results are plotted in Fig. IV. 8a-d.

In the case of Fig. IV.8a, for example, a background light fixed at 500nm is used, hence exciting mostly the P3HT:PCBM sub-cell. The modulated light generates a low current in the region below 550nm, since only the P3HT:PCBM sub-cell is active. However, above 550nm, the charge carriers produced in the $ZnPc/ZnPc:C_{60}/C_{60}$ cell can be extracted since the P3HT:PCBM cell is active. An overall maximum is observed at the overlap of the absorption spectra of the sub-cells. In Fig. IV.8b, the background light has been red shifted (560nm). The current delivered by the P3HT:PCBM cell at this wavelength is slightly reduced compared to the one collected at 500nm. Therefore, the current recorded above 550nm is smaller than in the previous case. In Figure IV.8c, the background light wavelength is located at the overlap of the absorption spectra (620nm): Therefore, both sub-cells are activated, and the current from their respective complementary cells can be recorded. Finally, in Fig. IV.8d, the situation is exactly opposite to the one of Fig. IV.8a. The background light (700nm) activates only the $ZnPc/ZnPc:C_{60}/C_{60}$ sub-cell, hence the photocurrent response of the P3HT:PCBM cell can be recorded. As in all cases, a maximum is observed at the overlap of the absorption spectra of the active materials.

Thus, Fig. IV.8a-d confirms that the current delivered by the tandem device is based on the extraction of charge carriers induced by the absorption of photons with a wavelength from 400nm to more than 800nm when the device is illuminated with broadband white light. Moreover, they show that such a tandem device based on active materials having complementary absorption spectra can be operated as two color detector according to the Boolean action AND.

In summary, the tandem connection of two organic solar cells of complementary absorption spectra is a very elegant way of increasing the spectral range of photon harvesting. A strict prerequisite of this concept is a careful balancing of the thicknesses of the subcells according to the incident light spectrum. This is also the most severe limitation of this device concept: the efficiency of tandem solar cells is rapidly dropping when the illumination conditions differ from the adjusted optimum, making them hard to use in mobile installations, which are probably the first applications for organic solar cells.
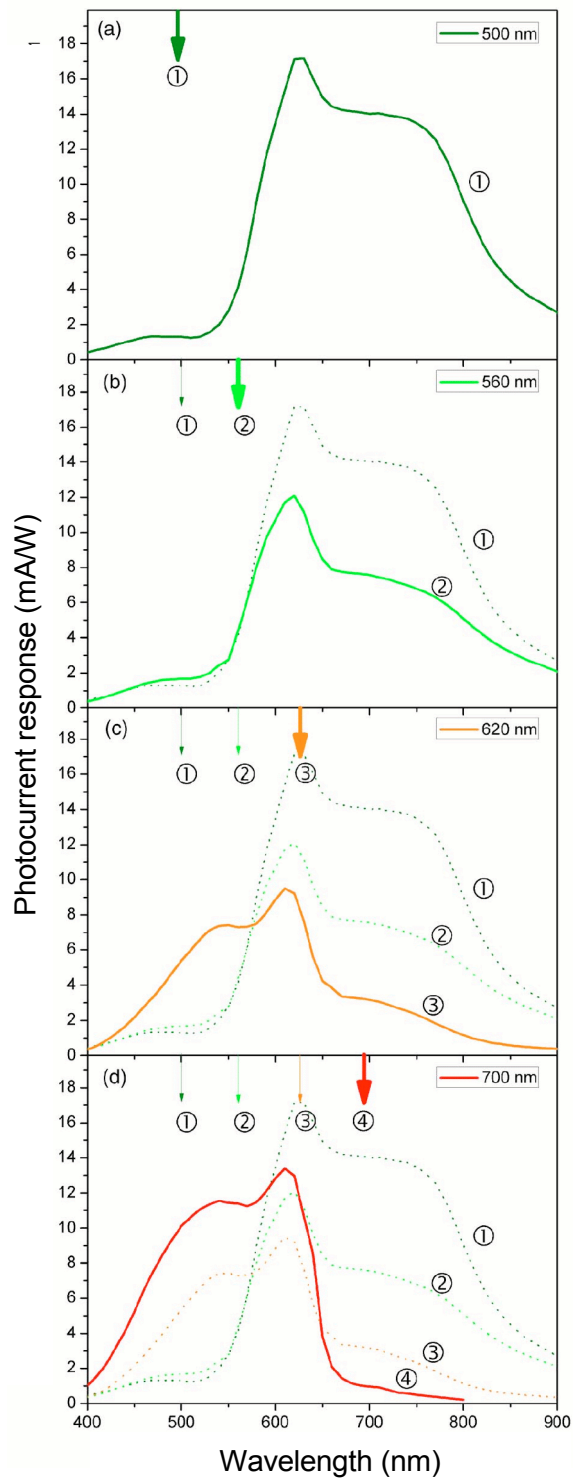
**IV.8** Photocurrent response of the organic tandem solar cell vs. the wavelength of the incident monochromatic light. In this experiment, a second monochromatic nonchopped light source is used, the wavelength of which is indicated by the arrow: **a** 500 nm, **b** 560 nm, **c** 620 nm, and **d** 700 nm. A schematic of the setup is shown on the left.

## IV.3. Organic Solar Cells with external absorbers

One of the major obstacles towards high efficiency organic solar cells is the limited charge carrier transport properties of the organic semiconductors. In most organic solar cells, the optimal thickness of the semiconductor layer does not yet provide enough absorption to ensure the maximum photon harvesting over the full absorption range of the materials. Thus it appears appealing to externalise the optical absorption with subsequent donation of the excitation energy to the solar cell in a spectral range that allows best energy conversion even with a rather thin active layer. Two basic concepts that might lead to this effect will be presented in the following.

### IV.3.1. Coupling external absorbers by luminescence

Photoluminescence is used for shaping the spectrum of light sources regularly in many applications. Most notably is the huge market of artificial lighting, where the radiation of electrically excited gas molecules in a sealed glass tube is one of the most efficient sources of generating illumination. The gas discharge has a rather limited spectrum of clearly distant sharp lines, not useful for white lighting applications. Here, inorganic phosphors applied to the inside of the tube are used to convert the spectrum of the gas discharge into white light via photoluminescence.

Luminescent concentrators [33, 34] work exactly the other way round. The broad spectrum of the sunlight is taken up by a material absorbing in a wide spectral range and reemitted as spectrally narrow luminescence. This luminescence should coincide with the best spectral response of a solar cell attached to the concentrator. As due to the Stokes-shift, the luminescence occurs always shifted to higher wavelengths compared to the absorption, the light can be only redshifted.

This process is accompanied by a loss in the photon energy, which is thermalised in the luminescent species and not usable for energy conversion. Other approaches of down- and upconversion without energetic losses (photon splitting and two-photon processes) require nonlinear material properties that usually are of low efficiency [35]. In luminescent concentrator applications, a beneficial effect can only be expected if the photocurrent generation in the applied solar cell is more efficient towards lower photon energies. As described in I., exactly this is the case in low energy gap organic solar cells.

The coupling of the solar cell to the luminescent concentrator is performed via photon emission by the luminescent species and absorption inside the solar cell. As photoluminescence is usually an isotropic process, an efficient guiding of the emitted light towards the solar cell is eminent. The currently most promising concept of integration is to attach an appropriate solar cell to the sides of a luminescent waveguide structure, as sketched in Fig. III.13a. In the following, the use of a luminescent concentrator together with low energy gap organic solar cells is studied.
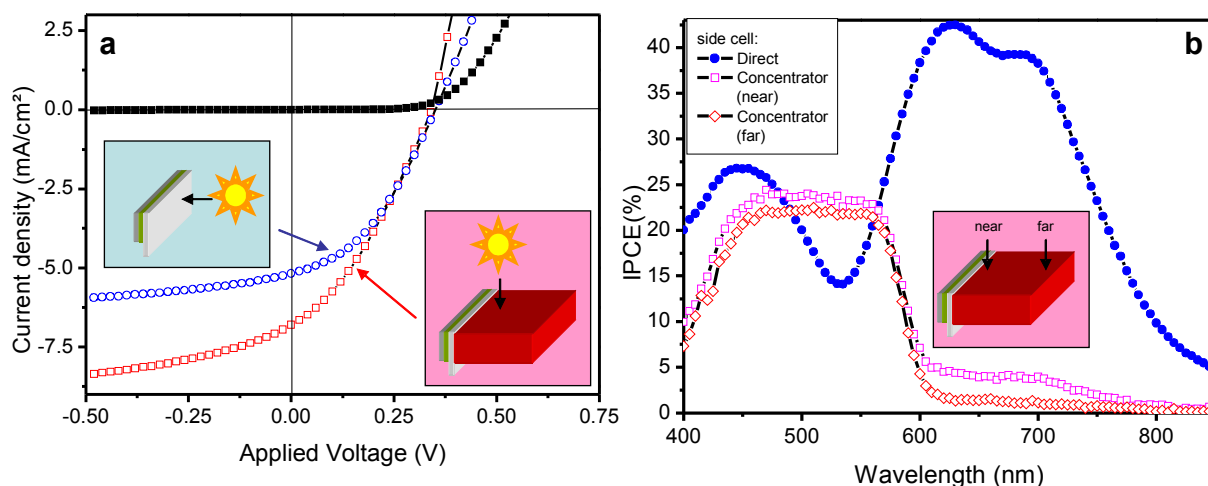
**IV.9 a** I-V characteristics of the "side cell" in the dark (black), under direct illumination (blue) and attached to the illuminated concentrator plate (red). **b** IPCE spectra of the side cell under direct illumination (blue) and attached to the concentrator plate illuminated near (pink) and far (red) from the side cell.

Both side and bottom cell are measured before and after assembling the luminescent concentrator structure as shown in Fig. II.13a. Under direct illumination, the side cell device shows the typical behaviour of an organic solar cell produced from ZnPc and $C_{60}$ (Fig. IV.9, blue spectra). A short circuit current density ($J_{sc}$) of around 10.5mA/cm² is accompanied by an open circuit voltage ($V_{oc}$) of around 360mV and a fill factor of 0.39. The IPCE spectrum corresponds roughly to the sum of the absorption spectra of the used materials and shows significant photon-to-electron conversion efficiencies in the range between 600 and 750nm while below 580nm the low absorption limits the IPCE.

After the solar cell is attached to the luminescent concentrator, it stands perpendicular to the incoming light and receives only light that is coupled into the waveguide by the luminescent dye. The $J_{sc}$ measured now relative to the full area of the concentrator plate amounts to 2.8mA/cm². As the active area of the concentrator plate is five times bigger than the side cell active area, the absolute photocurrent of the side cell increases by a factor of 1.3 with the concentrator in comparison with the cell under direct illumination.

The waveguiding mechanism is visible in IPCE spectra of the side cell attached to the concentrator (Fig. IV.9b). A clear correlation between the absorption spectrum of the dye inside the concentrator plate and the IPCE spectrum can be discerned. This is due to the fact that only light which is absorbed and reemitted by the dye can be efficiently waveguided to

the solar cell.

The luminescence spectrum of the dye is overlapping with the maximum in the conversion efficiency of the solar cell. Thus, the light absorbed by the dye in the concentrator can be converted more efficiently in the solar cell attached to the concentrator than under direct illumination. This can be seen by the absolute increase in conversion efficiency around 500nm and illustrates the high efficiency of the waveguiding structure.
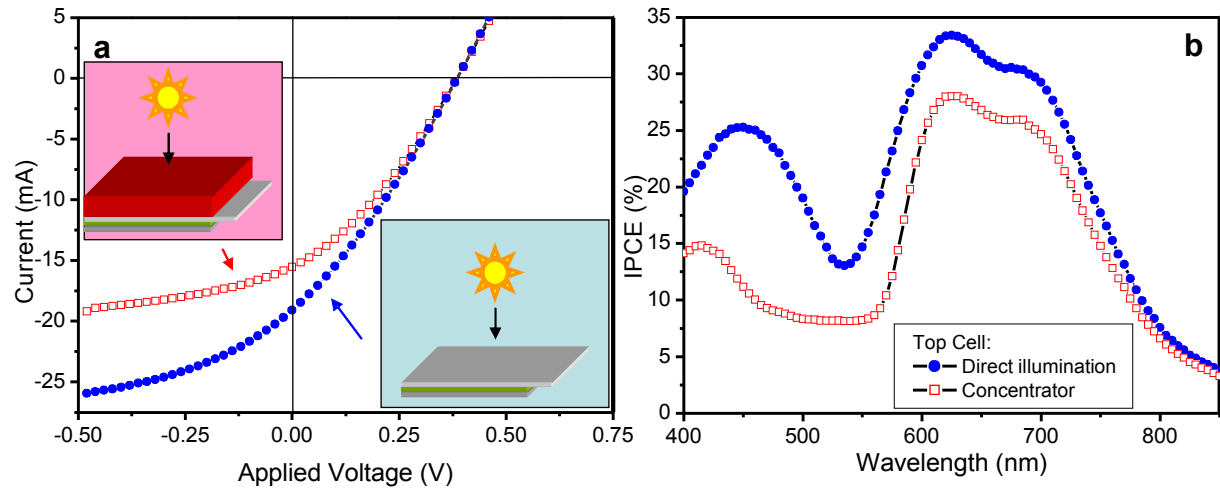


**IV.10 a** I-V characteristics of the bottom cell under direct illumination (blue) and illumination through the concentrator plate (red). **b** IPCE spectra of the bottom cell under direct illumination (blue) and illumination through the concentrator plate (red).

To estimate the effect due to the extended area of the concentrator plate, the IPCE spectrum is measured under illumination at different spots on the concentrator plate. The IPCE spectrum measured near the side cell shows only slightly higher conversion efficiencies of the waveguided light than the spectrum measured at the far end of the concentrator area. This indicates that a larger concentrator area could be used to harvest energy with a side cell. In applications for silicon solar cells, usually concentrator sizes of 50x50x3mm³ or even 100x100x3mm³ are used with high efficiencies [36].

Due to its larger size (2.25cm²), the bottom cell performance is limited by the high series resistance of the ITO electrode and shows a fill factor of around 0.3 as well as a $J_{sc}$ around 8.5mA/cm² (Fig. III.13a) under direct illumination. The IPCE spectrum under direct illumination is similar to that of the side cell with lower values corresponding to the lower $J_{sc}$.

Together with the concentrator, the $J_{sc}$ of the bottom cell decreases to about 7mA/cm². The IPCE spectrum of the bottom cell in the concentrator device (Fig. IV.10b) reveals that the loss

in conversion efficiency occurs mainly in the blue and green spectral region. Incoming light between 440 and 560nm is absorbed by the dye and reemitted in random directions. Most of the emission is coupled into the waveguide and harvested by the side cell. This light is not generating current in the bottom cell, therefore the efficiency in the range of absorption of the dye inside the concentrator is decreased.

Only some of the light is emitted inside the escape cone and leaves the concentrator towards the bottom cell, where it is converted with an efficiency of above 30%. This yields an effective quantum efficiency of around 8% between 440nm and 560nm, even though the concentrator plate is completely absorbing the incoming light. Red light is passing through the concentrator plate with slight reflection losses and can be directly converted by the bottom cell.
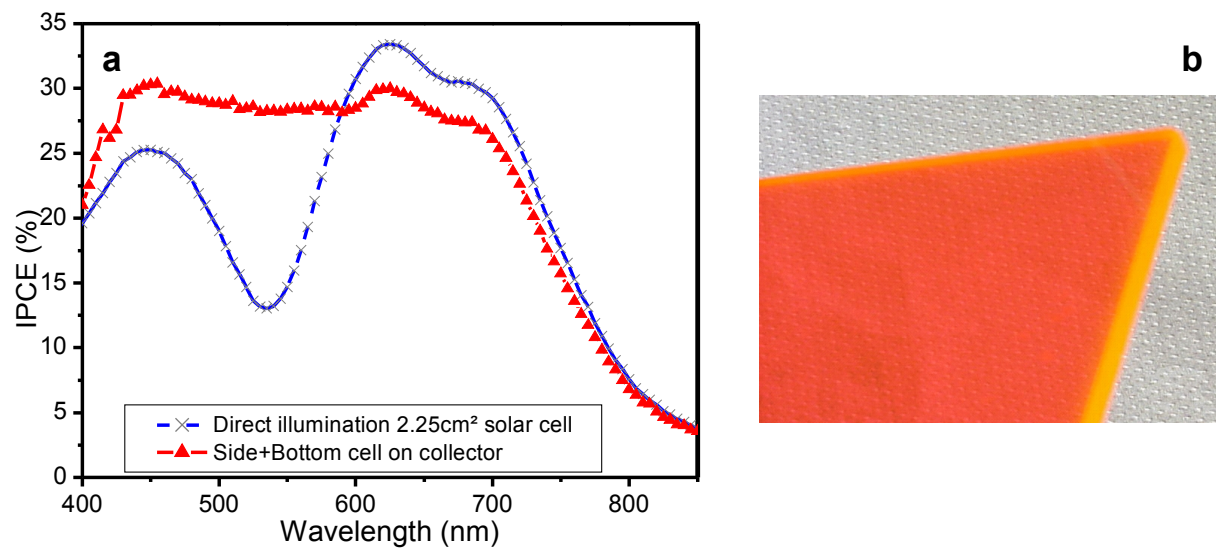


**IV.11 a** IPCE spectra of the bottom cell under direct illumination (blue) and the IPCE spectra of side and bottom cell attched to the concentrator added together (red). **b** a photograph of the concentrator plate.

If the reponse of the bottom and side cell in the concentrator device is added together (Fig. IV.11a, red), a strong increase in the conversion efficiency of blue and green light is apparent. This enhancement overcomes the reflection losses for red light in the concentrator and leads to an increase of the $J_{sc}$ from 8.5mA/cm² to around 10mA/cm². The power conversion efficiency of the integrated concentrator device is around 1.25%, while a single solar cell with the same surface area yields only about 1% under direct illumination. This efficiencies are reduced by the comparably large active area of the devices used, where the series resistance of the ITO-glass severely limits the fill factor. But generally, all solar cells with a significantly

lower external quantum efficiency in the blue and green spectral region will benefit from this arrangement, always adding to the efficiency of the single device.

In conclusion, this concept of combining organic solar cells and luminescent concentrator plates (a photograph of the plate used can be seen in Fig. IV.11b) enhances the performance of organic solar cells with limited quantum efficiencies in the blue and green spectral range. As organic solar cells can be fabricated without substrate heating, the concentrator itself can be used as a support, leading to a better coupling of the side cell to the waveguide. An additional benefit of this arrangement is an inherent UV protection of the solar cells potentially reducing the degradation of the active materials. The perhaps biggest drawback is the issue of luminescent dye stability, as the concentrator plate will lose efficiency under long-time full solar irradiation due to photobleaching of the dye.

### IV.3.2. Coupling external absorbers by resonant energy transfer

The concentration of photon energies by photoluminescence as discussed in IV.3.1 has several major disadvantages in the context of photon harvesting for photovoltaics. The emission is isotropic, always leading to a certain part of the converted light being emitted back towards the source and lost to the solar cell. Also, the process is always limited by the quantum efficiency of the luminescent species to significantly below 100%.

Both these disadvantages can be avoided in a well tuned resonant energy transfer system, where a direct coupling between the transition dipoles of two photoactive species leads to a transfer of the excitation from donor to acceptor chromophore. According to the theory of Theodor Förster [37, 38] as described in II.2., resonant energy transfer is directed and can reach transfer probabilities very close to unity.

If the acceptor species in the energy transfer is a low energy gap organic solar cell material such as ZnPc, a chromophore absorbing around 500nm and emitting above 600nm could donate the absorbed energy via energy transfer, leading to an enhanced photon harvesting in the solar cell. This process would be directed and can have a very high efficiency, provided that the distance between donor and acceptor is in the range of a few nanometers. The sensitization of semiconductor materials by energy transfer from luminescent species has been envisioned already in several different material systems [39, 40, 41, 42, 43]. If the process is cascaded over several steps with the final transfer funneling the energy onto the solar cell material, a large excitation density can be achieved on a thin layer of active material.

This concept is also applied in natural photosynthesis, where a multistep energy transfer funnels excitations towards the photosynthetic reaction center, thus enhancing the harvesting of solar radiation [44]. Nature uses extremely complex structures incorporating dozens of carotenoid and chlorophyll molecules with energy levels that are precisely adjusted by deformation in the surrounding protein matrix. These structures can funnel energy over dozens of nanometer distances and tens of single transfer steps to the reaction center, where the high concentration of light energy is needed to drive the chemical reaction of hydrocarbon formation from oxygen, water and carbon dioxide. The reaction center alone would have a too low absorption cross section to harvest enough sunlight to power these chemical reactions. Higher lifeforms could not exist without this mechanism. A scheme of such photosynthetic light harvesting complexes of purple bacteria is shown in Fig. IV. 12.
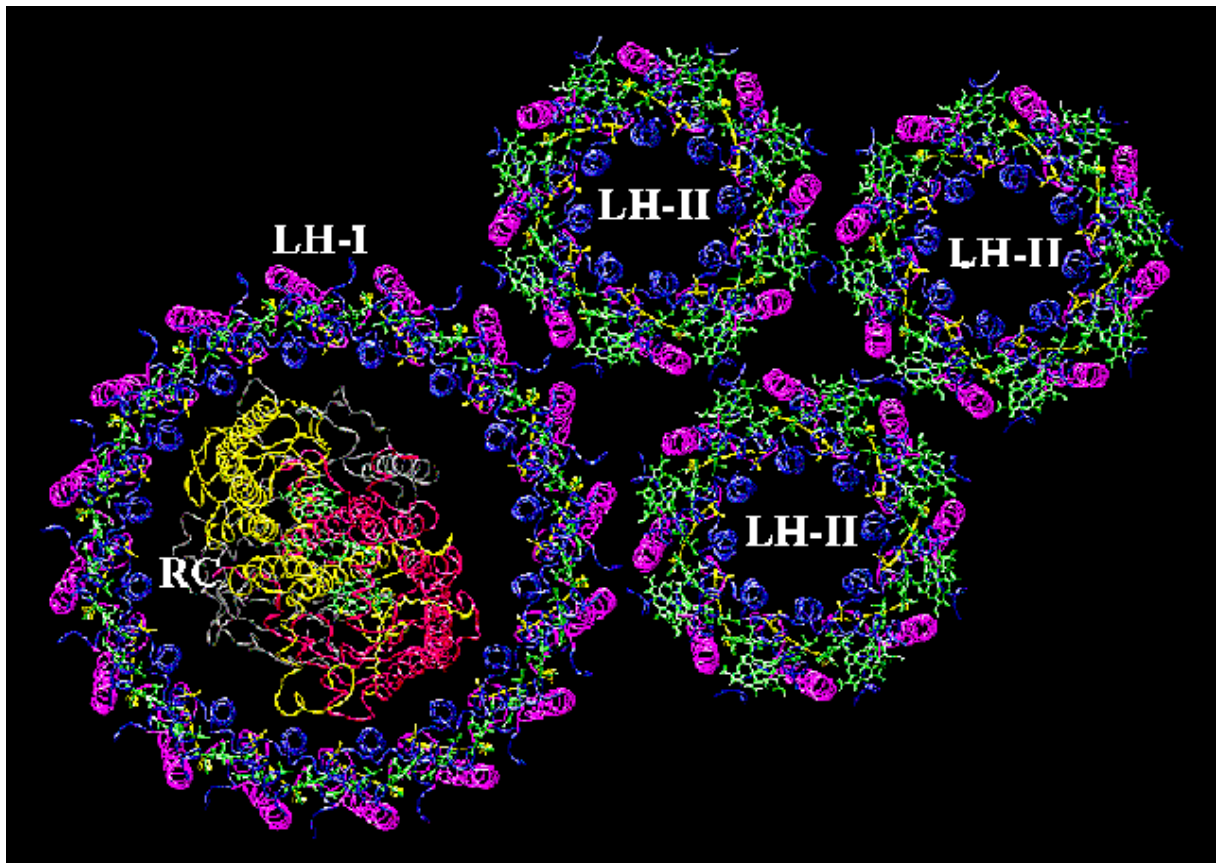
**IV.12** The setup of light-harvesting complexes in the photosynthesis system of purple bacteria. LH I and LH II are the light harvesting complexes I and II with protein backbones marked in purple and blue. The green and yellow molecules in LH I and LH II are chlorophylls and carotenoids, respectively. RC denotes the photosynthetic reaction center, a large protein complex, in and around which the chemical reactions take place.

Picture courtesy of Theoretical Biology Group - University of Illinois at Urbana-Champaign

The spectral as well as spatial concentration of the illumination might as well be beneficial for organic solar cells. The strong distance dependence of the resonant energy transfer brings the necessity for a nanoscale engineering of the energy transfer cascade organic solar cell system, though. Two concepts of energy transfer cascade systems and first approaches towards the integration in low energy gap organic solar cells will be presented in the following.

### IV.3.2.1. Energy transfer between semiconductor nanocrystals and zinc-phthalocyanine

A material class that fits well into the scheme of organic semiconductors for electronic applications [4, 45] are colloidal semiconductor nanomaterials. They exhibit very interesting optical properties such as strong absorption and high photoluminescence yield as well as solution processability. These properties can be tuned by changing the material, the size and the shape of the nanocrystals [46, 47]. The chemical properties of these nanoparticles are mostly determined by a shell of organic ligands that provide good compatibility with organic semiconducting materials.

Advanced photon harvesting systems, in which light absorption is occuring in photosystems separated from the materials providing charge generation and transport might be a way to expand the possibilities of common organic solar cell donor-acceptor material combinations. Resonant energy transfer is predestined to play a major role in all concepts of advanced photon harvesting. Especially the long range energy transfer mechanism as described by the Förster theory described in II.2 [37, 38] is applicable to funnel photon energy from electrically inactive but absorbing materials to the electrically active species with a lower overall absorption. This allows for very thin active layers, possibly improving the electrical characteristics of the organic solar cells limited by the low conductivities of the materials used.

As a photon harvesting system, colloidal CdSe/ZnS core-shell nanocrystals [48] are used. They show a high absorption cross section in the desired wavelength range as well as a strong luminescence above 600nm, required for the energy transfer to the ZnPc. A second advantage is the organic ligand shell around the nanocrystals, electrically insulating them from the surrounding matrix. This ensures that the long range energy transfer will be the leading mechanism and not the charge transfer requiring an overlap of donor and acceptor wavefunctions [49]. Charge transfer is not desirable in this case, as the transport of the charges remaining on the nanocrystals is usually unfavourable.

Steady state absorption and fluorescence spectroscopy is used to study the interaction between the two species. The nanoparticle ligands are altered to probe the dependence of the transfer efficiency on the distance between donor particle and acceptor matrix. Photodiodes with and without an intermediate nanoparticle layer are compared and a significant change in the external quantum yield spectrum is observed.
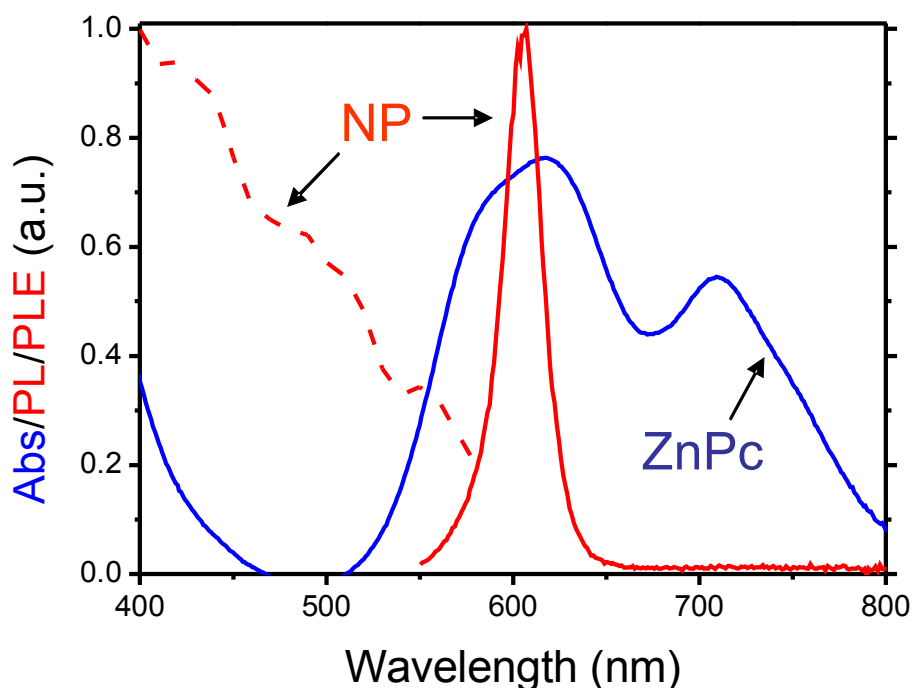
**IV.13** Absorbance spectrum of ZnPc together with the photoluminescence excitation and photoluminescence spectra of the CdSe/ZnS semiconductor nanoparticles used

In Fig. IV.13, the absorption spectra of thin films of ZnPc on glass can be seen as well as the photoluminescence and photoluminescence excitation spectra of thin nanoparticle films. The absorption spectrum of the evaporated film of ZnPc (solid line) shows a strongly broadened Q-band in the red and near infrared part of the spectrum. This is due to a $\pi-\pi$ interaction of the ZnPc molecules in a close packed film that leads to a Davydov splitting and broadening of the absorption peak. The nanoparticle films (dashed line) show a very strong and narrow luminescence centered at 605nm with a photoluminescence excitation spectrum extending in the blue region of the spectrum. Noticeable is the strong overlap of the nanoparticle luminescence with the ZnPc absorption, a prerequisite for efficient resonant energy transfer. The nanoparticles can be efficiently excited in the range of low absorption of the ZnPc.

In order to quantify the possible resonant energy transfer interaction between the molecules, a quenching experiment was performed in dilute solution and the results plotted in a Stern-Volmer plot as shown in Fig. IV.14a. The photoluminescence of a nanoparticle solution was monitored during the stepwise addition of small amounts of ZnPc. A linear increase of the inverse luminescence intensity change on the molar concentration of the ZnPc

is observed, indicating quenching according to the Stern-Volmer formalism. The quenching rate $k_q$ can be thus obtained via the gradient of the inverse luminescence intensity $K_{sv}$ with the Stern-Volmer formula:

$$K_{SV} = K_q * \tau_F \qquad \text{Form IV.1}$$

The resulting quenching rate constant calculates to around $10^8$/s, with the measured nanoparticle luminescence lifetime $\tau_F$ of about 7ns and a calculated nanoparticle molar mass of $75*10^3$g/mol.
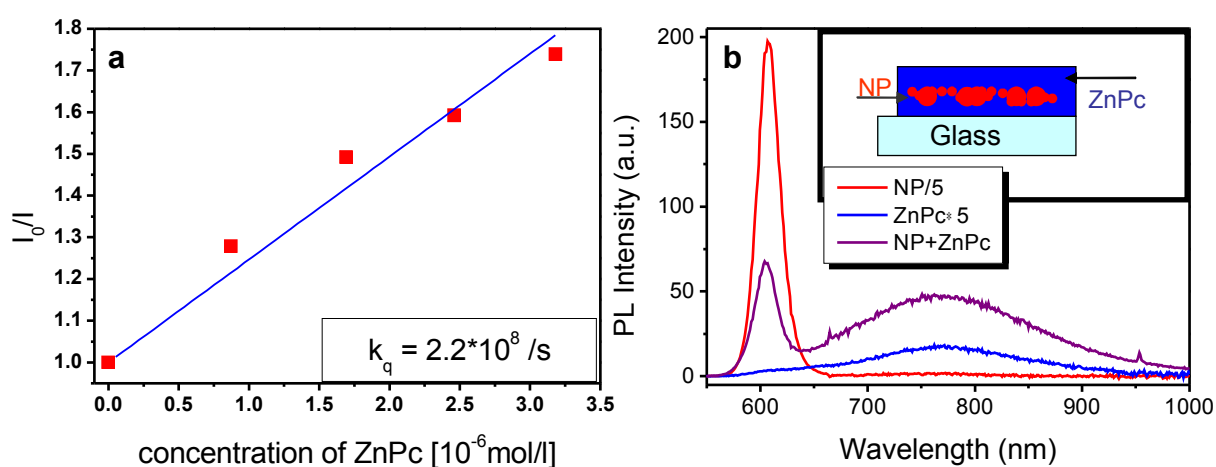


**IV.14 a** Stern-Volmer plot of the quenching of the nanoparticle solution luminescence by addition of ZnPc.
**b** luminescence spectra of a film of ZnPc doped with nanoparticles (violet) in comparison with the luminescence of a pure film of ZnPc (blue) and a comparable density of nanoparticles deposited on glass (red)

Thermally evaporated films of ZnPc, such as used in the fabrication of organic solar cells, show packing induced intermolecular $\pi$–$\pi$-interactions which strongly quench the ZnPc luminescence, as radiative transitions from the lower Davydov-level are forbidden. The weak luminescence of a 40nm thick film of evaporated ZnPc is broadened and featureless, as can be seen in Fig. IV.14b (dashed line, magnified 10x). When nanoparticles are added to the film, the luminescence signal (solid line) of the ZnPc in the range of 800nm increases by a factor of approximately 15, indicating a transfer of energy from the nanoparticles to the ZnPc. The nanoparticles show a much higher absorption at the excitation wavelength of 514nm than the pure ZnPc layer. At the same time, the luminescence of the nanoparticles is considerably quenched as compared to a layer of similar thickness deposited on clean glass (dotted line,

divided by 5). The increase of luminescence in the ZnPc-layer is a strong indication that there is a resonant energy transfer rather than charge transfer occuring between the ZnPc and the nanoparticles.

Another way of identifying and quantifying resonant energy transfer is to study the dependence of the donor luminescence quenching on the thickness of the insulating shell between donor and acceptor matrix. For this reason, nanoparticles are scattered from dilute solution on a glass substrate with subsequent evaporation of ZnPc. Thus we can make sure that almost all of the nanoparticles are in close contact with ZnPc molecules held at a distance by the ligand shell. As expected, the nanoparticle luminescence is strongly quenched (Fig. IV. 15a).
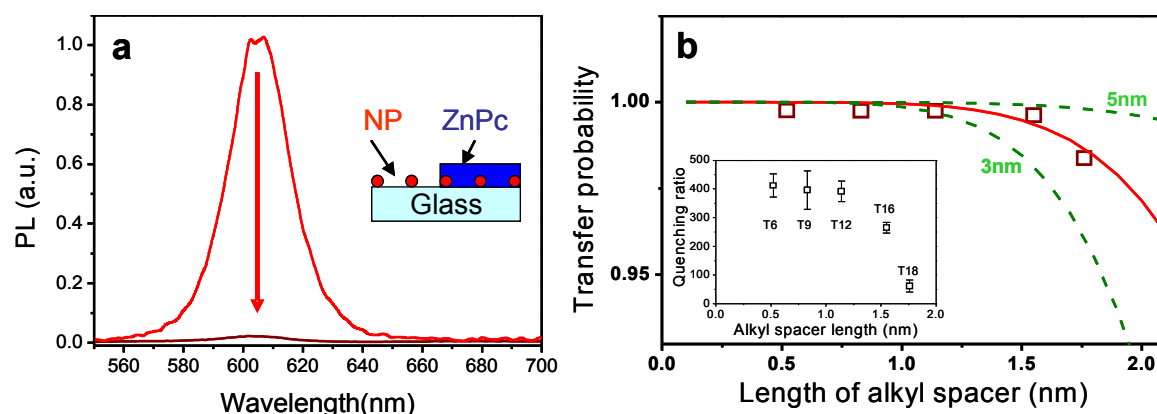


**IV.15 a** PL of nanoparticles dispersed onto a glass slide with (dark red) and without (light red) a ZnPc layer deposited on top. **b** Dependence of the quenching ratio (inset) and the transfer probability on the length of the alkyl chain of the nanoparticle ligands. The red as well as green dashed lines are calculations of the transfer probability according to Förster theory. A fit to the data points (red line) yields a Förster radius of 3.6nm, while the green dashed lines are corresponding to 3nm (lower) and 5nm (upper) Förster radius.

The inset of Fig. IV.15b shows the dependence of the nanoparticle luminescence quenching ratio on the length of the ligands covering the particles, assuming they are tightly packed and therefore fully elongated. 514nm laser excitation leads to a strong photoluminescence signal of the nanoparticles which then is significantly quenched in the presence of ZnPc on top of the nanoparticles. As expected, the quenching ratio increases with smaller shell thickness, but saturates at spacer lengths of less than 1nm. The quenching ratio is then over 400:1.

The donor-acceptor distance dependence of the energy transfer probability according to Förster's theory can be described by Form II.9 as given in the introduction to resonant energy

transfer in II.2. The dependency is sketched in Fig. II.2a.

$R_0$, the so-called Förster radius, is the donor-acceptor distance at which the transfer probability is 50%. In well-tuned energy transfer systems it can reach values of around 5nm. Comparing calculations according to the formula above with the measured data, we can estimate an effective Förster radius between 3 and 5nm. Fig. IV.15b shows the data points together with the calculated behaviour for a Förster radius of 3.6nm (solid red line) as well as 3.0 and 5.0nm (green dashed lines).

This rather large distance indicates that charge transfer between the compounds is unlikely, because an overlap of the wavefunctions is required [49]; calculations show that in a model system of two conjugated polymers only at donor-acceptor distances much less than 1nm efficient charge transfer can be expected [51].
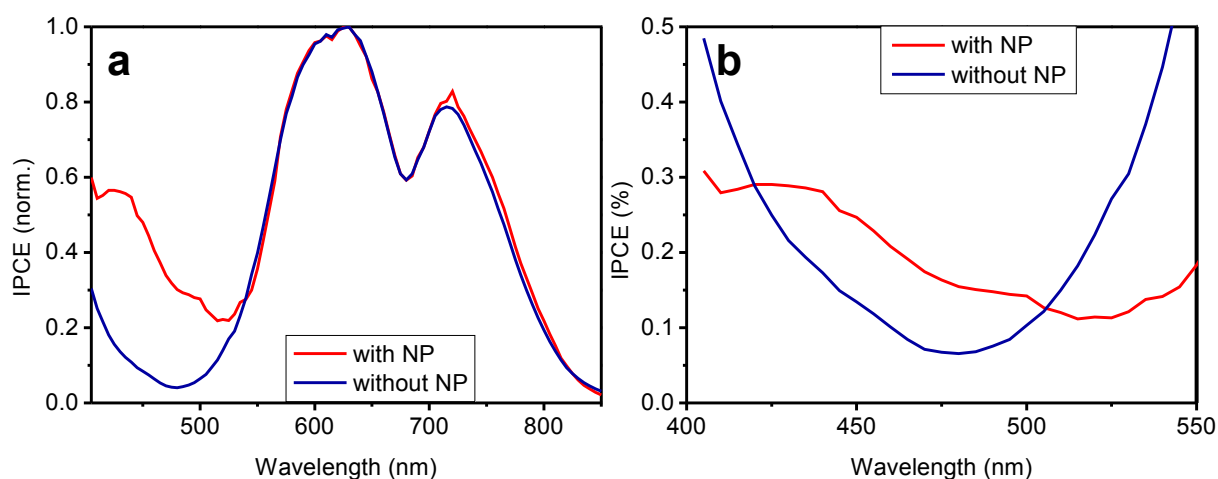


**IV.16 a** normalized IPCE spectra of ZnPc photodiodes with (blue) and without (red) nanoparticles deposited into the active layer. **b** absolute IPCE values in the range of low absorption of ZnPc indicating a sensitization of the photodiode by an energy transfer from the nanoparticles to the ZnPc

Fig. IV.16a shows the Incident Photon to Electron Conversion efficiency (IPCE) versus the wavelength of the incident light of a ZnPc photodiode with (solid line) and without (dashed line) nanocrystals deposited into the ZnPc layer normalized to the peak efficiency at 635nm. The introduction of the nanoparticles into the active layer of the photodiode shows a distinct sensitization of the photocurrent generation in the spectral range of low ZnPc absorption around 500nm. Above 580nm, the nanoparticles do not absorb any light and the IPCE spectrum of both samples shows the same shape.

The absolute values of the IPCE shown in Fig. IV.16b indicate that the overall conversion

efficiency is decreasing, most probably due to the hindered transport in the ZnPc film with interspersed nanocrystals. Around 500nm though, a significant increase of the absolute quantum efficiency values can be observed due to the absorption of the nanocrystals with subsequent energy transfer to the ZnPc.

It is very probable that this increase in the photocurrent response of the photodiode is due to light absorption in the nanocrystals and subsequent energy transfer to the surrounding ZnPc. This leads to an enhanced effective absorption cross section in the spectral range of low absorption by the ZnPc and high absorption by the nanocrystals.
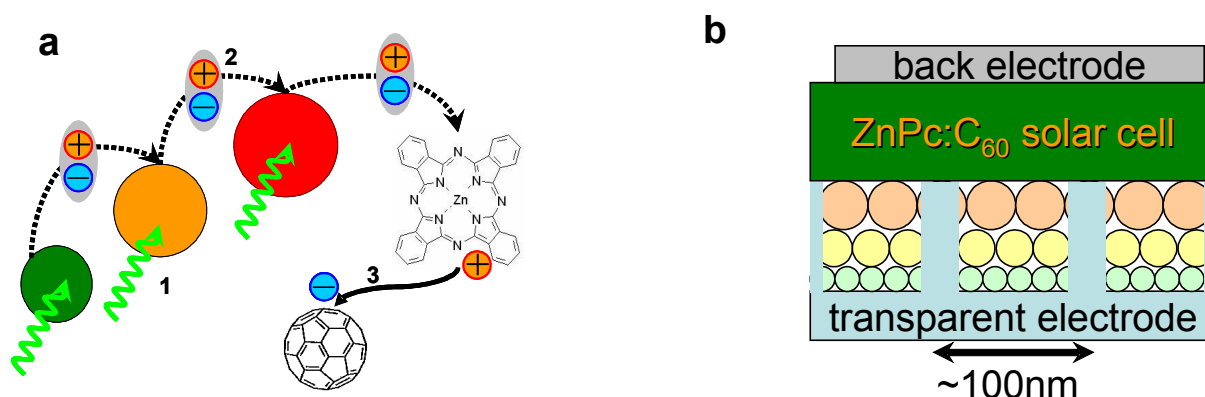


**IV.17 a** scheme of the cascaded energy transfer light harvesting featuring a multistep energy transfer between semiconductor nanoparticles of different sizes with a final energy transfer step onto ZnPc and subsequent charge transfer in a solar cell. **b** integration scheme of a nanoparticle energy transfer cascade with a ZnPc:C60 organic solar cell.

These measurements indicate that an energy transfer process can couple external absorbers such as semiconductor nanocrystals to a low energy gap organic solar cell material such as ZnPc to enhance the photocurrent generation. To avoid the problems of charge transport over external absorbers mixed into the solar cell, more advanced geometries to couple the absorbers to the solar cell have to be considered. A first approach towards such a geometry is sketched in Fig. IV.17b.

In this context, a specially noteworthy property of semiconductor nanocrystals is the possibility to change the optical properties by varying the size and shape of the colloids [46, 47]. This allows an exact tuning of the absorption and emission spectra due to the quantum confinement effect. The emission of semiconductor nanocrystals based on CdSe can be thus shifted through the entire visible spectrum.

As the most important prerequisite for resonant energy transfer is an overlap between

67

donor emission and acceptor absorption, semiconductor nanocrystals of different sizes can perform a very efficient unidirectional energy transfer towards the larger crystals with the most redshifted spectra [52, 53]. In recent studies, T. Franzl et al. [54, 55] presented multilayer CdTe nanocrystal structures fabricated by a layer-by-layer self assembly process. They observed a very efficient energy transfer between layers of differently sized nanocrystals. If the nanocrystals are stacked in layers of increasing size, the absorbed energy is funneled towards the last layer with the biggest nanocrystals in an energy transfer cascade.

This is shown by photoluminescence measurements, where in such a multilayer structure only the emission of the biggest crystals can be observed. Quantitative comparisons yield that the photoluminescence intensity is significantly increased in comparison with a single layer of the biggest nanocrystals. The effect is shown for a structure of seven nanocrystal monolayers, which shows already a significant absorption of around 5% in the green spectral region.

In effect, these structures or similar ones [56] can be used to efficiently funnel optical excitations towards a planar interface. To use this for photon harvesting in low energy gap organic solar cells, the last step has to be an energy transfer to the active material of the solar cell.

The final scheme for using cascaded energy transfer structures as photon harvesting antennae in organic solar cells is depicted in Fig. IV.17a. The first step is that light is absorbed in the elements of the cascaded energy transfer structure, such as differently sized nanocrystals. Secondly, the excitations are funneled via resonant energy transfer onto the low energy gap solar cell material, such as ZnPc. As third step, the charge separation and transport to the electrode has to occur.

The biggest challenge in this concept is to provide a channel for the extraction of the charge carriers generated in the device. This involves a nanostructuring of the cascaded energy transfer structure, as due to the low conductivity of the organic solar cell materials, the collecting electrode cannot be much further away from the point of charge carrier generation than approximately 100nm. How a straight-forward way of integrating a cascaded energy transfer structure could look like is sketched in Fig. IV.17b. This includes a pattern of conductive leads connecting the solar cell through the harvesting layer to the transparent electrode which could be generated by soft lithography or similar techniques.

### IV.3.2.2. Energy transfer between dye filled zeolite L crystals and zinc-phthalocyanine

A second approach towards an external absorber that can be coupled to an organic solar cell via energy transfer are dye-filled zeolite L crystals. Using the aluminosilicate framework of a zeolite micocrystal as scaffold for highly luminescent dye molecules, a nanostructured assembly of monodirectional light-harvesting antennas can be produced. Detailled luminescence studies on the interaction between dye-filled zeolite L crystals and ZnPc is performed and an efficent energy transfer from the dyes inside the zeolite crystal to ZnPc is identified. A large part of these studies, especially the synthesis and characterisation of the dye-filled zeolite L crystals were done by Dr. Olivia Bossart in Prof. Gion Calzaferris laboratory in Berne, Switzerland.
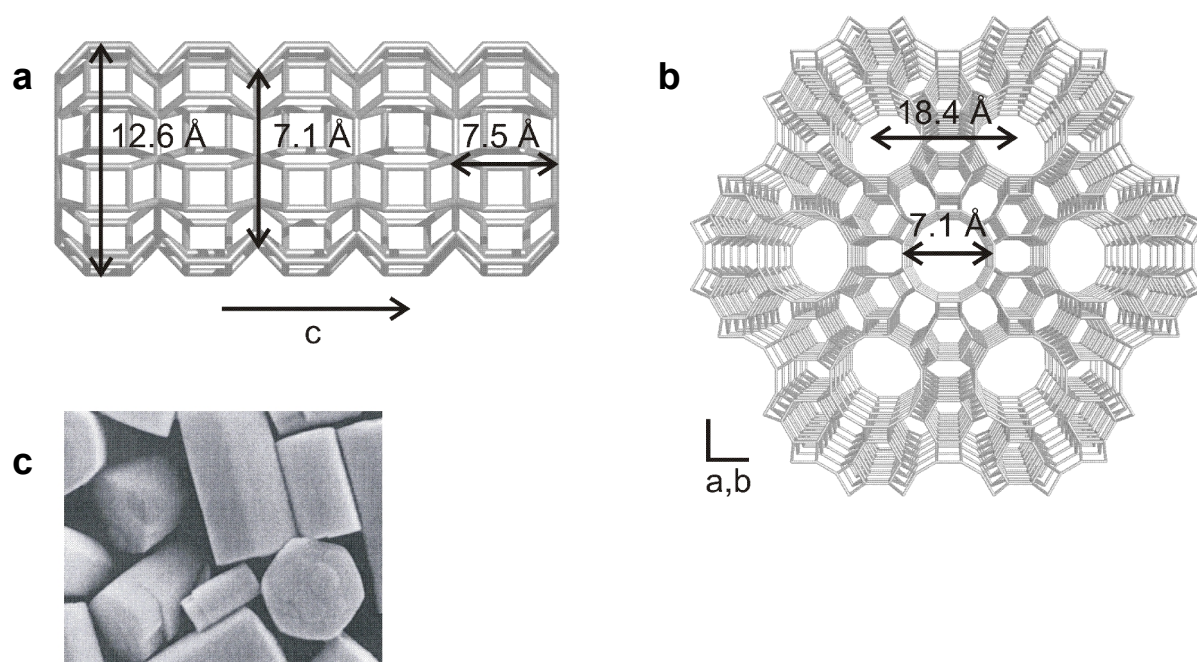
**IV.18 a** structure and dimensions of zeolite L in the a,c-plane. **b** structure and dimensions of zeolite L in the a,b plane. **c** SEM micrograph of zeolite L crystals, showing the cylindrical shape. The c-axis extends along the cylinder.

Zeolite L is a crystalline aluminosilicate with a one-dimensional channel system running along its c-axis. The channels consist of 7.5 Å long unit cells with a free open diameter of 7.1 Å at the smallest and 12.6 Å at the widest place. The centre-to-centre distance between two neighbouring main channels is 18.4 Å [57].

The framework of zeolite L is depicted along the crystal c-axis and in the a,b-plane in Fig. IIV.18a and IV.18b, respectively. Fig. IV.18c is a scanning electron micrograph showing the cylindrical shape of zeolite L. By assuming a cylindrical shape, the number of parallel channels $n_{ch}$ in a crystal can be calculated as follows:

$$n_{ch} = 0.267 \, (d_z)^2$$

where $d_z$ is the diameter of the cylinder in nanometer. Therefore, a zeolite L crystal of 550 nm in diameter incorporates approximately 80000 parallel channels. Due to its vast one-dimensional channel system zeolite L is an ideal host material.

Dye molecules with appropriate dimensions can enter the channels and occupy one, two

70

or more unit cells, depending on its size. The amount of unit cells that are covered by one dye molecule is described as site. Hence, the length of one site depends on the dimensions of the inserted dye. The occupation probability $p_{dye}$ in a dye-loaded zeolite crystal ranges from 0 for an empty zeolite to 1 for a fully loaded one and is defined as follows:

$$p_{dye} = \frac{\text{number of occupied sites}}{\text{number of total sites}} \qquad \text{Form IV.2}$$

Inside the crystal channels, the dyes are highly organised with a short intermolecular distance. Additionally, the dyes are prevented from aggregating by the confinement in the channels. The insertion of fluorescent dyes into the channels of zeolite L provides a stable photoactive material with a high monomeric dye concentration reaching up to 0.4mol/L.

An interesting material can be synthesised by loading zeolites with two or more different dyes [58]. As the dyes cannot pass each other once they are inside the zeolite channels, a highly ordered antenna material can be obtained. Depending on the sequence of donor and acceptor chromophores, the energy is directed to the crystal centre or to the channel entrances by multiple energy transfer steps terminating on the dyes with the lowest excitation energy.
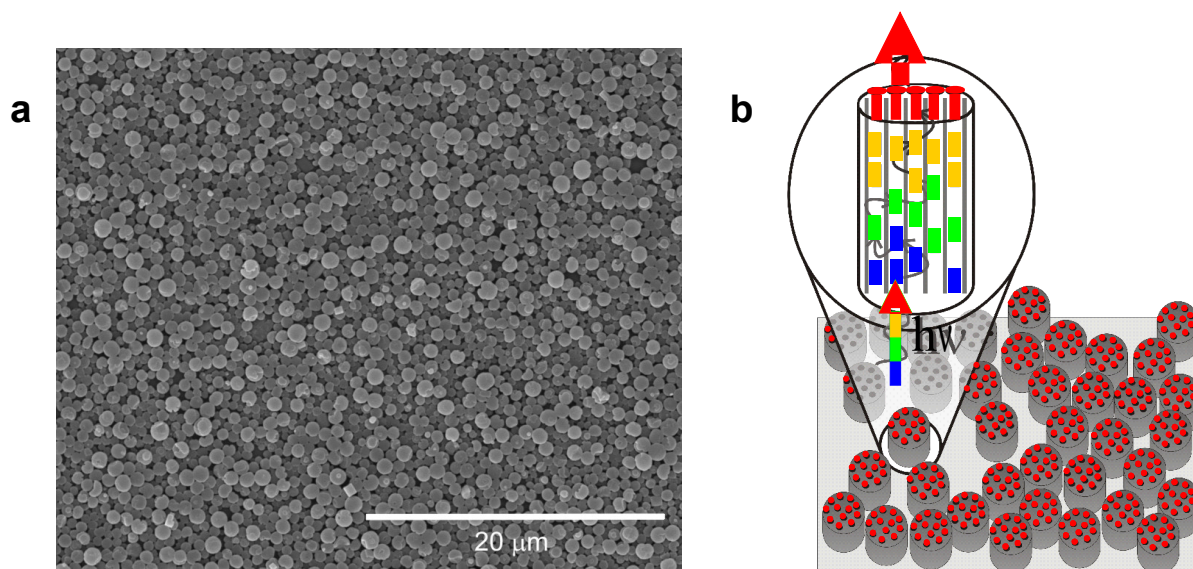


**IV.19 a** SEM micrograph of a zeolite L monolayer on glass. **b** scheme of monodirectional energy transfer in a zeolite L monolayer. The energy absorbed in the zeolite crystals is concentrated in the stopcock layer on top of the zeolites, from where it can be transferred into the solar cell.

The entrances of dye-loaded zeolites can additionally be modified with so-called stopcock molecules [59]. Stopcock molecules are fluorescent dyes which have a tail that can penetrate the channel entrances and a head that is too large to enter. They can participate in resonant energy transfer (RET) processes in the same way as chromophores that are fully inserted into the channels. Stopcock molecules connect the dyes inside the zeolites to the crystal environment. This enables further incorporation of dye-zeolite materials into photonic devices, such as for example solar cells.

Recent advances in the synthesis of zeolite L monolayers have added new functionality to zeolite L antenna materials [60, 61]. In Fig. IV.19a, a SEM image of a zeolite monolayer on a glass support is shown. As one end of the crystal is sealed by the substrate, the chromophores can only be inserted from one side of the zeolite channels. Thus, monolayers enable the synthesis of a unidirectional antenna material. A schematic image of such a material and the energy transfer cascade from the dyes inside the zeolites to the stopcock molecules at the channel entrances is shown in Fig. IV.19b.
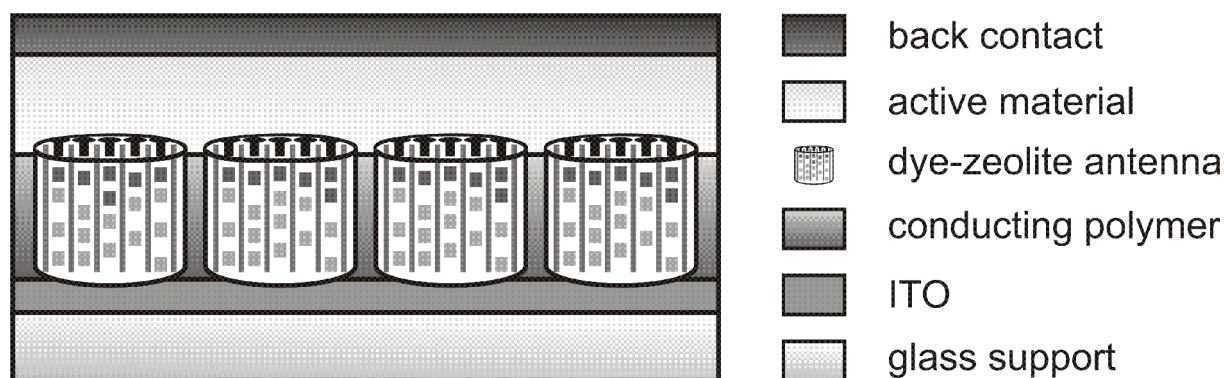


**IV.20** Integration scheme of zeolite L photon harvesting antennas into an organic solar cell

Dye-loaded zeolite L monolayers which absorb light between 400 and 600 nm are interesting for further incorporation into ZnPc solar cells, as ZnPc has a very low absorption coefficient at these wavelengths. The dyes filled into the crystal channels absorb light and transfer it onto ZnPc via the stopcock molecules. A possible integration concept of dye filled zeolites into a solar cell is shown in Fig. IV.20.

The green fluorescent dye neeliglow yellow 43 (NY43) can readily be inserted into the channels of zeolite L. NY43 can transfer excitation energy onto the stopcock molecule ATTO-565 which can be covalently bound to the channel entrances of zeolite L [62]. Their excitation and emission spectra as well as the absorption spectrum of ZnPc are presented in

Fig. IV.21c. The emission spectrum of ATTO-565 exhibits a large overlap with the absorption spectrum of ZnPc, a prerequisite for Förster type energy transfer to occur. The structures of NY43 and ATTO-565 are shown in Fig. IV.21a and Fig. IV.21b, respectively. The excitation spectra of NY43 and ATTO-565 nicely fill the gap in the absorption spectrum of ZnPc.
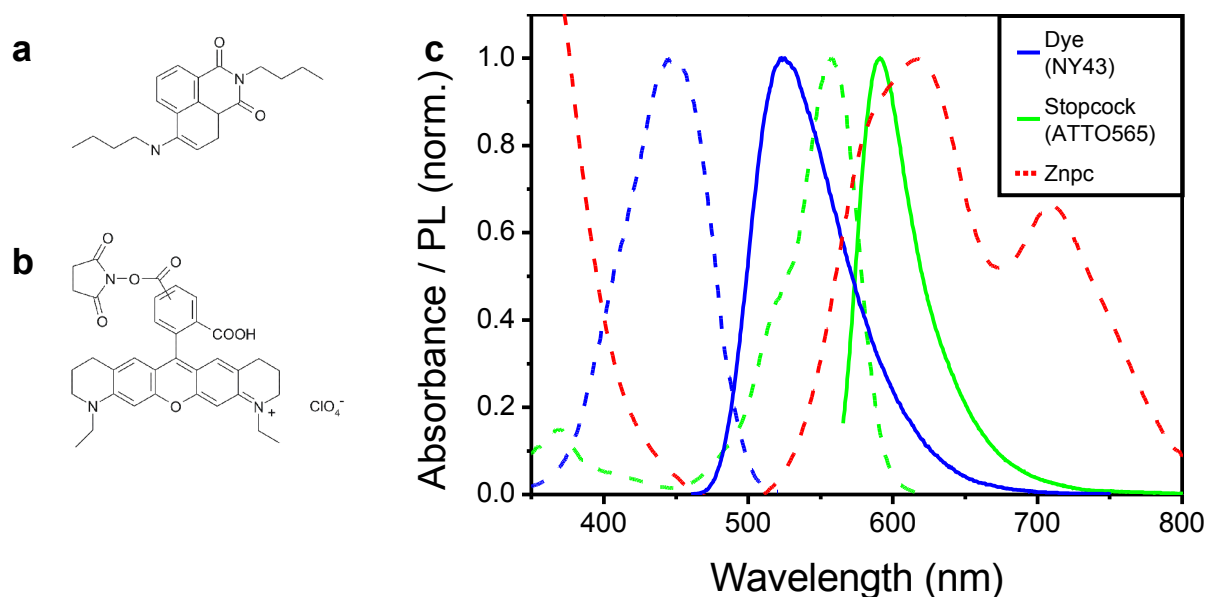


**IV.21** Chemical structures of **a** NY43, the dye filled in the channels of the zeolite L crystal, **b** ATTO565, the stopcock molecule blocking the channel entrances. **c** absorption (dashed) spectra of NY43 (blue), ATTO565 (green) and ZnPc (red) together with the PL (solid) spectra of NY43 (blue) and ATTO565 (green)

Preliminary experiments show that excitation energy from NY43 loaded zeolites is indeed transferred to ZnPc via the ATTO-565 stopcock molecules located at the channel entrances of the crystals. To demonstrate the energy transfer cascade 60 nm long zeolites with a diameter of approximately 350 nm were loaded with NY43. The final loading probability $p_{(NY43)}$ was 0.5. In a second step, the channel entrances were covalently modified with ATTO-565.

These dye-loaded zeolites were drop-cast onto a zinc phthalocyanine layer on a glass substrate. As a reference, the same amount of zeolite was drop-cast onto a clean glass substrate. Emission spectra of both sample and reference excited at 450 nm are shown in Fig. IV.22a. An additional excitation spectrum of the reference sample was recorded at 645 nm to confirm that the ATTO-565 emission at 590 nm is due to excitation energy transfer from the donor NY43. The emission spectrum of the zeolites on ZnPc is considerably quenched compared to the sample on the clean glass substrate.
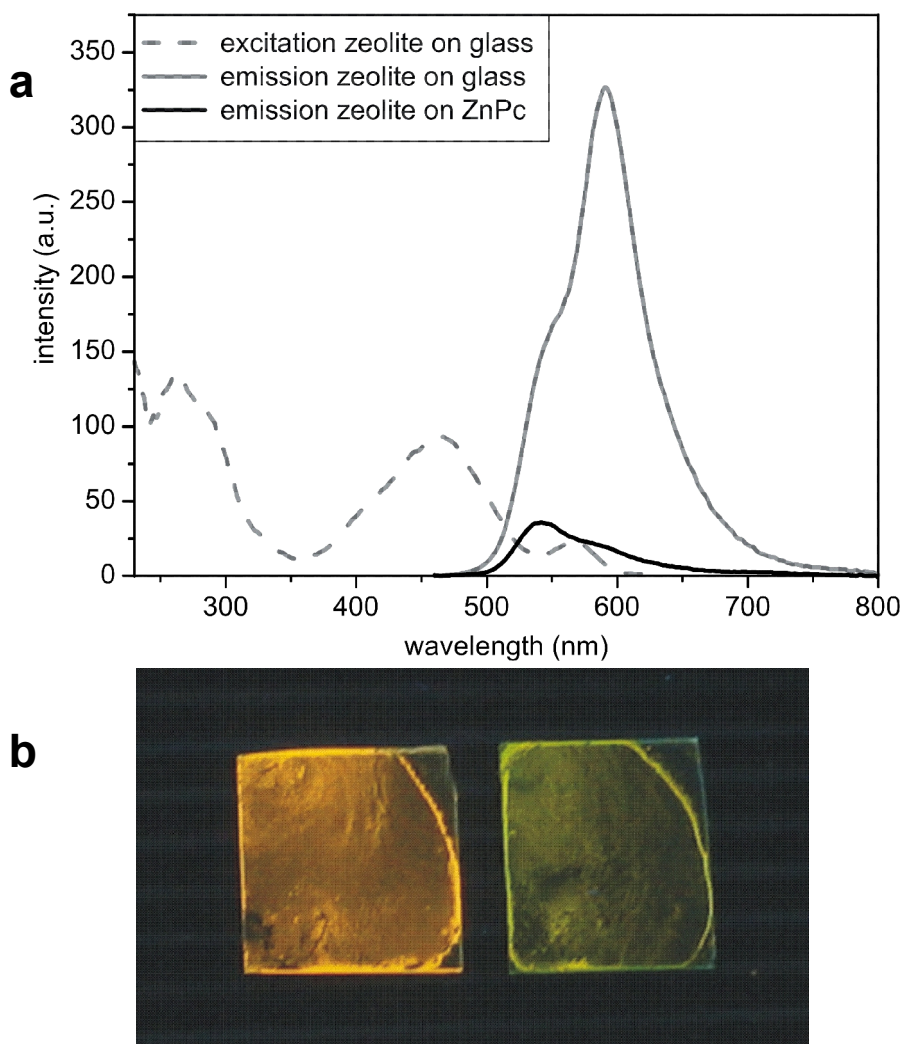
**IV.22 a** PL spectra (solid line) of dye loaded zeolite L crystals on glass (gray) and ZnPc (black) together with the PLE spectrum (dashed line) of dye loaded zeolite L crystals on glass. **b** true colour photograph of dye loaded zeolite L crystal films on glass (left) and on ZnPc (right) under UV illumination showing the spectral change of the zeolite PL.

Additionally, there is a change in the peak ratio, as the ATTO-565 emission at 590 nm is reduced more than the NY43 emission around 540 nm. This results in a colour change of the sample fluorescence which can be observed by eye under UV illumination. A photographic picture of the two samples under a UV lamp is shown in Fig. IV.22b.

The strong quenching of the dye-zeolite emission when in contact with ZnPc evidently indicates an interaction between the ATTO-565 and the ZnPc. However, it is not clear if the quenching is due to resonant energy or photoinduced electron transfer. To find out which process dominates, dye-loaded zeolite L and ZnPc was embedded in an inert and transparent polystyrene (PS) matrix. The polymer serves as physical barrier between the donor ATTO-565

74

stopcocks and the acceptor ZnPc acting as insulator participating in neither excitation energy nor charge transfer [63]. The amount of ZnPc was varied in order to observe the distance dependence of the luminescence quenching.

8 samples were prepared each containing the same concentration of dye-loaded zeolite in PS. Varying amounts of ZnPc resulting in final mean donor-acceptor distances ranging from 52 Å to 188 Å were added. Additionally, a sample containing no PS and a sample containing no ZnPc were prepared to observe the maximum and minimum quenching, respectively. Emission spectra of the samples were recorded upon excitation at 450 nm. The resulting spectra are presented in Fig. IV.23a.
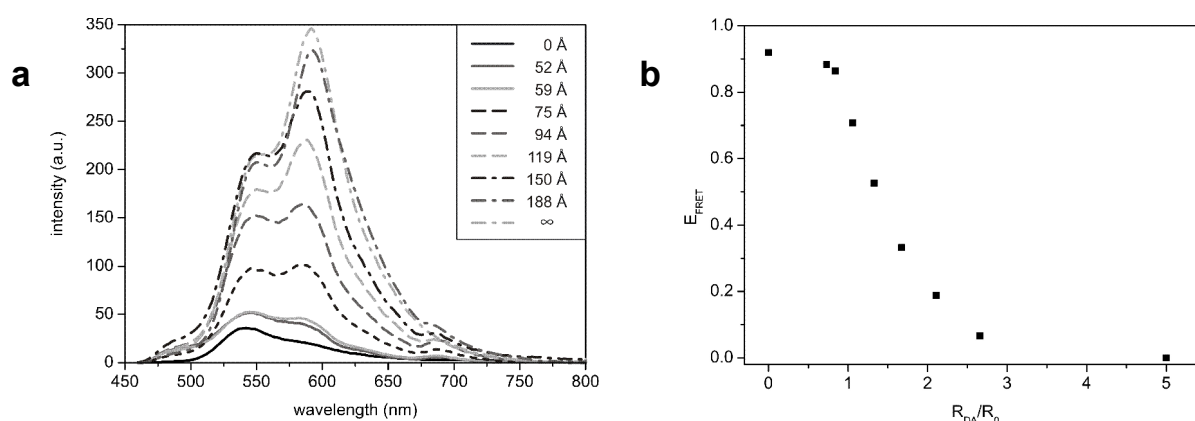


**IV.23 a** PL of dye loaded zeolite L crystals mixed into polystyrene with different amounts of ZnPc showing the quenching at differnet average distances. **b** plot of the energy transfer probability derived from the quenching experiment shown in a plotted against the average zeolite-ZnPc distance in units of the calculated Förster radius of R0=7.1nm

To evaluate the distance dependence of the quenching, the probability for energy transfer $E_{RET}$ was calculated according to the theory of resonant energy transfer given in II.2 using Form II.9, where $I_{DA}$ and $I_D$ are the fluorescence intensities of the ATTO-565 molecule at 590 nm in presence and absence of the ZnPc acceptor, respectively. The probability of RETwas calculated and plotted against $R_{DA}/R_0$. The resulting graph is shown in Fig. IV.23b. The $R_{DA}/R_0$ value for the sample containing no ZnPc was set to 5. The Förster Radius $R_0$ for excitation energy transfer from ATTO-565 to ZnPc was calculated to be 71 Å with Form II.8 according to Förster theory.

The plot shown in Fig. IV.23b shows the same curve progression as the theoretical probability for Förster type excitation energy transfer sketched in Fig. II.2a. It approaches

unity at small distances and then decreases rapidly after a certain donor-acceptor distance has been reached. The 50% probability of energy transfer in the measured progression is quite close to the calculated value for $R_0$.

A photoinduced charge transfer process would show a much shorter range of efficient transfer. As it requires an overlap of wavefunctions, distances between the donor and acceptor have to be an order of magnitude smaller than in the prepared samples [8, 49, 51]. This is clearly indicative of an energy transfer process between the ATTO-565 dye and the ZnPc.

The experiment presented here clearly indicates efficient excitation energy transfer from the excited dyes inside the zeolite channels to the ZnPc acceptor via ATTO-565 stopcock molecules. Together with the recent achievements towards oriented zeolite L monolayers, this shows the feasibility of using dye-loaded zeolite L crystals as photon harvesting antenna materials for organic solar cells.

A very promising feature of the zeolite L crystals is that they are inherently nanostructured and together with the possibility to form directed monolayers, this can lead to interesting structures, where the zeolite L crystals are used to "tunnel" the photon energy through an electrode layer in between the crystals. The electrode then does not have to be necessarily transparent in itself. As this would work both ways, a similar structure could be used in organic LEDs to channel the light out of a structure between two metal electrodes.

Shape control of dye-loaded zeolite L or similar microcrystals could improve the light harvesting potential dramatically. A truncated cone shape could concentrate the harvested light onto the solar cell while still leaving enough space for an efficient electrode. This is illustrated in Fig. IV.24.
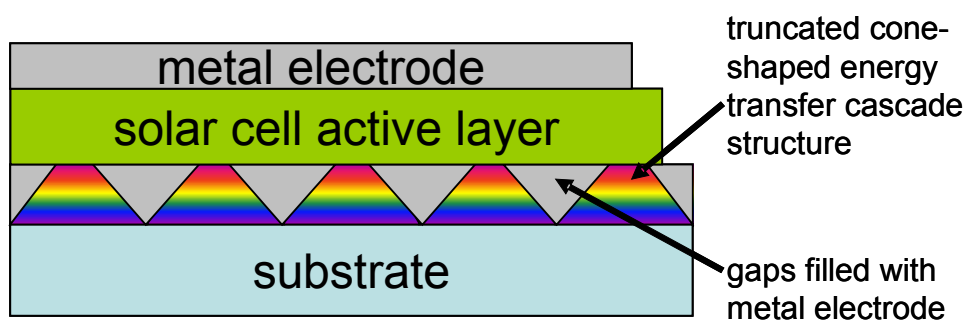


**IV.24** a solar cell structure employing truncated-cone shaped external absorbers to funnel the energy towards the active layer without obstructing the extraction of charges from the device.

## V. Summary and Outlook

This work describes different concepts of photon harvesting in organic solar cells to achieve an as wide spectral coverage as possible. The mismatch between the absorption spectra of organic semiconductor materials and the very broad white solar spectrum makes this a very important issue for further developments in organic solar cells. Decreasing the energy gap of organic semiconductor materials leads to difficulties in exploiting the blue and green spectral regions due to the localized transitions with a limited bandwidth of the absorption features. To fill this gap, materials absorbing in this region have to be chosen and coupled to an organic solar cell employing a low energy gap material.

The most straightforward technique is to add such a material directly to the active layer of a solar cell. However, as efficient organic solar cells utilize blends of donor and acceptor materials with very finely tuned interface properties, often this would only lead to reduced charge transfer or transport properties in the active layer and reduce the photocurrent. As shown in III.1.1, coordination chemistry can be a tool to influence and engineer interfaces in organic solar cells employing compounds such as ZnPc and PyF that spontaneously form supramolecular complexes during the deposition of the active layer.

Exploiting this effect, a blue and green absorbing conjugated polymer can be introduced into the fullerene phase of a diffuse bilayer organic solar cell with ZnPc and fullerenes as donor and acceptor phase, respectively. Balancing the ratio of complexing and non-complexing fullerene, the interface between the fullerene/polymer blend and the ZnPc can be activated, so that an efficient photoinduced charge transfer occurs between ZnPc and the fullerenes. The holes generated on the polymer by the photoinduced charge transfer between polymer and fullerenes can still be extracted via the ZnPc layer. Using this interface engineering, multicomponent organic solar cells can be fabricated that efficiently convert light from 400nm to 800nm and generate appreciably high short circuit currents with a maximal solar simulator power conversion efficiency of above 2%.

In the future, the interfaces between donor and acceptor phases in organic solar cells employing more than two compounds could be engineered, improved and stabilized by designing organic semiconductors with chemical groups that form a coordination complex between selected donor and acceptor compounds during the active layer formation. An improvement of the final solar cell efficiency can only be expected if the energy levels of the different donor and acceptor materials are well aligned.

Another way to extend the absorption range of organic solar cells is to take two independent devices with complementary spectral response and couple them via a series connection in an organic tandem solar cell as described in IV.2. Using a P3HT:PCBM diffuse bilayer and a $ZnPc/ZnPc:C_{60}/C_{60}$ solar cell coupled with a thin gold recombination contact, a tandem cell with an open circuit voltage of over 1V and short circuit currents of more than 4mA/cm² under 100mW/cm² simulated AM1.5 illumination is realized and the feasibility of the concept proven. In recent publications of other groups [64, 65], this concept has been developed further and efficiencies exceeding those of the best organic single junction solar cells are reached.

Additional to the rather complicated buildup with many different layers, which might complicate the fabrication process, tandem solar cells are very sensitive to the illumination spectrum. This makes them poorly suited to applications in changing illumination conditions like e.g. powering portable devices indoor as well as outdoor. But as multijunction tandem devices will probably be the best way to reach very high power conversion efficiencies, bulk electricity generation with organic solar cells will most probably be only feasible with these devices. Of the approaches presented in this thesis, the organic tandem solar cells are probably the most promising concept for applications in the near future.

Luminescencent concentrator plates as presented in IV.3.1 are a straightforward way to use external absorbers not involved in the charge transfer and transport processes to concentrate and shift the spectrum of the incoming light. The concentrator plate channels the red luminescence of highly fluorescent dyes absorbing in the blue and green spectral range efficiently to a low energy gap solar cell attached to a side of the plate. A second low energy gap solar cell is utilizing the red light being fully transmitted through the concentrator plate.

As the solar cells reach their highest conversion efficiency in the spectral region of the dye emission, the whole setup is more efficient as a solar cell with the same active area under direct illumination. This concept can be extended if solar cells with different spectral responses are used for the side and bottom cells. The side cell can be tuned to efficiently convert just the rather narrow emission of the dye at a high open circuit potential while the bottom cell converts as much of the red and infrared light passing through the concentrator as possible. In principle, this enhanced setup can reach similar efficiencies than a tandem solar cell but without the limitations induced by the requirement to match the currents in the serially connected device, as the solar cells applied to the concentrator can be contacted independently.

This concept can only work with a dye that shows an extremely high luminescence efficiency as well as good stability to withstand exposure to direct sunlight for an extended period of time. A definite drawback is the more complicated setup of the device, even though the concentrator plate can be used directly as substrate for the organic solar cells, making the integration quite straightforward. The concentrator plate of course reduces the lightness and flexibility of a final device significantly compared to a normal organic solar cell on plastic foil.

An intriguing possibility of coupling external absorbers to organic solar cells is by nonradiative resonant energy transfer. This approach is one of the prerequisites for higher lifeforms on earth, as efficient photosynthesis is based on the funneling of energy from strongly absorbing antenna molecules to the photosynthetic reaction center. In a similar process, excitation energy could be transferred from absorber molecules to the active materials in an organic solar cell.

The first model system studied in IV.3.2.1 are strongly absorbing semiconductor nanoparticles that can donate excitation energy efficiently to the low energy organic solar cell material ZnPc. As there is a shell of insulating ligands around the nanoparticles, charge transfer is inhibited, but long range energy transfer as described in Förster's theory is still happening with a very high probability. The dependence of the energy transfer probability on the length of the ligands is studied with the result that even an alkyl chain of 12 carbon atoms does not reduce the energy transfer efficiency significantly.

Photodiodes from ZnPc with and without interspersed semiconductor nanoparticles are produced and characterized. The spectral response of the diodes with added nanoparticles is significantly enhanced in the blue and green spectral region where ZnPc shows a very low absorption. Several possible application schemes are presented, utilizing a cascaded energy transfer between semiconductor nanoparticles of different sizes with a final transfer step to ZnPc and a subsequent charge transfer between ZnPc and fullerene.

A big challenge with all concepts like this is the extraction of charge carriers, which has to be performed in the same space as the energy transfer cascade. To avoid this conflict, the energy transfer cascade system could be arranged as shown in Fig. V.1, but an easy fabrication of such a structure would require very advanced nanoengineering probably involving well controlled self-assembly. Here, the energy transfer happens in columns where the energy is concentrated from both sides in the middle height of the column, from where it is transferred (black arrows) into the solar cell active layer (green). The advantage of such an arrangement

would be the unobstructed transport of charge carriers, while retaining a large cross section for light absorption in the external absorber.
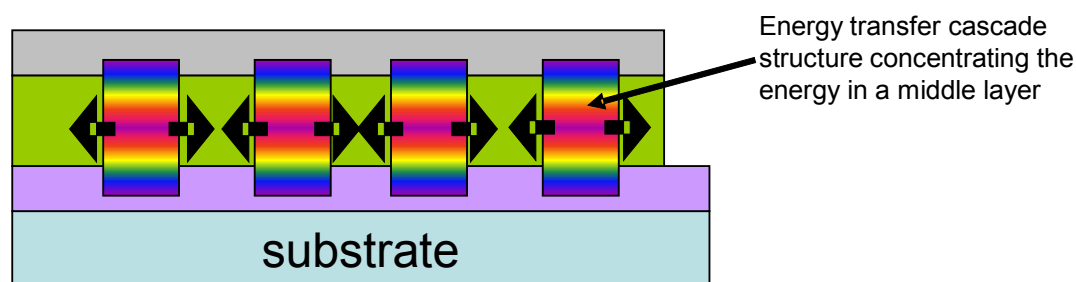


**V.1** a solar cell structure employing external absorber columns (rainbow colours) using cascaded energy transfer to donate the energy into the active layer (green). Thus, an obstruction of the extracting electrodes (violet and gray) can be avoided. The final energy transfer step is indicated by the black arrows.

The second system are zeolite L microcrystals with dye molecules filled in the zeolite channels such as presented in IV.3.2.2. These fascinating photonic structures show large absorption cross-sections and a high degree of ordering of the dye molecules inside the channels. Due to this ordering, energy transfer along the channel direction is highly efficient and by sequentially inserting dyes with overlapping emission and absorption spectra, the excitation energy donated by a large number of chromophores can be concentrated on dye molecules attached to the ends of the zeolite channels.

From there, an efficient energy transfer could couple the dye filled zeolite L crystal to a low energy gap organic solar cell material. Photoluminescence studies suggest such an interaction between ZnPc and zeolite L microcrystals of appropriate size. The possibility of arranging zeolite L crystals as a monolayer on a solid substrate with subsequent filling with dye molecules opens an interesting way of integrating the zeolites as external absorbers in organic solar cells. Light absorbed by the dyes in the zeolite crystals gets funneled by the efficient energy transfer to the upper end of the crystal, where it interfaces with the organic solar cell, thus boosting the charge carrier generation efficiency in the spectral region where the dyes absorb.

As energy transfer allows for the concentration of excitation energy in space, a very appealing point of coupling external absorbers to organic solar cells by energy transfer is that the overall absorption of the active layers is not limiting any more the photocurrent generation. Thus, external absorbers could donate the energy they absorb onto a very thin organic solar cell reducing the limitations imposed by bad charge carrier transport properties

of the semiconducting materials.

The most difficult challenge in this very advanced mode of photon harvesting by coupling an external absorber via energy transfer to a low energy gap organic solar cell material is the extraction of the generated charges. This is due to the limited range of energy transfer, which means that the external absorber has to be in very close contact with one of the solar cell materials and will be in the way of charge extraction.

A very elegant way to solve this problem might be the special properties of thin silver films which are reported to allow the passage of excitation energy from a luminescent material on one side to an absorber on the other. The proposed mechanism is a surface plasmon enhanced energy transfer over the silver film [66]. Recently, a first application in organic photodiodes was shown with a slight increase in the conversion efficiency of a copper phthalocyanine:$C_{60}$ device in the green spectral region [67]. Up to now, the maximum possible efficiency of this process is hard to quantify, but by further optimization, it could allow the implementation of the advanced photon harvesting concepts described in IV.3.2. to enhance the efficiency of organic solar cells.

## VI. References

1.  A two-layer organic solar cell. C.W. Tang, Appl. Phys. Lett. 48, 183 (1986)
2.  Organic Solar cells. D. Wohrle, D. Meissner, Adv. Mater. 3, 129 (1991)
3.  Semiconducting polymer-buckminsterfullerene heterojunctions: Diodes, photodiodes and photovoltaic cells. N.S. Sariciftci, D. Braun, C. Zhang, V.I. Srdanov, A.J. Heeger, G. Stucky, F. Wudl, Appl. Phys. Lett. 62, 585 (1993)
4.  Flexible conjugated polymer-based plastic solar cells: From basics to applications. G. Dennler, N.S. Sariciftci, Proc. IEEE 93(8), 1429-1439 (2005)
5.  Organic solar cells: An overview. H. Hoppe, N.S. Sariciftci, J. Mater. Res. 19(7): 1924-1945 (2004)
6.  Small molecular weight organic thin-film photodetectors and solar cells. P. Peumans, A. Yakimov, S.R. Forrest, J. Appl. Phys. 93(7), 3693-3723 (2003)
7.  Highly efficient p-i-n type organic photovoltaic devices. D. Gebeyehu, M. Pfeiffer, B. Maennig, J. Drechsel, A. Werner, K. Leo, Thin Solid Films 29, 451–452 (2004)
8.  Photoinduced electron-transfer from a conducting polymer to buckminsterfullerene. N.S. Sariciftci, L. Smilowitz, A.J. Heeger, F. Wudl, Science 258, 1474 (1992)
9.  Organic photovoltaic films. J. Nelson, Current Opinion in Solid State & Materials Science 6(1), 87-95 (2002)
10. A brief history of the development of organic and polymeric photovoltaics. H. Spanggaard, F.C. Krebs, Sol. En. Mater. Sol. Cells 83(2-3), 125-146 (2004)
11. Low band gap polymer bulk heterojunction solar cells. M.M. Wienk, M.P. Struijk and R.A.J. Janssen, Chem. Phys. Lett. 422(4-6), 488-491 (2006)
12. Low-bandgap alternating fluorene copolymer/methanofullerene heterojunctions in efficient near-infrared polymer solar cells. F.L. Zhang, W. Mammo, L.M. Andersson, S. Admassie, M.R. Andersson and O. Inganäs, Adv. Mater. 18(16), 2169 (2006)
13. Poly(diindenonaphthalene) and poly(indenofluorene) - Tuning the absorption properties of low bandgap cross-conjugated polymers. E. Preis and U. Scherf, Macromolecules Rap. Comm. 27(14), 1105-1109 (2006)
14. Low bandgap polymers for photon harvesting in bulk heterojunction solar cells. C. Winder and N. S. Sariciftci, J. Mater. Chem. 14(7), 1077-1086 (2004) and references therein

15. Efficient methano[70]fullerene/MDMO-PPV bulk heterojunction photovoltaic cells. M.M. Wienk, J.M. Kroon, W.J.H. Verhees, J. Knol, J.C. Hummelen, P.A. van Hal, R.A.J. Janssen, Angew. Chem. Intern. Ed. 42(29), 3371-3375 (2003)

16. Hybrid nanorod-polymer solar cells. W.U. Huynh, J.J. Dittmer, A.P. Alivisatos, Science 295(5564), 2425-2427 (2002)

17. Hybrid solar cells based on nanoparticles of $CuInS_2$ in organic matrices. E. Arici, N.S. Sariciftci, D. Meissner, Adv. Funct. Mater. 13(2), 165-171 (2003)

18. The semiconductivity of organic substances. Part 1, D. D. Eley, G. D. Parfitt, M. J. Perry and D. H. Taysum, Trans. Farad. Soc. 49, 79 - 86 (1953)

19. Conjugated Macrocycles .32. Absorption spectra of tetraazoporphines and phthalocyanines - formation of pyridine salts. M. Whalley, J. Chem. Soc. 866 (1961)

20. Efficient 2+3 cycloaddition approach to synthesis of pyridinyl based [60]fullerene ligands. P. A. Troshin, S. I. Troyanov, G. N. Boiko, R. N. Lyubovskaya, A. N. Lapshin, N. F. Goldshleger, Fuller. Nanot. Carb. Nanostruct. 12, 413 (2004)

21. Thickness dependence, in situ measurements, and morphology of thermally controlled interdiffusion in polymer-C-60 photovoltaic devices. M. Drees, R. M. Davis and J. R. Heflin, J. Appl. Phys. 97, 036103 (2005)

22. High-mobility n-channel organic field-effect transistors based on epitaxially grown $C_{60}$ films. T.B. Singh, N. Marjanovic, G.J. Matt, S. Günes, N.S. Sariciftci, A. Montaigne Ramil, A. Andreev, H. Sitter, R. Schwödiauer, S. Bauer, Org. Electr. 6, 105-110 (2005)

23. Organic p-i-n solar cells. B. Maennig, J. Drechsel, D. Gebeyehu, P. Simon, F. Kozlowski, A. Werner, F. Li, S. Grundmann, S. Sonntag, M. Koch, K. Leo, M. Pfeiffer, H. Hoppe, D. Meissner, N.S. Sariciftci, I. Riedel, V. Dyakonov, J. Parisi, Appl. Phys. A 79, 1-14 (2004)

24. 2.5 % Efficient Organic Solar Cells. S.E. Shaheen, C.J. Brabec, N.S. Sariciftci, F. Padinger, T. Fromherz, J.C. Hummelen, Appl. Phys. Lett. 78, 841-843 (2001)

25. Nanoscale morphology of conjugated polymer/fullerene based bulk-heterojunction solar cells. H. Hoppe, M. Niggemann, C. Winder, J. Kraut, R. Hiesgen, A. Hinsch, D. Meissner, N. S. Sariciftci, Adv. Funct. Mater. 14, 1005 (2004)

26. Enhanced spectral coverage in tandem organic solar cells. G. Dennler, H.-J. Prall, R. Koeppe, M. Egginger, R. Autengruber, N.S. Sariciftci, Appl. Phys. Lett. 89, 073502-1 (2006)

27. Organic tandem solar cells comprising polymer and small-molecule subcells. A. Colsmann, J. Junge, C. Kayser, U. Lemmer, Appl. Phys. Lett. 89(20), 203506 (2006)

28. Supramolecular Association of Pyrrolidinofullerenes Bearing Chelating Pyridyl Groups and Zinc Phthalocyanine for Organic Solar Cells. P.A. Troshin, R. Koeppe, A.S. Peregudov, S.M. Peregudova, M. Egginger, R.N. Lyubovskaya, N.S. Sariciftci, Chem. Mater. 19, 5363 (2007)

29. High photovoltaic performance of a low-bandgap polymer. D. Mühlbacher, M. Scharber, M. Morana, Z. Zhu, D. Waller, R. Gaudiana, C. Brabec, Adv. Mater. 18, 2884 (2006)

30. Morphology of polymer/fullerene bulk heterojunction solar cells. H. Hoppe, N.S. Sariciftci, J. Mater. Chem. 16, 45-61 (2006)

31. 29.5-percent-efficient GaNP/GaAs tandem solar cells. K. A. Bertness, S. R. Kurtz, D. J. Friedman, A. E. Kibbler, C. Kramer, J. M. Olson, Appl. Phys. Lett. 65, 989 (1994)

32. Physics of Solar Cells. P. Würfel, Wiley 2004, New York

33. Solar-energy conversion with fluorescent collectors. A. Goetzberger, W. Greubel, Appl. Phys. A 14, 123 (1977)

34. Luminescent solar concentrators .1. theory of operation and techniques for performance evaluation. J.S. Batchelder, A.H. Zewail, T. Cole, Appl. Optics 18, 3090 (1979)

35. Modifying the solar spectrum to enhance silicon solar cell efficiency - An overview of available materials. C. Strümpel, M. McCann, G. Beaucarne, V. Arkhipov, A. Slaoui, V. Svrcek, C. del Canizo and I. Tobias, Sol. Energy Mater. Sol. Cells 91(4), 238-249 (2007)

36. Performance of single layer luminescent concentrators with multiple dyes. L.H. Slooff, R. Kindermann, A.R. Burgers, A. Büchtemann, R. Danz, T.B. Meyer, A.J. Chatten, D. Farrell, K.W.J. Barnham, and J.A.M. van Roosmalen, Proc. SPIE Photonics Europe 2006 in Strasbourg

37. Zwischenmolekulare Energiewanderung und Fluoreszenz. T Förster, Ann. Physik. 1948, 6, 55

38. 10th Spiers memorial lecture - transfer mechanisms of electronic excitation. T. Förster, Disc. Faraday Soc. 27, 7-17 (1959)

39. 2 ideas on energy-transfer phenomena - ion-pair effects involving the OH-stretching mode, and sensitization of photo-voltaic cells. D.L. Dexter, J. Lumin. 1979 (18/19) 779

40. Förster energy transfer from a semiconductor quantum well to an organic material overlayer. D. Basko, G.C. La Rocca, F. Bassani, V.M. Agranovich, The Eur. Physical Journal B 8, 353-362 (1999)

41. Energy-transfer pumping of semiconductor nanocrystals using an epitaxial quantum well. M. Achermann, M.A. Petruska, S. Kos, D.L. Smith, D.D. Koleske and V. Klimov, Nature 429 (2004) 642

42. Sensitization of low bandgap polymer bulk heterojunction solar cells. C. Winder, G. Matt, J.C.Hummelen, R.A.J. Janssen, N.S. Sariciftci and C.J. Brabec, Thin Solid Films 403, 373-379 (2002)

43. Using resonance energy transfer to improve exciton harvesting in organic-inorganic hybrid photovoltaic cells. X.Y. Liu, M.A. Summers, C. Edder, J.M.J. Frechet and M.D. McGehee, Adv. Mater. 17(24), 2960 (2005)

44. How nature harvests sunlight, X Hu, K Schulten, Phys. Today 1997, 50, 28 and references therein

45. Manufacturing and commercialization issues in organic electronics. J.R. Sheats, J. Mater. Res. 19(7), 1974 (2004)

46. Shape control and applications of nanocrystals. E.C. Scher, L. Manna, A.P. Alivisatos, Phil. Trans. R. Soc. Lond. A 361, 241 (2003)

47. Electrical and optical properties of semiconductor nanocrystals. C.E. Finlayson, D.S. Ginger, E. Marx, N.C. Greenham, Phil. Trans. R. Soc. Lond. A 361, 363 (2003)

48. Synthesis and characterization of strongly luminescing ZnS-Capped CdSe nanocrystals. M.A. Hines, P. Guyot-Sionnest, J. Phys. Chem. 100(2), 468-471 (1996)

49. Theory of photoinduced charge transfer in a molecularly doped conjugated polymer. M.J. Rice, Y.N. Gartstein, Phys. Rev. B 53 (1996) 10764

50. Study of conduction mechanism and electroluminescence in CdSe/ZnS quantum dot composites. R.A.M. Hikmet, D.V. Talapin, H. Weller, J. Appl. Phys. 93(6), 3509 (2003)

51. Theory of photoinduced charge transfer in weakly coupled donor-acceptor conjugated polymers: application to an MEH-PPV : CN-PPV pair. M.W. Wu, E.M. Conwell, Chem. Phys. 227, 11 (1998)

52. Picosecond energy transfer in quantum dot Langmuir-Blodgett nanoassemblies. M. Achermann, M.A. Petruska, S.A.Crooker and V.I. Klimov, J. Phys. Chem. B 107, 13782 (2003)

53. Fast energy transfer in layer-by-layer assembled CdTe nanocrystal bilayers. T. Franzl, D.S. Koktysh, T.A. Klar, A.L. Rogach, J. Feldmann, N. Gaponik, Appl. Phys. Lett. 84, 2904 (2004)

54. Exciton recycling in graded gap nanocrystal structures. T. Franzl, T.A. Klar, S. Schietinger, A.L. Rogach, J. Feldmann, Nano Lett. 4, 1599 (2004)

55. Super-efficient exciton funneling in layer-by-layer semiconductor nanocrystal structures. T.A. Klar, T. Franzl, A.L. Rogach, J. Feldmann, Adv. Mater. 17(6), 769-773 (2005)

56. Light amplification in organic thin films using cascade energy transfer, M. Berggren, A. Dodabalapur, R. E. Slusher and Z. Bao, Nature 389, 466-469 (1997)

57. Atlas of Zeolite Framwork Types. C. Baerlocher, W.M. Meier, D.H. Olson, Elsevier 2001, 5th ed., Amsterdam

58. Host-guest antenna materials. G. Calzaferri, S. Huber, H. Maas, C. Minkowski, Angew. Chem. Int. Ed. 42, 3732 (2003)

59. Trapping energy from and injecting energy into dye-zeolite nanoantennae. H. Maas, G. Calzaferri, Angew. Chem. Int. Ed. 41, 2284 (2004)

60. Organizing supramolecular functional dye-zeolite crystals. A. Zabala Ruiz, H. Li, G. Calzaferri, Angew. Chem. Int. Ed. 45, 5282 (2006)

61. Facile monolayer assembly of fluorophore-containing zeolite rods in uniform orientations for anisotropic photoluminescence. J.S. Lee, H. Lim, K. Ha, H. Cheong, K.B. Yoon, Angew. Chem, Int. Ed. 45, 5288 (2006)

62. Sequential functionalization of the channel entrances of zeolite L crystals. S. Huber, G. Calzaferri, Angew. Chem. Int. Ed. 43, 6738 (2004)

63. Resonance energy transfer from organic chromophores to fullerene molecules. Y.-X. Liu, M.A. Summers, S.R. Scully, M.D. McGehee, J. Appl. Phys. 99, 093521 (2006)

64. Double and triple junction polymer solar cells processed from solution. J. Gilot, M.M. Wienk, R.A.J. Janssen, Appl. Phys. Lett. 90(14), 143512 (2007)

65. Efficient tandem polymer solar cells fabricated by all-solution processing. J.Y. Kim, K. Lee, N.E. Coates, D. Moses, T.Q. Nguyen, M. Dante, A.J. Heeger, Science 317, 5835 (2007)

66. Energy transfer across a metal film mediated by surface plasmon polaritons. P. Andrew, W.L. Barnes, Science 306(5698), 1002 (2004)

67. Surface plasmon polariton mediated energy transfer in organic photovoltaic devices. T.D. Heidel, J.K. Mapel, M. Singh, K. Celebi, M.A. Baldo, Appl. Phys. Lett. 91(9), 093506 (2007)

**Publications describing the results of this thesis:**

**III.1.1:**

Complexation of pyrrolidinofullerenes and zinc-phthalocyanine in a bilayer organic solar cell structure. R. Koeppe, N.S. Sariciftci, P.A. Troshin, R. N. Lyubovskaya, Appl. Phys. Lett. 87(24), 244102 (2005)

Photoluminescence studies on the supramolecular interactions between a pyrollidinofullerene and zinc-phthalocyanine used in organic solar cells. R. Koeppe, P.A. Troshin, A. Fuchsbauer, R.N. Lyubovskaya, N.S. Sariciftci, Full. Nanotubes Carb. Nanostruct. 14(2-3), 441 (2006)

**IV.1:**

Supramolecular Association of Pyrrolidinofullerenes Bearing Chelating Pyridyl Groups and Zinc Phthalocyanine for Organic Solar Cells. P.A. Troshin, R. Koeppe, A.S. Peregudov, S.M. Peregudova, M. Egginger, R.N. Lyubovskaya, N.S. Sariciftci, Chem. Mater. 19, 5363 (2007)

**IV.2:**

Enhanced spectral coverage in tandem organic solar cells. G. Dennler, H.-J. Prall, R. Koeppe, M. Egginger, R. Autengruber, N.S. Sariciftci, Appl. Phys. Lett. 89, 073502-1 (2006)

**IV.3:**

Advanced photon harvesting concepts for low-energy gap organic solar cells. R. Koeppe, O. Bossart, G. Calzaferri, N.S. Sariciftci, Sol. Energ. Mat. Sol. Cells 91(11), 986 (2007)

**IV.3.1:**

Enhancing photon harvesting in organic solar cells with luminescent concentrators. R. Koeppe, N.S. Sariciftci, A. Büchtemann, Appl. Phys. Lett. 90(18), 181126 (2007)

**Eidesstattliche Erklärung:**

Ich erkläre an Eides statt, dass ich die vorliegende Dissertation selbstständig und ohne fremde Hilfe verfasst, andere als die angegebenen Quellen und Hilfsmittel nicht benutzt bzw. die wörtlich oder sinngemäß entnommenen Stellen als solche kenntlich gemacht habe.

Linz, Dezember 2007

_____

(Robert Koeppe)

**Acknowledgments:**

But nevertheless, a lot of people had a lot of influence on my life over the last four years and therefore deserve to be acknowledged:

First, I would like to mention the person in charge of everything: Prof. N. Serdar Sariciftci. You are the Boss, after all...

Then, of course, all the former and present colleagues at LIOS, a great team of utterly chaotic people. It was a pleasure to work with you in this really nice place. Especially I would like to mention my dear long-term office mates Anita and Martin without whom I would probably have finished a bit sooner but also a lot less knowledgeable about chemistry. Non-scientific thanks go also to Gerda, Petra and the mobbing expert Fredl, not just for technical, economical and juridical help, but also for getting me acquainted with all the austrian idiosyncracies that make life here a constant source of joy.

Colleagues from all over the world helped me a great deal and some of them also became good friends over the time. Pavel and Olesya in Chernogolovka, Olivia in Berne, Zoltan and Andras in Budapest, Bertrand in LA, Claudia in Konstanz, Mike in Portland, I wish you all the best. It is a pleasure that I got to know you!

And of course, even though I am a physicist, there were other people supporting me and helping me to enjoy my life. My parents, of course, are anyway somehow to blame that I am around and I am really thankful for that and everything else. Birgit and Nellie expanded my horizon in a totally different direction. The usual suspects from Linz are to thank for giving me company on my beloved mountains.

**And everyone I did not mention, thank you anyway!**

# Curriculum Vitae

of **ROBERT KOEPPE**

**since 2003** scientific staff at the Linz Institute for Organic Solar Cells of Prof. Sariciftci. Scientific interest: Photophysics of organic semiconductor materials, organic solar cells.

**2003** Scientific staff at LMU, faculty of physics, Photonics and Optoelectronics Group of Prof. Feldmann. Scientific interest: Optoelectronical properties of II-VI semiconductor nanocrystals, conjugated polymers and applications of these materials

**2002** Graduated at LMU, faculty of physics with the twelve months Diploma Thesis "Realization of an Organic Microcavity Photodiode" performed at the Photonics and Optoelectronics Group of Prof. Feldmann. Grade "very good"

**2001** Diploma exams in theoretical and experimental physics. Both graded "very good"

**2001** Five months science project in Prof. Beton's group at the University of Nottingham, Department of Physics and Astronomy. Scanning probe and electrical measurements on polymeric materials and inorganic nanotubes. Funded by the EU through the ERASMUS/SOCRATES programme

**2001** Diploma exams in astrophysics and biophysics. Both graded "very good"

**2000/2001** working student at the Bavarian Center for Applied Energy Science (ZAE Bayern e.V.), scientific work on various aspects of energy efficiency and renewable energy sources

**2000** Two months science project at CERN in Geneva. Thesis: "First steps towards a scintillating coil particle detector"

**1999/2000** Official student's representative in the "Fachbereichsrat" (faculty council) of the faculty of physics at LMU

**1999** Change in studies towards Physics (Diplom)

**1999** Vordiplom in Meteorology at the Ludwigs-Maximilians-Universität in Munich (LMU). Grade "very good"

**1996/97** Mandatory social service in the Klinikum Ingolstadt at the Institute for Radiation Therapy and Radiological Oncology.

**1996** Graduated from secondary school (Abitur). Grade 1.6 (scale from 1 (very good) to 6 (insufficient))

born **February 16, 1977** in Ingolstadt/Donau